Predicting Motions of Fast Ships in Following Seas using a Time Domain Potential Flow Simulation

Erik Verboom

October 13, 2014

Submitted to the Department of Maritime Engineering
on October 13, 2014 in partial fulfillment of the
requirements for the degree of
Master of Science.

Abstract

One aspect that significantly influences the operational safety of a fast sailing vessel is its behaviour in steep stern quartering waves. Especially course stability plays a great roll when it comes to preventing uncontrollable and potentially dangerous situations in these sea states. During the design process of such a vessel, it is of interest predict its behaviour mentioned conditions, give an idea about which conditions are still save for operation and in a next step, try to maximise the set of those conditions. Due to the computational power of modern desktop computers, one way for obtaining such a prediction within a limited time frame are time domain potential flow simulations. Through reproduction of series of model tests, captive and free sailing, with and without waves, this report gives a thorough validation of such a potential flow code for following sea states up to conditions that possibly lead to a capsize of the vessel. The main conclusion is that the motions of a vessel in the tested conditions are predicted well by the simulation in all tested sea states. The risk of exceeding certain motion amplitudes is very similar in simulations and model tests. Nevertheless, there exist a couple of findings in the simulation results that are worth mentioning. The prediction of dynamic trim and sinkage is a weak point for the tested potential flow code. Vessels in the simulation consistently show larger dynamic rise and less bow up trim. The exact reason of this inaccuracy remains unknown. Further more, the results of free sailing conditions including irregular waves showed an extreme sensitivity for small variations in the simulation input. Especially since in without exception the input that matched the the model test the closest also lead to the best fit in the simulation results, further investigation would be interesting into whether this sensitivity actually exists in model tests or whether it is only a result of the chosen simulation method.

Thesis Supervisors: Prof. dr. ir. Rene Huijsmans
Dr. ir. Frans van Walree
Dr. ir. Pepijn de Jong

Contents

1 Introduction

Fast mono hulls are often relatively small vessels (up to about 60 meters) that, due to their purpose (i. e. rescue, coastguard or military vessels), have to operate in rough sea states , putting high demands on vessel and crew. Depending on the wave direction, the primary aspect of concern switches from operability and structural loads due to vertical movements and accelerations in head waves to course stability and operational safety in stern and stern quartering waves. These stern quartering waves of wave lengths exceeding the ship length will cause phenomena like surf riding, bow diving and broaching. Especially broaching and bow diving lead to a loss of control if the vessel and large heel angles. In extreme cases, a vessel can capsize within seconds, creating a possibly fatal situation for the vessel and its crew. Therefore it is of great interest to be able to predict the behaviour of such a fast vessel in stern quartering waves and give a good estimate of the sea states and conditions that are safe for operation. If this prediction can be made during early design stage, vessels can be optimised and the scope of conditions that are safe for operation can be increased significantly. Unfortunately, research into the phenomena leading to surf riding and broaching is quite hard to accomplish. The vessel is sailing in severe sea states, waves lengths exceed the ship length and cause large amplitude motions in all six degrees of freedom. Most phenomena that play a role are highly nonlinear and small differences in the vessel's position in a wave might decide between a complete loss of control, broaching and capsizing or a harmless surf ride down the wave. On top of that, in an irregular sea state, due to the described sensitivity with respect to the considered wave, the vessel's position in the wave, and even small details like instantaneous rudder angle or autopilot settings, the occurrence of extreme cases that pose a danger to crew and vessel can be very rare. Extensive testing time and multiple capsizes are necessary to make a well informed decision what conditions are safe for operation and which ones are not. Obviously, in most cases it is not possible to perform such tests on a full scale vessel. But even model tests or time domain simulations are very time consuming since a large number of wave encounters is necessary and the encounter frequency can be extremely low, approaching zero in some cases. On top of that, a completely free sailing vessel is necessary, that can handle large amplitude motions in all six degrees of freedom.

This thesis project focuses on the possibilities of a potential flow code to predict the vessel's motions in stern quartering waves. As the computational resources necessary to run such a program are available in a modern day desktop environment, it has the potential to be an easy to use tool that can give a good estimate of the vessel's course stability and manoeuvrability already in early design stages. Moreover, when the computational time of one simulation run drops down to reasonable values, the number of design cycles, optimising the vessel for operational safety in multiple conditions can be increased significantly. However, in order to be able to run free sailing simulations with large amplitude motions within a reasonable time frame on a desktop pc, significant simplifications have o be made to the physics that play a role in such simulations. Due to these simplifications of the flow model, force components have to be calculated separately, often using empirical data from previous measurements. Each of these separate calculations and especially empirical methods often have an applicability that is limited to certain conditions and geometries and limit the applicability of the entire simulation program. As a result of that, such a program needs to be validated extensively for several conditions separately to draw a set of conditions and hull shapes in which it delivers reliable results.

The goal of this report is to investigate the capabilities of such a program for stern quartering waves. To do this, a number of model tests on different hull shapes will be reproduced as accurate as possible within the simulation. Through the comparison of model test and simulation results, conclusion can be made about the reliability of the simulation results. In order to get a complete and detailed idea of the simulation results, not only model tests in stern quartering waves will be reproduced, but also captive and free sailing tests in calm water. This can help to analyse different components of the forces and moments on the hull and helps to isolate reasons for differences between model tests and simulations. Based on these tests in calm water, some variations in the simulation method can be made in an effort to improve the simulation results. Afterwards, model tests in actual steep stern quartering waves can be reproduced in simulations and conclusions can be drawn on the its ability of the simulation method to predict a vessel's motions and course stability in these conditions as well as its ability to predict the risk of the occurrence of severe broaches and capsizes.

In order to achieve this goal first a thorough description and analysis of the problem of a fast hull in stern quartering seas will be given. In section 2 said description is given as well as a number of approaches that are available in literature to predict a vessel's behaviour in stern quartering waves, including their advantages and disadvantages. Finally, this section can be seen as an argumentation for the use of a time domain 3D potential flow simulation for vessel's in said conditions, provided the currently available computational power. Secondly, in section 3, a description of the simulation method used is given. A detailed overview of the principles of a time domain simulation as well as the decomposition of forces on the hull and the choices of mathematical models for each of those force components is shown. Afterwards, with the provided knowledge about vessels in stern quartering waves and the simulation methods used, sections 4 and 5 are used to describe in detail verifications and validations on the bases of respectively captive and free sailing model tests that were carried out during this project. This includes the reproduced calm water model tests as well as the tests in stern quartering seas. From those validations, some points of interest and possible variations in the simulation method could be isolated that are worth examining and trying out into further detail. Section 6 provides a verification of some of these variations in the pursuit of improving the given simulation method.

2 Problem Description

As described during the introduction, the objective of this project is to validate predictions for ship motions in stern quartering waves. For this validation, it is important to understand the dynamics of a hull in stern and stern quartering waves as well as how such a 3D potential flow code is structured. This section will first explain some background knowledge for manoeuvring and seakeeping in stern quartering waves. Afterwards, methods for predicting a ship's behaviour in stern quartering waves will be explained and examined in order to give a motivated choice for the 3D time domain potential flow code used in the remainder of this report.

For head waves and trim and sinkage in calm water, a validation of the considered panel code is given by de Jong in [24]. However, since the points of focus for a simulation of a ship in head waves are different than for a ship in stern quartering waves, a separate validation for these conditions is necessary.

2.1 Dynamics in Regular Stern Waves

While the high encounter frequencies in head waves move the focus mainly towards accelerations and structural loads caused by highly dynamic peak pressures, a ship in stern waves has much lower encounter frequencies. In fact, the encounter frequency in the situations of interest is so low that during past research, often a quasi-static position of the hull with respect to the (regular) wave has been assumed. This assumption helps to understand part of the dynamics of surf riding, broaching and nose diving. When the vessel is located on the front of the wave, its stern is lifted up by the incoming wave while the bow is located near the wave trough. In this situation, the stern is not only lifted, but also being pushed forward by the wave and gravity. First of all, this will lead to a significant acceleration. This acceleration is only stopped by the bow digging deep into the wave trough or the back of the next wave and the resulting sudden increase of local drag. Depending on the maximum speed obtained during this acceleration three things might happen. In case the maximum speed of the vessel is lower than the wave speed, it will be overtaken by the wave and move on to the next wave. If the maximum speed is equal to or a little higher than the wave speed, a stable equilibrium might be found in which the vessel rides on the front of the incoming wave. The last possibility is that the vessel starts overtaking the wave. In this case, the bow will "'bump"' into the previous wave, decelerating the vessel back to a speed lower than the wave speed. In some cases this might lead to the vessel into a periodic trajectory between the front and the back of one wave trough.

Within this simple model, one clear definition of the meaning of the terms surf riding, broaching and nose diving can certainly be given. The most common phenomenon of those three certainly is surf riding. This describes the accelerated situation on the front of the wave. In itself surf riding does not pose an increased risk to the safety of crew or vessel. If anything, higher speeds can be obtained with equal or less fuel consumption. However, as Spyrou mentions in [8] it is commonly acknowledged that surf riding is a precursor to more dangerous events like nose diving and broaching. As described in the previous paragraph, surf riding is initialised by a large accelerating force acting on the stern and ended by a sudden increase of drag in the bow. Here, it can easily be seen that in both situations, a large force is "'pushing"', acting (in the direction of the force) in front of the centre of gravity of the vessel. In these "'pushing"' situations small yaw rotations cause yaw moments that tend to increase the rotation further. Whenever these exciting moments become larger than restoring moments due to hull drag and steering, a dynamic instability occurs, causing a rapid change of course. Whenever this kind of dynamic instability occurs, it is safe to assume that a combination of hydrostatic, and centripetal and wind forces cause a heeling moment large enough to pose a significant thread of capsizing. Depending on whether this instability occurs during the acceleration or during the deceleration, the result will be referred to as respectively broaching or nose diving.

One approach to the prediction of broaching are -linear and nonlinear- mathematical manoeuvring models. For these models the described regular stern wave and the longitudinal position of the vessel in that wave are taken as starting point for predictions. Often not only the 3 DOFs for manoeuvring in calm water (yaw, sway and surge), but also the roll motions and/or rudder angles are taken into account. The controlled variables are rudder angle or auto pilot course and in some cases the propeller revolution rate. With these

models, a set of conditions where surf riding and/or the loss of directional stability occurs can be predicted. When such a dynamic instability occurs, the periodic trajectory between the front and the back of one wave trough meets an unstable equilibrium of surf riding. Some of these methods are discussed in [2], [4], [15]. As input, these models use manoeuvring coefficients that depend on the ship and the wave that is to be examined. These coefficients can be obtained from model tests, simulations or comparison with other designs. These mathematical models have the advantage that, when the necessary coefficients are known or can be estimated, a region of conditions (such as wave height, wave steepness, wave angle, but also auto pilot settings) where broaching occurs can be given without the need for extensive time domain simulations or model testing. As Umeda shows in [15], his model can even be used to create an autopilot that can reduce the risk of broaching. The disadvantage however is that these models take only into account regular stern waves. Effects of irregular waves or waves coming in from angles smaller than 360 degrees can also cause directional instability, but are not taken into account.

2.2 Irregular Stern Quartering Waves

In the previous section, the problem of predicting the ship's behaviour in stern quartering seas was simplified to predicting regular waves coming directly from behind. In order to fulfil the goal of this thesis however, we have to look at at stern quartering waves as well, including irregular waves. In these conditions, it is not possible anymore to only look for dynamic instabilities as a result of the stern being lifted by a wave. Since waves do also come in from the side, the hydrostatic forces will not only lift the stern and push it forwards, but also partly to the side introducing a considerable yaw and heel moment. Without the occurrence of any dynamic instability, this can already introduce significant yawing angles that may lead to dangerous situations. Therefore the previous definition of a broach does not hold anymore.

Instead there is fluent transition between waves that introduce smaller and rather harmless yawing moments to waves that cause the vessel to broach until the waves come in from the side. In literature, there have been some cases of broaching being defined as a strict set of conditions being fulfilled. For example de Jong in [25] defined a broach as a situation in which a certain combination of yaw angle, rate and acceleration, as well as instantaneous rudder angle is exceeded. This can be helpful when looking for a certain set of wave conditions that pose a thread to vessel and crew, or for a comparison between two concept designs. However, when it comes to validating a time domain simulation, there is no reason to define a clear set of conditions that define a broach. Rather, effort should be put into evaluating the ship's motions in general. A validation should be given for motions in all six degrees of freedom, including small and harmless heave and pitch motions as well as large roll and yaw motion possibly leading to a capsize. For this reason, if the term "'broach"' will be used at all, it will be in the sense of the rather vague definition "'A rapid change in yaw and heel angle introduced by a stern incoming wave, posing a significant thread to the safety of crew and vessel."'.

2.3 Time Domain Simulations

One way to predict the risk of broaching, including stern quartering and irregular are time domain simulations. Here an attempt is made to simulate all instantaneous forces and moments acting on the sailing vessel and use them to predict the ship's motions in six degrees of freedom for each point in time. Under this category, model tests as well as CFD simulations can be summarised. In both cases, and in contrast to the mathematical models described in the previous section, there is no way of easily predicting any region of conditions that will lead to broaching. Instead, a large number of wave encounters has to be simulated to show with statistical significance if broaching is likely to occur in the simulated conditions. The fact that there also is a large range of conditions that might be worth testing and the wave encounter frequencies that are often very low illustrate that, no matter what simulation method used, this approach is very time consuming. On top of that the simulation of ship's motions in stern quartering seas posts high demands on the used simulation method. The simulation method needs to be able to handle large motions in the vertical and horizontal plane, the ship needs to be free sailing, self propelled and self steered and preferably any wave direction between 270 and 360 degrees should be realisable. On the other hand, simulation data can be used

to obtain manoeuvring coefficients for the mathematical manoeuvring models, who in turn can broaden the spectrum of conditions for which predictions can be made. Moreover, the physical simulations can give a better insight into what is actually happening around the hull. Therefore it can lead to the optimisation of design parameters and safer vessels in the future. All the requirements make model tests as well as CFD simulations very costly and explain the search for efficient simulation methods.

In the past decades, the interest in - as well as the possibilities of - numerical simulations of manoeuvring and seakeeping has increased consistently. This is not hard to explain when realising that the availability of computer power kept - and for the foreseeable future most probably will keep - on improving while its costs decrease. Generally, the principles of these simulation algorithms work as follows: Through one way or the other, an estimation is made for all forces acting on a vessel at any moment in time. This includes hydrodynamic pressure on the hull, hydrostatic pressure on the hull as well as manoeuvring and propulsion forces and appendages like bilge keels or stabilising fins. In some cases even a simple representation of wind forces can be included. When all forces are added up, the equations of motion can be solved for the entire vessel. To do this, a discretisation in time is necessary. Depending on the simulation method chosen, the equations used for the force estimations vary. Especially evaluating the hydrodynamic forces accurately poses some significant mathematical challenges. The next paragraphs give a short explanation of the different approaches used for time domain computer simulation up to the present time.

2.3.1 Hydrostatic Solution

When looking at a vessel, it is solely surrounded by gas and fluid flow. All forces that act on it are in some form due to fluid dynamics and fluid statics. Hence, all forces can be computed by integrating pressures and shear forces over the complete vessel's surface. To evaluate those at each time step as accurate as possible, they are split up into components, adding up several physical phenomena that take place around the hull. One component that will be neglected in most cases is any wind introduced flow. With that, a solution of any flow above the instantaneous waterline, as well as modelling of on-deck structures can be avoided. For the remaining hydrodynamic problem of the flow around the hull, splitting up of the forces will depend on the simulation method chosen. However, some general guidelines can be given. First of all, a split between hydrostatic and hydrodynamic pressures is very useful. The hydrostatic solution contains any pressures on the hull that would still exist if the instantaneous situation was frozen, and all water and ship motions are eliminated. For a static calm water situation, this would result in a pressure on the hull $p = \rho \cdot g \cdot h$, depending solely on the depth of the point that is being evaluated. Even in cases including the ship's motions and free surface waves, this hydrostatic component is easy to evaluate when the local instantaneous wave height and hull position is known. Replacing the h used before with the depth from the local hull surface to the undisturbed local wave height, the so called Froude-Krilov forces can be evaluated, giving the hydrostatic forces on the hull.

2.3.2 Hydrodynamic Solutions

Evaluating the hydrodynamic solution is a bit more complicated. This contains all forces that are in any form caused by fluid particle motions and ship or appendage movement, including any pressure distribution and waves caused by forward speed of the vessel and local currents within a wave as well as forces caused by appendages like rudders, stabilizing fins and the propulsor. Generally, this hydrodynamic solution can be obtained by solving the Navier-Stokes equations for a given fluid domain with a set of fitting initial and boundary conditions. However, unfortunately, within foreseeable future, it will not be possible to obtain sufficient computational power to do that. Therefore, several simplifications to the Navier-Stokes equations have been developed in the past that provide approximate solutions. On top of that, in many cases it is easier to exclude appendages like propellers and lifting surfaces from the hydrodynamic solution. This way the modeling process as well as the hydrodynamic solution can be simplified. Forces caused by these appendages can then be modeled using open water diagrams and well validated empirical lift and drag coefficients.

URANS One possible simplification to the NS equations are so called '(Unsteady) Reynolds Averaged Navier-Stokes' (RANS) solvers. Here the flow speed's and pressures are interpreted as statistical quantities, where only the average value is being calculated, basically eliminating turbulence and its unsteady effects withing a boundary layer. The calculations of average flow speeds would be exact if the energy dissipation from small to large eddies (vortices within turbulent boundary layers) could be modeled exact. However, for this energy dissipation, RANS solvers have to rely on empirical turbulence models that can only be accurate up to a certain point. During the past years a significant amount of research has been dedicated to extending the capabilities of RANS solvers. In [16], Jacquin et al. describe a RANS solver that can simulate the manoeuvring of a free sailing, self propelled ship in calm water. While moving appendages can be taken into account, the propulsion is simplified to an actuator disc or a steady force. This means that a large number of viscous flow effects and appendage-hull interaction is included in the hydrodynamic solution naturally. In [19], Ferrant et al. describe steps towards including incident waves into the unsteady RANS solver used by Jacquin. However, even with modern high performance computers these simulations still need an excessive amount of computation time. Especially simulations of longer time spans (that will be necessary for sea keeping) are beyond reach for most practical applications.

Potential Flow When simplifying the NS-equations even further to potential flow, the computational time necessary will reduce significantly. Essentially, potential flow describes a special case of flow, where there is no viscosity and no rotation. In this case there is no need anymore to evaluate the flow in the complete fluid domain. Rather, evaluation of the stream traces on the surface of the domain boundaries is sufficient. However, this comes at a cost of a significant difference between the calculated flow and the flow encountered in reality. Moreover, viscous effects are no longer included in the hydrodynamic solution, creating the need for additional formulations for lift forces, viscous drag and flow separation. However, most of this viscous forces (for example lift and flow separation) strongly depend on the submerged volume and the flow speed and direction considered. Empirical methods used to describe them are often curve fittings of systematic series of measurements. The further the simulated case deviates from the case used to develop the empirical formulations, the less accurate results can be expected. This partly creates the need for programs specialised for specific vessel types or sailing conditions.

A number of tools based on potential flow theory have been developed in the past 20 years that can deal with large amplitude motions of self propelled and self steered vessels. Generally, these programs in most cases can handle the requirements for simulating course keeping and manoeuvring in steep stern quartering seas within reasonable computation time. However, between them there are significant differences in choices for evaluating the potential flow equations and dealing with (non)linear boundary conditions. De Kat [5] developed a simulation program named FREDYN, calculating the forces of the potential flow on the hull based on strip theory. The forces on the hull are obtained by superimposing Froude-Krylov forces, as evaluated for the instantaneous wetted surface and linear radiation and diffraction forces. Due to the use of strip frequency domain strip theory, this initially excludes secondary effects of forward speed (like the bow and stern wave systems) from the hydrodynamic solution. Additional forces due to viscous effects and manoeuvring are added separately.

Later on, a couple of 3D full time domain potential flow programs were developed that naturally include effects of forward speed, seakeeping and manoeuvring forces. In 2010, Yen [21] published validation of the Large Amplitude Motion Program (LAMP). LAMP can calculate its results based on a body-linear or a body-nonlinear approach. Either way, the hydrodynamic forces are calculated using a potential flow panel method, which naturally includes the effects of incident, diffracted and radiated waves. These free surface effects are calculated using Green's functions as well as panels on the water surface. Viscous effects like viscous resistance, damping and lift on the hull and or appendages, as well as any form of propulsion forces are added using empirical or semi empirical formula's. In his paper, Yen obtains reasonable results for manoeuvring tests like the turning circle and zig-zag manoeuver.

In a similar way, in his PhD thesis [7], Raven developed a program named RAPID. In this case a body and surface nonlinear approach was chosen to determine wave making resistance and account for dynamic

trim and sinkage. RAPID is limited to a steady incoming flow. The free surface effects are taken into account by a panel distribution on the free surface. The RAPID program will be used later on in this report to get another comparison for certain Panship results.

In [9] van Walree developed Panship, a potential flow program using the transient Greens function to include free surface effects and eliminate the need for free surface panels. Thereby, computational effort can be further reduced. Again, two versions are developed, one with non-linear body and free surface boundary conditions and a linearized version. The details about the mathematical models used within Panship will be discussed in section 3. Later on, a detailed validation of results obtained by Panship, will be described.

2.4 Validation of Potential Flow Simulations

Due to the extend of simplifications applied to the flow, but also due to the relatively large number of added empirical calculations and forces, all potential flow methods need extensive testing and validation for different conditions and submerged geometries, before they can be used as a predicting tool. This section will give some insight into methodology and necessary steps for a validation of free sailing simulations in stern quartering waves.

Performing a validation of a vessel in stern quartering seas posts a number of difficulties. The objective is to validate the ship's motions as a result of incoming waves, propulsion and autopilot steering. In this situation, the simulation result is a sum of a very large number of force components that are taken into account. Even if these simulation results seem to reproduce measurements well, it might just be that errors in several force components cancel each other out in the one tested case. Therefore, in order to achieve a reliable validation, as many force components as possible should be tested separately, and as many cases as possible should be validated. This way a good idea can be given about the actual accuracy of the simulations.

Reference Cases Simulations are generally performed in order to predict a real full scale vessel's behaviour. Therefore, a validation of a simulation method should preferably use measurements from such a full scale vessel's motions as a reference case. Assuming accurate measurements as well as valid measurement methods, this would imply that the measurement results can be directly taken as for comparison of the simulation results. However, accurate and detailed full scale measurements are very expensive and often hard -if not impossible- to take. Moreover, sailing in conditions that might lead to broaches and capsizes poses a significant thread to crew and vessel.

A better choice for reference cases can be model tests. Model tests have been carried out for a long time and measurement techniques as well as the variety of different tests that are performed on a vessel are very refined. On top of that, the conditions during model tests can be controlled far more accurate than during full scale measurements. The effect of the relative difference in viscosity between full scale vessels and models are well known and can be taken into account while comparing test and simulation results. One problem that remains with any measurements is that only the sum of all forces/motions/pressures can be measured. Force components that are calculated separately within the simulation can not be compared separately from one measurement. This restriction can be overcome by not only looking at model tests for a free sailing vessel in irregular stern quartering waves. Instead, for example the force components caused by incident waves can be eliminated by validating simulations on calm water. A useful addition can also be captive simulations with forced heel or yaw variations in order to validate the effect of heel and yaw angles that in reality might be introduced by incoming waves. Generally, it is a good idea to validate a large scale of model tests run in different conditions. This way, not only a better estimate of the quality of simulation results in irregular stern quartering waves can be given, but also possible causes of errors in these results can be pinpointed and ideas for possible improvements can be given.

Analyzing Results in Irregular Waves When simulations including irregular waves are validated, attention has to be given to the recreation of the waves encountered during the model tests. Generally, there

are two possibilities to compare simulations in irregular waves with model test results. These validations can be done by statistical analysis of the time traces or by a recreation of the wave train encountered during model testing (a deterministic approach). For the statistical analysis, only the wave spectrum from the model test has to be recreated. Based on this, statistical data like mean values and standard deviations of the ship's motions can be compared between model tests and simulation. If the amount of wave encounters is sufficient, this is a valid approach to validate a simulation. However, for aft incoming waves it is often a problem to get a sufficient amount of wave encounters in a model test. Due to the low encounter frequency this would lead to an excessive amount of runs per condition.

Therefore, the second option is to recreate the wave train that was realized during the model test, and make a one on one comparison of the ship's motion. This method is harder to accomplish, first of all since the wave during the model test has to measured and afterwards recreated. Then during the simulation the initial position of the vessel has to be correct, including initial values for speed and orientation. Secondly, errors in the ship's motions accumulate over time, so that a small initial error can cause a completely different resulting time trace, even when the simulation is valid.

Existing Validations The computer programs Fredyn and Panship developed by de Kat and van Walree were compared and validated by van Walree in [22] for stern quartering waves. In this paper, special attention was given to deck submersion in case of large heel angles. Several ways of computing the free surface along the hull were tested in this respect. Afterwards, a short detour into the occurrence of broaches in stern waves was taken. While the tested simulations and model tests had too little wave encounters to be statistically representative, the results indicate that the conditions necessary for a broach to occur are reasonably well predicted by Panship. For Fredyn, the results are a little further away from the model tests. With Panship, additional deterministic validations were carried out. These show reasonable similarity between the model test and simulations up to about 150 seconds into the run. Afterwards, the simulated position of the vessel in the waves is different from the experimental one, resulting in very different motions.

In [23], van Walree performs another validation of Panship in stern quartering seas. When it comes to the deterministic analysis of the vessel's time trace, van Walree found a way to eliminate the accumulation of small errors over time. This is done by calculating the forces on the hull based on the experimentally measured position of the vessel at each time step (instead of the actually calculated position). Afterwards Panship solves the equations of motions based on the simulated forces resulting from the experimental wave. This way, even if there are errors in the simulated forces at each time step, the x-y position of the vessel in the wave of the next time step will be identical in the simulation and the model test. The results of these deterministic validation shows remarkable resemblance between simulated and measured motions, however, the exact amplitude of motions seems hard to predict.

2.5 Bow Waves

Some of the model tests that are available for validations within this report include pressure and wave height measurements in the bow area. This opens the opportunity to validate not only the motions of the entire vessel, but also get a more detailed impression of the flow dynamics within the bow area. For the over all resulting forces and moments on the hull, the dynamics within this bow section are of great importance. This is due to the fact that, for most hull forms, high pressures and steep pressure gradients occur mostly in the bow area. On top of that, the highest radiated wave for steady forward speed is the bow wave, extending a high pressure area far above the still water wetted surface. Obviously, these high local pressures have a large impact on the steady state trim and sinkage as well as on the ship's motions in waves.

Unfortunately, especially for fast ships, the bow wave is almost always always a breaking wave with a considerable amount of spray. Both are effects that are (partly) caused by viscosity and include rotation in the flow pattern. Hence, these effects are not included correctly by potential flow simulations. It therefore is save to assume that the pressure distribution and the wave height in the bow area predicted by Panship will differ from measured values. Especially since in the semi linear version of Panship free surface boundary condition is linearized and the wave height and pressure distribution has to be estimated based

on the pressure on the still water free surface, there is a need understand the physics of a breaking bow wave.

In the past there have been published several papers analyzing breaking bow waves of slender ships. Through different approaches the researchers were in most cases focused in describing the shape and height of the bow wave, going into detail as far as possible. In many cases this lead to empirical formulations for wave height, steepness and position of the highest point.

In [10], Waniewski et al looked at bow waves produced by wedge shaped hulls in a towing tank and inclined plates in a flume. Both the plates and the wedges entered the water at half bow angles varying between 13 and 26 degrees. Amongst other things, Waniewskis paper leads to proposals for scaling for the height and x-position of the highest point of the contact line between bow wave and hull:

$$Z_b = C^W \cdot d \cdot F_n^{1.5} \cdot \theta$$

$$X_b = C^X \cdot F_n^{\frac{7}{3}} \cdot R_n^{-\frac{1}{3}} \cdot d$$

Here,C^W and C^X are unknown constants and θ represents the half bow angle and d is the draft of the model. It should be noted that in general, when considering the bow wave, for the calculation of the Froude number, the draft is used instead of the length of the towed body. These formulations can be used to give an empirical estimation of the dimensions of a bow wave. However, from Waniewski's plots we can see that these the accuracy that can be expected by these methods is not more than ± 20 to 30%.

In his two papers [12] and [14], Noblesse uses a series of measurements from earlier papers (amongst which also [10]) to develop his own expression for x and z position of the highest point of the bow wave of the ship. All measurements considered were made on wedge shaped hull forms. On top of the results from [10] and [20], Noblesse also looked into the actual values of the non dimensional constants C^W and C^X. Additionally, Noblesse adds some expressions to translate the dimensions of the wedge shaped hulls into actual hull shapes. This way he is able to improve his predictions for Wigley hulls.

$$Z_b = C^W \cdot d \cdot \frac{F_n^2}{1 + F_n} \cdot \frac{\tan\theta}{\cos\theta}$$

For the non dimensional constant C^W, Noblesse finds that for all wedge shaped hulls this value lies somewhere around 2.2. For the longitudinal position of the peak height the following expression is found:

$$X_b = C^X \cdot d \cdot \frac{F_n^2}{1 + F_n}$$

Where again for the wedge shaped hulls the value of C^X is constant around 1.1. To translate his findings about wedge shaped hulls into real hull forms, Noblesse introduces an effective draft $\overline{d}$ and an effective entrance angle $\overline{\theta}$ that can be calculated on the base of the actual hull shape considered.

Maxeiner [20] focused his dissertation on the breaking waves produced by a 2D + t wave, simulating simple bow-like shapes. This way he was able to very accurately visualize the wave profile at each time step. Like Waniewski, Maxeiner formulates a scaling rule for the contact line height, however, for a slightly wider range of simplified bow shapes. The resulting formulation is quite similar:

$$Z_b = C_W \cdot F_n^{1.33} \cdot d \cdot \left(\frac{a_b}{g}\right)^{0.15}$$

Here, a_b is the wave board acceleration of the 2D wave maker and can be translated into the half bow angle θ. Another parameter that Maxeiner described is the time to peak contact point height, which can

be translated into the longitudinal position at which the maximum bow wave height is reached in a 3D environment. However, in contrast to Waniewsky, Maxeiner concludes that (for breaking waves) the time to the contact line peak height is constant, independent of Froude number and Reynolds number at around 0.35 seconds.

In [18], a closer look is given to the stretching of the pressure in body and surface linear codes. While the wave height can be estimated based on the hydrodynamic pressure on the waterline, the pressure above the still water waterline can not be obtained from the potential flow equations (since these are located outside of the fluid domain). De Jong suggests to extend the hydrodynamic pressure evaluated at or near the still water free surface linearly as hydrostatic pressure up to the actual free surface. In a wave trough, the pressure above the actual free surface can be set to zero. This way there are no jumps in the pressure distribution, and at least for non-breaking waves this should give a reasonable approximation of the actual pressures in a wave.

3 Simulation Method

As explained in section 2, the general working principle of a 3D time domain manoeuvring and seakeeping simulation program is evaluating the sum of all forces acting on the vessel and based on that, solving the equations of motion in a discrete time domain. This section will give a short description of the mathematical methods validated during this project. Within that objective, an explanation will be given about the breakdown of the forces into components that are evaluated separately. An interpretation of the applied simplifications and an estimate of the resulting errors can be made. Afterwards, some attention is drawn towards the verification of input choices and the time and space discretization.

There exist many different approaches to predicting manoeuvring and seakeeping behaviour of ships. Even within the range of potential flow methods, every day new simulation methods are developed focusing on specific fields of application. The mathematical model validated in this report was developed with the goal of delivering a manoeuvring and seakeeping simulation tool for fast ships that is applicable for research and design purposes. It has been realized in a program called Panship. In this context, fast means between $F_n = 0.5$ and $F_n = 1.2$. In this range, depending on the hull shape, most vessels are in semi-planing mode. In order to be useful within the research and design trajectory of a vessel, it should be workable on a modern desktop environment by ship designers and naval architects. This implies that the program should deliver reliable results within a reasonable time frame. Excessive computational effort, as well as a specialist's knowledge about the mathematical models used should not be necessary.

To achieve this goal, a compromise between the physical accuracy and correctness of the simulation model on one hand and the necessary computational time on the other had to be found. In the end, a 3D panel method has been chosen in order to deal with arbitrary large amplitude motions as well as large forward speed effects. This model has been extended by adding empirical and semi empirical elements to improve the over all results. Special attention has been drawn to problems like a ventilated stern, that are typical for fast ships. The details and limitations of the mathematical method applied will be discussed in this section.

Due to the fact that the potential flow model does not account for all physical effects, these forces are a summation of several components.

- Hydrostatic forces on the hull
- Hydrodynamic forces on the hull
- Viscous drag on the hull in x and y direction
- Viscous damping
- Forces on appendages
- Propulsion

For each time step, all forces are calculated, summed up and used as input for the equations of motion. The rest of this section will give a short overview on what methods are used for the evaluation of the force components. For a more thorough explanation of the mathematical models used, one can refer to chapter 3 of de Jong's PhD thesis [24].

3.1 Definitions and Coordinate Systems

In order to understand the input and output described in this report correctly, a number of definitions have to be made. This section will focus on the definitions that are handled during this report as well as for the in and output of the simulations.

For a simulation program capable of running simulations of a ship in sailing in a straight line, as well as doing manoeuvring tests, at least two coordinate systems are necessary to conveniently describe the input and output data. In some cases, an earth fixed axes system makes interpreting the results easier, while for

other applications, a ship fixed system is to be preferred. For this reason, output is given in both coordinate systems. On top of that, for the geometrical input a ship reference frame is defined.

For the output of forces acting on the hull, a dimensional and non dimensional value is given. Since there are several options for making forces and moments non dimensional, a definition for the force and moment coefficients will be given.

Hull Reference Frame For the geometrical input of panel locations, as well as empirically formulated appendages and the center of gravity, a ship fixed reference frame is used with it's origin at the aft perpendicular and on the keel line of the vessel. This is indicated in figure 1. Here, the z-axis is pointing upwards, the x-axis is pointing from the stern towards the bow, and y is positive to port side of the vessel.

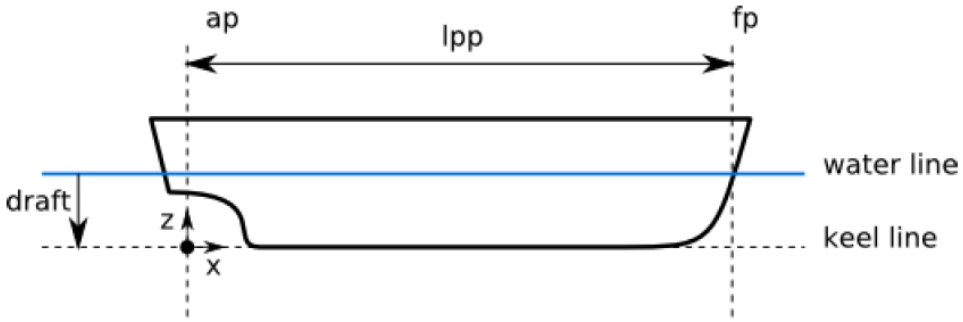

Figure 1: Reference frame for geometrical input. Source: *Panship User Manual Version 2.3*

Coordinate Systems The vessels motions during a simulation are presented in two coordinate systems. One ship fixed and one earth fixed. Like with the hull reference frame, both coordinate systems are a right handed Cartesian coordinate systems with the x-axis pointing from stern to bow. However, the origin of the ship fixed coordinate system coincides with the center of gravity of the vessel. The earth fixed system has it's origin on the still water free surface, and unless otherwise specified, at the start of the simulation the rotation between ship and earth fixed systems is zero.

Both coordinate systems are indicated in figure 2.

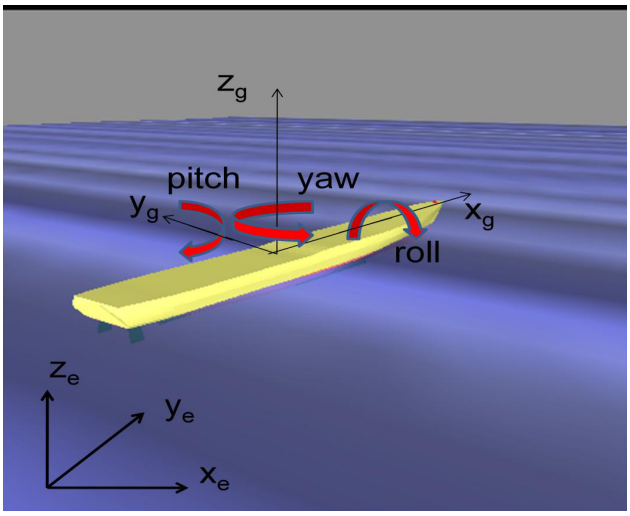

Figure 2: Coordinate systems and rotation directions. Source: *Panship User Manual Version 2.3*

Non Dimensional Values The forces and moments that are obtained during the simulation are presented within the ship fixed reference frame. In order to make simulation results comparable independent of the size of the actual vessel tested, non dimensional force and moment coefficients are given as well as values in Newton and Newtonmeters. The non dimensional coefficients are defined as follows:

Forces: $C_F = \frac{2F}{\rho U^2 S}$
Moments: $C_M = \frac{2M}{\rho U^2 S L}$

Where S is the wetted hull surface and L is the length between the perpendiculars.

3.2 Hydrostatic Forces

Hydrostatic pressures are caused by the water column resting on top of the location. As such, they can be evaluated at any location by:

$$p = \rho \cdot g \cdot h$$

Where h describes the local instantaneous distance to the water surface. Within the presented time domain simulation method, the hydrostatic pressures are calculated for every panel at every time step based on the calculated instantaneous position of the ship and height of the undisturbed wave.

3.3 Hydrodynamic Forces

The component of the forces on a vessel that is the most difficult to evaluate accurately are the hydrodynamic forces. These hydrodynamic forces are described by the Navier-Stokes equations. For three dimensional (compressible) flow this is a set of five differential equations describing the dynamics of a continuous fluid. Unfortunately, for most boundary conditions (including all conditions of interest for a seakeeping and manoeuvring simulation) there is no analytical solution for these equations. On top of that, a numerical solution for an entire vessel within a reasonable time and space discretization demands computational power that is orders of magnitudes higher than what is currently available even on the most powerful super computers.

3.3.1 Flow Simplifications

Within the described simulation method, the choice has been made to simplify the Navier-Stokes equations that govern the flow around the hull significantly in order to limit the computational resources that are necessary for a simulation. The resulting potential flow neglects all viscosity, rotation and compressibility in actual water flow, resulting in a set of equations that can be solved numerically with only a fraction of the computer power that otherwise would be necessary. This is (partly) due to the fact that the governing equations for potential flow only need to be evaluated on the domains boundaries. For example, for a 3D flow around a vessel, one only needs to calculate the streamlines along the hull and the free surface surrounding the hull. Potential flow describes the flow velocity as the gradient of a scalar function Ψ (the velocity potential).

$$\vec{v} = \nabla \Psi$$

Since the curl of a gradient is always zero, this automatically states that the flow is irrotational.

$$\nabla \times \nabla \Psi = \nabla \times \vec{v} = 0$$

One can proof that, in combination with incompressibility, this automatically implies an inviscid flow. With these simplifications, the governing Navier-Stokes equations reduce to the Bernoulli equation and the Laplace equation for the potential. In detail, this simplification is shown in appendix B. The resulting differential equation for the velocity potential is shown below:

$$\frac{p}{\rho} + \frac{\partial \Psi}{\partial t} + \frac{1}{2} \nabla \Psi \cdot \nabla \Psi - gz = C$$

$$\nabla^2 \Psi = 0$$

To solve these equations for the potential function $\Psi(x, y, z, t)$, there have been developed a large number of numerical techniques. The panel method used in the Panship code will be discussed briefly during this section.

For the purpose of simulating a vessel sailing, it is useful to decompose the potential Ψ into a sum of several components.

$$\Psi(x, y, z, t) = \Phi_w(x, y, z, t) + \Phi(x, y, z, t)$$

Here, Φ_w is the disturbance potential caused by incident waves and Φ is the disturbance potential caused by diffraction and radiation of waves from the submerged body. Previous to the simulation, the incident wave disturbance potential is known as a function of a given wave spectrum whereas the diffracted and radiated waves disturbance potential needs to be calculated during the simulation. Note that disturbance potential from several sources can be linearly superimposed for the final result.

Now, to summarize we have a flow that has the following three mayor simplifications with respect to the actual water flow around a hull: incompressibility, irrotationality and inviscidity. To give an idea about how this theoretical flow looks like, figure 3 shows the potential flow around a cylinder and around acorner. The dark blue lines represent stream lines and the lighter blue lines represent equipotential lines that are perpendicular to the flowdirection at all times.

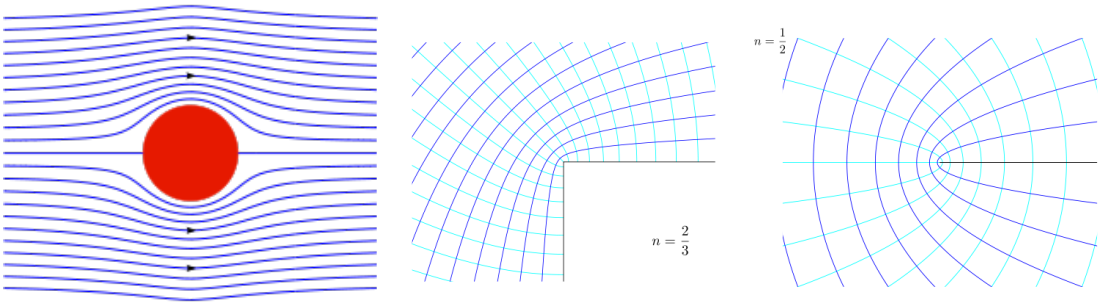

(a) Cylinder (b) Corner (c) Plate end

Figure 3: Potential flow around different geometries. Source: *http://en.wikipedia.org/wiki/Potential_flow*

Obviously, these flows differ significantly from what one would expect to see in a water flow. There is no flow separation, no vortices and no boundary layer at all. The particles adjacent to obstacles simply follow the obstacles geometry, even if that means a 180 degree turn as shown in 3c. This means that around sharp edges there are going to be extremely low local pressure peaks in places where normally flow separation would take place. On top of that, for any fully submerged body (like the cylinder in figure 3a) the total potential flow resistance sums up to zero. This is due to the fact that without viscosity and flow separation, the streamlines meet again at the trailing stagnation point, creating an equally high pressure around both stagnation points. The only energy that might be dissipated from a body and thus create resistance are radiated surface waves on the boundary of the fluid domain. Obviously this is only the case for surface piercing objects or objects close to a free surface.

3.3.2 Transient Green Function

The Green function is a mathematical function describing disturbance potential as a function of time and and space while satisfying all boundary conditions for the free surface and for domain sides and bottom at

plus/minus infinity as well as the Laplace equation governing the potential flow. It specifies the influence $G(p, q, t-\tau)$ of a singularity of unit strength (located at point $q(\xi, \eta, \zeta)$) on the disturbance potential Ψ at any position $p(x_0, y_0, z_0)$ within the fluid domain at any time $t - \tau$ between now and the start of the simulation. In case of multiple singularities, the resulting disturbance potential at point $q(\xi, \eta, \zeta)$ is a summation of all $G(p, q, t - \tau)$ terms from all singularities.

$$G(p, q, t - \tau) = G^0 + G^f$$
$$= \frac{1}{R} - \frac{1}{R_0} + 2\int_0^{\inf} [1 - cos\left(\sqrt{gk}(t - \tau)\right)]e^{k(z_0+\zeta)} J_0(kR)dk$$
$$for\ p \neq q, t - \tau \leq 0$$

Here, k symbolizes the wave number, G^0 is the source and biplane part and G^f is the free surface memory part of the Green function. J_0 is the Bessel function of order zero. Further more, R describes the distance between the singularity q and the evaluated point p, given by:

$$R = \sqrt{(x_0 - \xi)^2 + (y_0 - \eta)^2 + (z_0 - \zeta)^2}$$

and R_0 is defined by:

$$R = \sqrt{(x_0 - \xi)^2 + (y_0 - \eta)^2 + (z_0 + \zeta)^2}$$

Now, using this Green function, when a condition for the disturbance potential is given at location p the necessary strength of a singularity at q can be calculated in the fashion of:

$$\Phi(p, t) = source\ strength \cdot G(p, q, t - \tau)$$

From here, it is easy to see that for multiple singularities this results in a solvable set of linear equations with an equal amount of unknown source strengths and boundary conditions for the disturbance potential. Note however, that every G term on itself contains a time integral that has to be solved numerically in the discretised time. Hence, the computational effort of this system of equations is still very considerable.

3.3.3 Spacial Discretisation

A second step that is necessary is the spacial discretisation. In the case of an arbitrarily shaped submerged body (like a vessel's hull) as a fluid domain boundary, the equations governing potential flow can not be solved in a continuous, analytical way. Instead, a spacial discretisation of said domain boundary is necessary. Since the potential flow equations only need to be solved on the boundaries of the fluid domain, the hull surface will be divided into a large number of flat panels. Each panel has to be chosen sufficiently small so that the local curvature of the hull can be neglected without changing the outcome of the simulation significantly. This spacial discretisation for potential flow is commonly referred to as panel method.

Technically, when such a panel method is used, the vessel's hull is not taken as a boundary of the fluid domain as the space enclosed by the hull is filled with fluid up to the free surface at $z = 0$. Then, for each panel, zero normal velocity is set: $\frac{\partial \Psi}{\partial n} = 0$. As described in section 3.3.2, to enforce such a boundary condition, for each panel a singularity within the fluid domain is necessary. Physically interpreted, such a singularity can be seen as a sink, source or dipole where fluid can be generated or removed in such a way that the flow across the panel is kept zero at all time. Mathematically interpreted, such a singularity introduces a jump in potential and (only in case of a source or a sink) a jump in the velocity component perpendicular to the panel's surface. The magnitude of these jumps define the strength of singularity and form the unknowns in the resulting linear system of equations.

Here, as long as the lift forces created by a body are small and can be neglected, source/sink singularities are sufficient. For the largest part of the hull, only source/sink panels are used. However, when the Kutta condition is used to solve the transom flow, a wake sheet of dipole panels, as well as a few rows of dipole panels near the transom edge are necessary. For other lifting surfaces like rudders and fins, wake sheets with dipole panels are always necessary. Physically spoken, the dipole panels introduce rotation to the flow. That rotation is necessary for the development of any lift forces.

Note that, since the boundary conditions are only fulfilled on average over the entire panel, it is important to make the panels sufficiently small. On the other side, the more panels there are, the higher the demand for computational power and computer memory. Finding a good balance for the number of panels will be part of the numerical verification of the spacial discretisation.

3.3.4 Linearisations

For a manoeuvring vessel's hull, as well as a free surface with arbitrarily high waves, boundary conditions apply on the previously unknown instantaneous location of the hull/free surface. Since this location will vary over time and is a priori unknown, these have to be nonlinear boundary conditions. This implies that the system of equations described in 3.3.2 has to be solved at every time step, with new boundary conditions.

One way to significantly reduce the computational effort necessary for a simulation is to assume small wave heights and small deviations from the straight course and constant speed of the vessel. Then, the boundary conditions are applied on the expected average locations of free surface and hull position instead of the actual instantaneous locations. The hydrodynamic forces in the simulation are calculated based on a vessel sailing a straight line at constant speed and waves are only simulated as pressure fluctuations within a static fluid domain. In this case, Green functions have to be calculated only once, prior to the time domain simulation.

Free Surface Boundary Condition For the free surface, two conditions need to be fulfilled. First, a kinematic condition is necessary, that ensures that the vertical velocity of water particles on the free surface is equal to the vertical velocity of the free surface itself. Secondly, a dynamic condition ensuring the pressure on the free surface is equal to the atmospheric pressure (set to zero). When linearised, this translates to the vertical velocity and the pressure at $z = 0$ being set to zero. Further more, all higher order terms from the Bernoulli equation are neglected, assuming small wave steepness.

$$\frac{\partial \eta}{\partial t} = \frac{\partial z_0}{\partial t}$$
$$\frac{\partial \Psi}{\partial t} + g\eta = 0$$

Here, $\eta(x_0, y_0, t)$is the instantaneous free surface elevation at (x_0, y_0) and z_0 is the vertical displacement of a water particle. Since we are looking at the linearised free surface, these equations have to hold for $z_0 = 0$ instead of $z_0 = \eta$.

Body Surface Boundary Condition On the hull's surface (as well as on appendages), the normal flow has to be zero. This means that the local flow velocity has to be equal to the local velocity of the considered surface. This results in the following boundary condition:

$$\dot{\vec{\delta}}_0 \cdot \vec{n} = \frac{\partial \Phi}{\partial n} + \frac{\partial \Phi_w}{\partial n}$$

Here, Φ and Φ_w are respectively the disturbance and wave potential. $\vec{\delta}$ refers to the local instantaneous body velocity. For the linearised case, this condition has to be applied on the hull's position when it is moving at the average speed, trim and sinkage. The linearisation of this boundary condition is worked out by de Jong in [24].

3.4 Viscous effects

Due to the fact that the hydrodynamic forces are calculated based on non viscous potential flow, additional force terms have to be applied to account for the viscosity of water. This includes additional drag terms caused by flat plate resistance and flow separation as well as lifting forces. Here, especially accurately modelling the effects of flow separation is hard to accomplish and, as the local flow over the hull's is strongly dependent on flow separation, also viscous drag can be hard to estimate.

This is one point where the specialisation for fast vessels is of significant interest as flow separation, and wether it's forces can be neglected or not very strongly depend on the considered submerged geometry and even the degree of freedom that is of interest. For a full time domain simulation for manoeuvring and seakeeping, motions in all six degrees of freedom have to be taken into account. For fast vessels, a slender, approximately wig shaped hull with a dry stern can be considered as typical for planing and semi planing vessels.

3.4.1 Viscous Drag

Hulls that are optimised for either planing or semi planing usually approximate a wig shape quite well and have a cut off stern that is dry when sailing at design conditions. Such a geometry generally causes an absolute minimum amount of flow separation when sailing strait forward without drift angle. Only around bilge keels or hard chines that are not completely aligned with the flow direction, some small areas of flow separation will be found.

However, a different scenario can be found when a drift angle or a yaw rotation are applied. In that case a (local) transverse component of the flow will appear that encounters the significantly less streamlined transverse cross section of the hull. A significant amount of turbulence and separated flow will develop near the trailing hull - waterline intersection, increasing the local crossflow drag significantly. For that reason two different empirical formulations are used for viscous drag in longitudinal and in transverse direction.

For viscous resistance on a flat plate, the ITTC in 1957 formulated an empirical approach. As long as no significant amount of flow separation takes place, this approach gives a good representation of the added viscous resistance.

$$R_V = \frac{1}{2}\rho u^2 S C_f \cdot (1+k)$$

$$C_f = \frac{0.075}{(log_{10}(R_n)-2)^2}$$

Here, u is the forward speed, S is the wetted surface area, k is a form factor for the hull and R_n is the Reynolds number of the geometry considered. This formulation is applied for the longitudinal viscous drag on the hull, as well as all appendages. As soon as a drift angle is introduced, additional effects like flow separation and a transverse drag coefficient have to be taken into account. This is done by implementing an empirical crossflow drag method as discussed in further detail by Faltinson in chapter 10 of [11]. Generally, the transverse viscous force is assumed to be the sum of the transverse force on all cross section. To correct for large longitudinal velocities, C_D is made time dependent in a $2D+t$ approach.

$$F_Y = -\frac{1}{2}\rho \int_L [C_D(x)|\dot{\eta_2} + x\dot{\eta_6}| \cdot (\dot{\eta_2} + x\dot{\eta_6})\, A(x)]dx$$

Here, $A(x)$ is the local cross sectional area, the term $\dot{\eta_2} + x\dot{\eta_6}$ describes the local transverse velocity with η_2 being the sway position and η_6 the yaw rotation. Now, all that is left to calculate is the value of the drag coefficient C_D of the local cross section of the hull. C_D values are obtained based on curve fittings of systematical measurements on different cross sectional shapes.

3.4.2 Lifting Forces

Another effect that is caused by the viscous flow is lift created on the hull and appendages. For surfaces modelled with panels, the potential flow solution has to be enhanced in order to obtain lifting forces. Within plain potential flow, the trailing stagnation point would not lie on the trailing edge. This is indicated in figure 4a. The flow around the sharp trailing edge would locally cause infinitely high flow velocities. It is only due to the viscosity that flow around sharp corners is prevented, the trailing stagnation point is moved towards the trailing edge of the lifting surface and a vortex around the lifting surface is created.

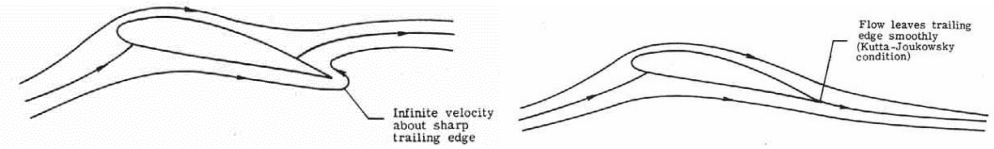

(a) Potential flow (b) Potential flow with Kutta condition

Figure 4: Potential flow around an inclined lifting surface. Source: *http://secretofflight.wordpress.com/incorrect-theories/*

Now, in section 3.3.1 it was mentioned that potential flow implicates irrotational flow, which is equivalent to zero vorticity. Technically this is not accurate as only the derivative of the vorticity has to be zero. Hence, jumps in the vorticity are still possible and are used to estimate lifting forces even within potential flow simulations. To do this, the so called Kutta condition is applied at the trailing edge. This is an additional boundary condition that prescribes equal flow velocities just above and below the trailing edge and hence enforces flow separation at the trailing edge. This is indicated in figure 4b. However, to apply this condition, a sheet of (infinitely thin) panels is necessary in the wake of the trailing edge. The wakesheet is discretised by means of doublet panels. The Kutta condition has to be applied in the wake of rudders and skegs that are modelled as a panel surface, but also at a ventilated transom to prevent unrealistic flow velocities about the transom edge. This also enables the calculation of lift forces around the hull in case of nonzero drift angles.

For empirically modelled lifting surfaces, lift and drag coefficients are calculated based on the geometry of the appendage. The lift forces are then calculated by:

$$F_L = -\frac{1}{2}\rho C_L v_i^2 A(x)$$

Where A is the area of the lifting surface and v_i is the inflow velocity. Depending on the aspect ratio, the method for calculating C_L is obtained with the help of lifting line theory or low aspect ratio theory.

3.4.3 Transom Flow

As already shortly mentioned in the previous paragraph, in potential flow, attention has to be given to the handling of ventilated sterns of fast vessels. If the hull form including stern would simply be modelled with panels, the flow would follow the sharp edge at the transom and create locally very high velocities and pressure gradients. Two methods for implementing a ventilated stern will be discussed within this section.

First, a wake sheet can be applied at the sharp stern edge, enforcing the Kutta condition at this position. This way, a pressure condition can be applied to reduced the pressure gradually to atmospheric level as the flow approaches the stern edge. To make this possible, combined source and doublet panels are necessary in the aft part of the hull and a wakesheet of doublet panels follows the transom edge. Lifting forces that are created by the hull in case of nonzero drift angles will be included in the hydrodynamic solution of the flow.

Second, an empirical correction to the pressure near the stern can be applied. When this approach is used, over the length a (as indicated in figure 5) the calculated total pressure is reduced by an empirically determined factor, resulting in the shown pressure distribution. This approach has been developed by Garme in [13]. In this case, lifting forces acting on the hull have to be calculated separately with the use of a lift

coefficient as described in section 3.4.2.

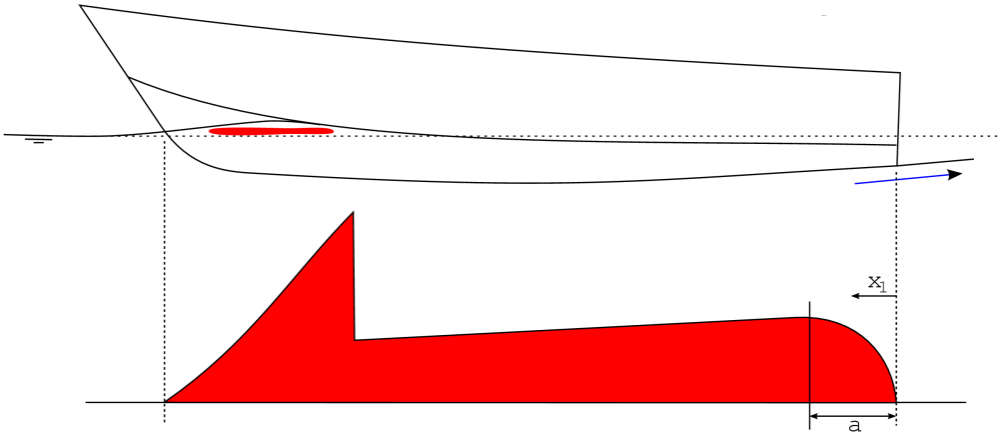

Figure 5: Pressure distribution along the hull. *Source: Panship User Manual Version 2.3*

In any case, for smaller Froude numbers, a simple empirical formulation for a partly wetted stern will be used.

3.4.4 Viscous Damping

Viscous damping is generally a significant term for roll motions only. However, for slender lightweight vessels viscous damping also becomes significant in the vertical plane (heave and pitch motions). For these motions, flow separation around the bilge area causes relatively large forces and moments. The magnitude of the damping force coefficient depends on a large number of variables. Amongst them are the oscillation frequency, Froude number and section shape. For Panship, the coefficient used only depends on the local section type.

$$F_Z V = \frac{1}{2}\rho V_r |V_r| S C_D$$

Here, V_r is the vertical velocity of the local section to the local flow. S is the horizontal projection of the section area. The drag coefficient C_D is the same as used for the crossflow drag described in 3.4.1.

Viscous roll damping is evaluated by:

$$K = b_{44l} p + b_{44q} p|p|$$

Where b_{44l} andb_{44q} are roll damping coefficients obtained from experimental data and p is the angular roll velocity.

3.5 Appendages

There are several reasons that create the need to model appendages separately and exclude them from the hydrodynamic solution. First of all, appendages, in combination with the hull create complicated geometries with a large number of sharp edges and wake sheets that intercept the hull's surface. This will in many cases not lead to reasonable results within the applied potential flow model. Secondly, during a design process, it is often desirable to try a large number of different appendages on one hull and examine the effect on the manoeuvring capabilities of a vessel. This is a lot easier if only a few geometrical quantities like chord length and aspect ratio need to be changed each time instead of an entire panel distribution on for example a rudder.

If Appendages are not modelled as part of the potential flow model, the forces acting on the appendages are not part of the hydrodynamic solution. In this case these lift and drag forces have to be modelled

separately as described in the sections 3.4.1 and 3.4.2. A number of different appendages can be added to better fit the real vessel:

- rudders
- trim flap
- bilge keels
- propeller shafts
- propellers
- waterjets

Controlled Surfaces For simulations in free sailing conditions, rudders and fins, but also trim flaps have to be controllable during the run. Regardless whether the considered lifting surface is modelled empirically or as part of the hydrodynamic solution, this can be done by creating an autopilot that specifies rotations, maximum rotation speed and angle as a function the vessel's motions. For each surface a separate autopilot can be defined.

Propulsor In case of a propulsor it is not efficient to model each lifting surface and it's motions relative to the vessels hull separately. Instead well validated empirical model can be used to estimate a propulsion force as a function of inflow velocity and rate of revolution.

As a propulsor, waterjets and propellers can be added to the model. Generally, the propulsor is modelled simply as a longitudinal force acting at a specified location. Effects of the propulsor on the flow underneath the hull are neglected. This means that also any form of propeller-hull interaction is neglected.

For a propeller, Wageningen B-series polynomials are used to determine thrust and torque coefficients based on the nondimensional advance ration J. This way, the calculated torque can be used to give an estimate of the required power. The incoming velocity that is used is calculated as follows:

$$V_a = u(1 - w_p) - \dot{\xi}_p$$

Here, u is the ship's velocity in longitudinal direction w_p is the wake fraction and ξ_p is the longitudinal wave induced velocity.

For waterjets, the propulsion force is based on the flow rate through the nozzle and the nozzle diameter. With a simple empirical formulation based on model tests, these quantities can be determined. Like rudders, waterjets can be actively steered using an autopilot. In this case the steering force is obtained using thrust deflection.

3.6 Numerical Verification

The goal of this report is to validate time domain potential flow simulations (amongst others) by reproducing model tests. However, before the simulation results are reliable, a numerical validation study has to be carried out. There are several parameters that need to be set and a good knowledge about their effects on simulation results is necessary. Next to the time and space discretisation, also the number of memory steps that has to be taken into account, as well as a switch on period have to be verified. Another aspect that arises from the body linear boundary condition is that the panel distribution and the trim and sinkage used in the geometry input should accurately represent the dynamic state at the simulation speed.

3.6.1 Panel Size and Distribution

One obvious step of simplification that has to be taken in order to get from reality to a numerically solvable simulation is the discretisation in space. As mentioned before, for potential flow it is sufficient to discretise only the boundaries of the fluid domain, and due to the Green functions this can be further reduced to only the hull and appendage surfaces. Within the panel method these surfaces are divided into a large number of so called 'panels', quadrilateral pieces of surface without any curvature. Obviously, by doing this the 3D, curved hull shape has to be changed slightly. For verification, it is of course necessary to make sure that obtained results are actually a consequence of the hull's geometry, and not a result of the spacial discretisation itself.

For the two hull shapes discussed during this report, a number of different panel distributions and sizes have been tested to make sure that the differences between them are small. Thereby, the total number of panels under the waterline was varied roughly between 1100 and 1900. Further more, the effects of aspects like wake sheets for the transom flow and skegs modelled with Panels on the over all results were investigated. For the m8325 87 meter patrol boat hull, an additional aspect were the two hard chines in the hull shape (as can be seen in figure 10). Putting a panel edge on each chine was tested against a simpler, yet geometrically less accurate distribution.

Another point of interest when it comes to the panel distribution is a consequence of the body linearity of the hydrodynamical solution. Since the flow is calculated at all times around the initial submerged geometry, dynamic effects on trim and sinkage are not included. However, for fast ships in free sailing conditions the static trim and sinkage may differ significantly from the situation at rest. This has been dealt with by creating separate panel files for each speed that has been tested. The trim and sinkage for the panel files was taken from the model tests or in an iterative procedure from Panship simulations with the initial zero speed submerged geometry.

3.6.2 Time Step

Next to the spacial discretisation, there is also the time discretisation. This holds, that results are calculated and available only for certain points in time. The Green function values of the hydrodynamic solution are assumed to be constant during one time step. Some attention has to be drawn to the size of the time steps chosen. Setting the time step too large might lead to inaccurate results or even numerical instabilities. Too small time steps lead to an excessive amount of computer resources necessary for the simulation.

Of course, the ideal time step depends on several factors and simulation parameters. For example, a simulation with a free sailing vessel in irregular waves will need a smaller time step than a captive simulation on calm water. Nevertheless, to get an approximate idea about the necessary order of magnitude of the time step, one simulation was carried out with a number of time steps between 0.05 and 0.8 seconds. When made non dimensional with the progression of panel lengths at the simulation speed this translates to 0.8 to 11 panel length progressions per time step. For reasons of simplicity a captive simulation of the m8325 hull has been chosen at a speed of 21.6 m/s and a yaw angle of 5 degrees. The resulting forces on the hull in three degrees of freedom are shown in figure 6.

Apparently, the changes between the different time steps are small for not too large time steps. Only for the largest time step considered, a significant deviance of about 20% can be observed. However, the computational time increases drastically, especially for the two shortest time steps. For the given, simple captive simulation, these can not be run on a normal windows pc anymore due to a restriction that windows enforces on the amount of memory that one program may use. Of course, using different simulation parameters (like a smaller amount of panels or memory time steps) might solve this issue. However, as Panship is targeted to be used on a normal desktop environment, for this case these small time steps should not be considered as practically applicable.

Looking at the calculated forces resulting as a function of the time step, the conclusion is that up until a time step of 0.4 seconds the differences are very small. After that, at 0.8 seconds, uncertainty seems to

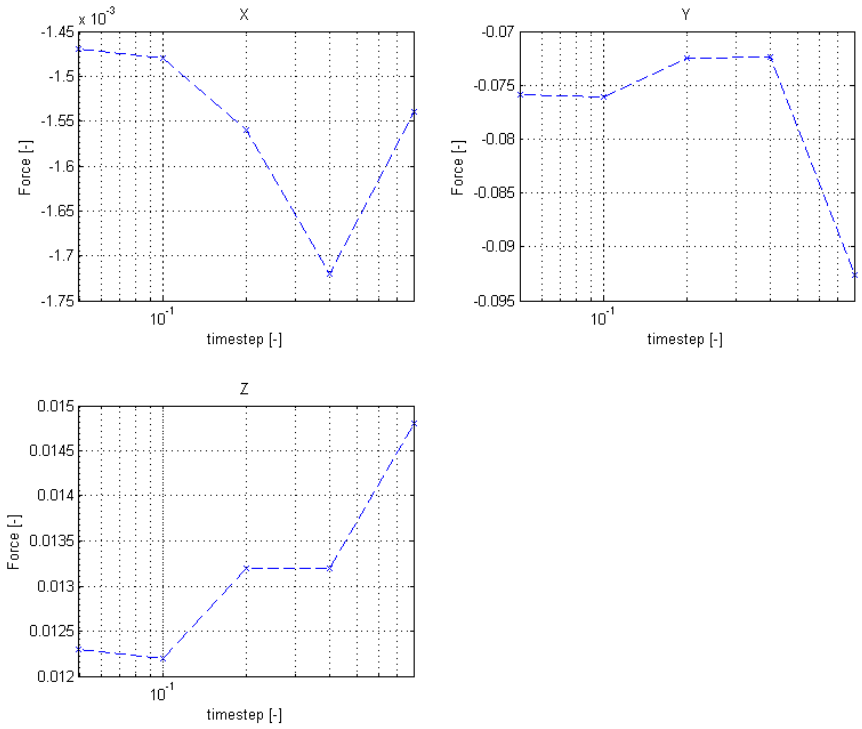

Figure 6: Non dimensional forces using different time steps

increase. Therefore, for the simulations evaluated in this report, a maximum time step of 0.4 seconds should be considered. Note that in case of free sailing simulations there is a feedback loop between calculated forces and the pressure on the hull and it's location. To prevent oscillations within this system, it can be necessary to further reduce the time step.

3.6.3 Other Numerical Aspects

Simulation Time Next to the discretization in time and space, there are a number of numerical parameters that influence the memory requirement and calculation time, as well as the result of a simulation. One of them is the total number of time steps, or in other words the time span that is simulated. For steady tests without waves, this simulated time span has to be at least as long as it takes for the flow to become stationary. How large this time span is depends on several parameters like for example the vessel's speed, the size of the time step, the number of history time steps, the panel distribution and hull shape. In figure 7, the time trace of the force in x-direction is shown for the simulation discussed in section 3.6.2 with a 0.2 seconds time step. As one can see, in this case 30 seconds were simulated and the simulation reached a steady state after around 10 seconds. For tests in (irregular) waves, a simulation time should be chosen so that a sufficient number of wave encounters are included, but at least the time it takes for a similar free sailing simulation without waves to get to a stationary condition.

Switch on Period Of course, when looking at the time traces in figure 7, results prior to 10 seconds into the simulation should not be taken into account when evaluating the simulation. These extreme fluctuations can be explained by the impulsive change in velocity at the start of the simulation as well as by the fact that initially no free surface memory effects are present. Only after the simulation has passed some time, the memory effects are obtained and slowly develop a steady state solution. For this reason, Panship offers a possibility to define a number of time steps at the start of the simulation that will be skipped for the

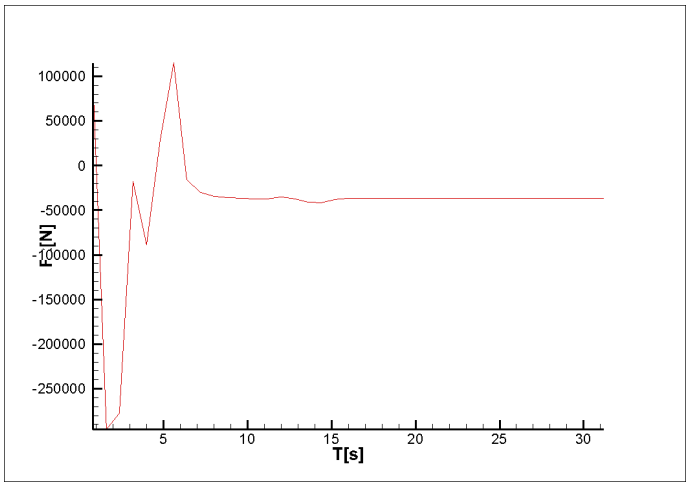

Figure 7: Time trace of x forces

statistical analysis of the output signals.

Another aspect of the switch on period is encountered when deterministic free sailing simulations in waves are run. In that case, a wave train that has been measured during the model test is copied into the simulation to compare model test and simulation results. However, since model test measurements start only after the carriage is at full speed, in the fully developed sea state, so should the calculations. Unfortunately, this is not possible due to the initially missing memory terms, first movements of the vessel will be calculated inaccurate, leading to an inaccurate position of the vessel in the waves, leading to even larger mistakes. To cope with this problem, a couple of options have been tested and the results have been compared. In detail, they will be described in section 5.2.2.

History Terms The Green function defines the influence of a source anywhere in the fluid at any time step on the potential at another point. Obviously, the influence of one source on the the potential is time dependent (think of surface waves), and in a simulation of a vessel sailing at an arbitrary forward speed even the location of the source will be time dependent. Now, technically during a simulation this means that for the full solution at the current time step, an integral has to be taken from the start of the simulation right until the current time step. This way, one can be sure that even waves and fluid disturbances from the very first time step are taken into account.

However, solving those time integrals, especially during long simulation runs, can be very time and computer memory consuming. Moreover, for ships running in an approximately straight line, it is very unlikely that flow disturbances from a long time ago have a significant effect on the current flow around the vessel. For this reason, Panship offers the possibility to cut off the memory integral after a certain amount of time steps. In [24] a minimum time that should be taken into account is mentioned as the time that it takes for the vessel to progress one ship's length. This is a logical choice as an absolute minimum, since this way at least the effects of the bow panels from when they were at the current stern location are taken into account. However, radiated waves from earlier bow positions that might have progressed to the current stern location are not taken into account. To get an idea of the effect of cutting of the memory effects, figure 8 shows the resulting forces in z direction in a captive test on hull m8325 at $21.6 m/s$. Note that in this case it takes 4 seconds for the vessel to pass it's own length of about 87 meters. Since the time step is set to 0.2 seconds, this is about 20 time steps.

Apparently, as soon as the number of history time steps drops below 25, the simulation outcome is hugely influenced. However, even the difference between 25 and 50 time steps is still almost 10%. This means that the number of history steps taken into account is indeed a very significant parameter for the simulation. In

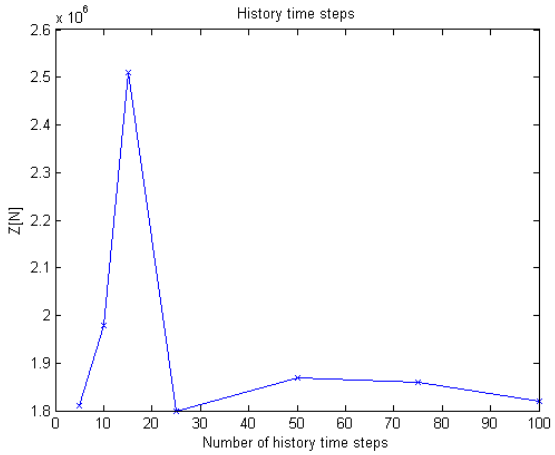

Figure 8: Effect of history time steps on the total z-force

order to be sure about the results, significantly more than the time it takes for the vessel to progress one ship's length should be taken into account.

	Magnitude	Unit
L_{PP}	86.9	m
L_{WL}	86.9	m
B	12.36	m
T_F	3.53	m
T_A	3.53	m
C_b	0.52	-
∇	1970	m^3
Δ	2020	t
S	1127	m^2

Table 1: Main particulars m8325.

4 Captive Steady Tests

This section will refer to all captive simulations carried out within the scope of this project. Part of them were validated by model tests carried out by Marin in 2005. Within the scope of validating the behaviour of a vessel in stern quartering seas, captive tests can be helpful to isolate certain components of the forces that act on the hull. During the considered model tests, the vessel sailed at a known and constant trim, sinkage and speed on calm water. This way, the hydrostatic forces, as well as linearised instantaneous location of the vessel that is used for the hydrodynamic solution in the simulation, can be assumed to be accurate, isolating the hydrodynamic solution and viscous forces. By looking at several drift angles, a good validation can be made of those force components for different orientations of the vessel.

By introducing drift angles in the steady captive tests, the submerged geometry of the vessel is changed in a way that (in viscous flow) more flow separation and lift forces occur around the hull and it's appendages. Since these physical aspects of the flow are not included in the potential flow model, empirical and semi empirical formulations like the Kutta condition and the crossflow drag method are used to estimate their effects on the hydrodynamic forces. Hence, the simulations including drift angles can be used to validate the forces and moments calculated by these formulations.

First, tests on a concept hull m8325 for a patrol boat of 87 meters will be discussed, afterwards the same tests will be carried out on the parent hull form of the systematic FDS series. Captive tests will be carried out with drift variations on calm water. That way, some important manoeuvring coefficients and coupling between motions can be validated.

4.1 M8325

The hull shape considered is a concept hull for a patrol boat. As this, it is a planing hull with a transom stern that (in most operating conditions) will be dry. The design speed was chosen at 42 knots which corresponds the a Froude number of 0.74, well into the semi planing speed range. In table 1, an overview over the main particulars of the hull is given.

From figure 9, a couple of characteristics can be pointed out that need to be taken into account while analysing the results of simulations and model tests. First of all, the vessel is propelled by a twin waterjet configuration. As Bulten states in [17] this might lead to significant vertical forces that influence trim and sinkage of the hull during model tests. In the simulation, only a horizontal thrust force is modelled. Then, the model is fitted with stabilising fins. Since these are calm water tests, these fins were not actively steered during the model tests. However, some attention should be drawn towards the correct modelling of these fins. The same goes for the skeg underneath the stern section of the hull and the trim flap. When it comes to the hull itself, there are two hard chines starting just aft of the bow section. These chines will certainly have an influence on transverse forces and might cause flow separation that can not be modelled with potential

flow. Moreover, when the panel distribution is chosen, hard chines can only be modelled as such if they lie on panel edges over their entire length.

4.1.1 Model Tests

The model tests on the m8325 hull were carried out in 2005 within the scope of a research project. Next to the PMM tests discussed in this report, also manoeuvring and powering tests were carried out. For this purpose a couple of concept hull forms were tested at Marin. Since the m8325 hull was the concept that was not further developed, the model tests results could be made available for purposes of validating Panship. For this project, part of the PMM tests will be used.

(a) Bow section, two hard chines.

(b) Side view, stabilizing fins and a skeg.

(c) Propulsion configuration, two waterjets

Figure 9: Model characteristics of m8325.

The model that was used had a scale of 1:18 and was fitted with a twin water jet configuration and two stabilizing fins, as can be seen in figure 9. The PMM tests were all carried out for a trim and sinkage condition corresponding to design conditions at 42 knots of speed. This results in a positive trim angle of 0.75 degrees and an average draft of 3.47 meters in full scale. During the tests, the vessel was captive in all 6 degrees of freedom. The tests were run approximately at self propulsion point, but without measuring the actual propulsion forces. A table of all test conditions that are going to be used during this report is given in 2.

4.1.2 Making Results Comparable

When it comes to sign conventions and coordinate systems, as well as definitions of nondimensional coefficients, there are some significant differences between the simulation output and the model test reports. For this reason, some effort has to be put into making the results of both comparable. First, the coordinate systems used during simulations and model tests differ. As described in 3.1 the simulation output is given in amongst others a ship fixed coordinate system. However, in case of a fixed trim, these rotations are

v[kn]	Fn[-]	drift angle[°]
20.6	0.36	-10, -5, -2.5, 0, 2.5, 5, 10
28.9	0.51	-10, -5, -2.5, 0, 2.5, 5, 10
42	0.74	-10, -5, -2.5, 0, 2.5, 5, 10

Table 2: Test matrix of captive tests.

already included in the geometry input, causing the ship fixed system to behave like a ship centred system with it's origin at the LCG, positive z always pointing straight upwards and positive x always pointing from stern to bow. In contrast to that, the model test results are given in a real ship fixed system, creating a rotation between both coordinate systems of exactly the prescribed trim angles. Moreover, the model test results are given in the propulsion and steering system that has the positive z-direction pointing downwards, introducing another 180 degree shift in Φ. A definition of the nondimensionised force coefficients has to be found that can be used for all output data.

Nondimensionalising Forces and moments As described in the model tests report, their results are made non-dimensional using the following formulas:

$$X' = \frac{X}{\frac{1}{2}\rho V_S^2 L_{pp} T} \qquad Y' = \frac{Y}{\frac{1}{2}\rho V_S^2 L_{pp} T} \qquad Z' = \frac{Z}{\frac{1}{2}\rho V_S^2 L_{pp} B}$$

$$K' = \frac{K}{\frac{1}{2}\rho V_S^2 L_{pp} T^2} \quad M' = \frac{M}{\frac{1}{2}\rho V_S^2 L_{pp} B^2} \quad N' = \frac{N}{\frac{1}{2}\rho V_S^2 L_{pp} T^2}$$

As Panship offers dimensional as well as nondimensional forces as output, the above equations will be used to nondimensionalise the simulation output by hand.

Axis Systems To transform the axis system used in the simulations to the one used for the model tests, the sign of the z-axis and y-axis, as well as pitch and yaw rotations had to be changed. Further more, to get from the earth fixed to the ship fixed coordinate system, a transformation matrix taking care of the ship's motions has to be taken into account:

$$T = \begin{bmatrix} cos\psi cos\theta & sin\psi cos\theta & -sin\theta \\ -sin\psi sin\phi + cos\psi sin\theta sin\phi & cos\psi cos\phi + sin\psi sin\theta sin\phi & cos\theta sin\phi \\ sin\psi sin\phi + cos\psi sin\theta cos\phi & -cos\psi sin\phi + sin\psi sin\theta cos\phi & cos\theta cos\phi \end{bmatrix}$$

However, since ψ is always zero between the given ship-fixed and a ship-centered coordinate system, this matrix can be simplified to:

$$T = \begin{bmatrix} cos\theta & 0 & -sin\theta \\ sin\theta sin\phi & cos\phi & cos\theta sin\phi \\ sin\theta cos\phi & -sin\phi & cos\theta cos\phi \end{bmatrix}$$

Force Measurements During the model tests, the measurements of forces and moments were zeroed while the vessel is at rest without propulsion, taking only hydrodynamic effects into account. However, at the applied trim and sinkage (taken from free sailing tests at 42 knots), there is a significant difference between buoyancy force and the mass of the vessel. In the simulation output, the sum of all z-forces is given, including buoyancy and gravity. This means that the simulation results have to be corrected for the difference between buoyancy and gravity force at the applied trim and sinkage. This has to be done taking into account that the simulation output is given in the ship fixed coordinate system, where the z-axis is not necessarily exactly vertical.

Another aspect is the (in direction and strength) unknown propulsion force. The tests were carried out near the self propulsion point, but the actual thrust force was not measured. The only thing that is known is that for all captive tests at the same speed, the same rate of revolution was kept for the waterjets. This creates an unknown component of the X and Z forces that cannot accurately be reproduced by the simulations.

However, a few assumptions can be made to at least be able take some usable conclusions from the simulated X and Z forces, as well as the pitching moment. The simulations use an empirical model to calculate the waterjet propulsion forces. Just like the open water model used for propellers, this model takes into account the inflow velocity at the intake of the waterjet. Assuming that this model is approximately correct (errors are small compared to the total propulsion force), the the difference between the propulsion forces in the model tests and in the simulations will be constant as long as the rate of revolution is kept constant. This way, the X forces can be compared up to a constant. When further assuming that the z-component of the propulsion force is approximately constant during all model tests considered (differences in propulsion Z forces are small compared to the hydrodynamic Z forces), one can also compare the pitching moment up to a constant.

For the Z force, Bulten in [17] gives an indication about the magnitude of the z-component of waterjet propulsion compared to the propulsion force. In extreme cases this can go up to 20% of the propulsion force. However, in normal operating conditions as present during the considered tests, this percentage drops to below 5%. For the model considered, at the highest speed, comparing the values of the displacement and the total propulsion force can give a maximum value for the inaccuracy introduced by not taking the z-component of the propulsion into account.

total propulsion force	$= 1346$ kN
displacement	≈ 20200 kN
z-component prop force	≤ 51.5 kN
as percentage of disp:	0.25%

4.1.3 Results Drift Variations

When trying to reproduce the given model tests in Panship, there are a number of choices that have to be made regarding the input and mathematical models used. These vary from the way appendages are modelled, the panel distribution all the way to choices for some important input parameters. This section will focus on the choices made in this respect and show the resulting effects on the simulated flow and over all forces and moments.

First, different options for simulation input will be verified. After that, simulation results can be compared to model test results. The goal is to get a good idea about the effect of different choices within the simulation method on the manoeuvring behaviour of the vessel. Later on, this knowledge can be used to identify inaccuracies in free sailing simulations including waves. Note that in these cases the forces did not need to be compared to model tests. For that reason, the waterjets were removed from the model in order to be able to compare the pure hydrodynamic solution. This way, it is easier to estimate the significance of differences in the results. Afterwards, simulation results will be compared directly to the model test results to get an idea about the accuracy of force and moment predictions.

Within this section first results from the design speed of 42 knots are presented. Afterwards, the over all forces and moments at lower speed will be shown to give an idea about the differences. All figures in this section take into account the ship-centred resistance and propulsion axis system with positive z pointing downwards.

Propulsion One aspect that needs some attention was the waterjet propulsion. As mentioned in section 4.1.2, in any case the resulting X force can only be compared to the model test up to a constant. For reasons of simplicity, the waterjet model was taken out of thesimulations. This might not be exactly accurate, since the waterjet propulsion force during the model tests might vary as the inflow velocity in x direction decreases with larger drift angles. However, this effect is assumed to be small.

Viscosity All model tests were reproduced using full scale dimensions and viscosity, thus at a different Reynolds number than the original model tests. However, Since a panel method with inviscid flow is used, this only effects the empirical correction for viscous resistance. The overall difference between model scale and full scale simulation results was checked for a few tests and turned out to be negligible.

Panel Size As discussed before, there are several characteristics to this hull shape that have to be taken into account when creating the input for a simulation. A couple of panel distributions were tested in order get an idea of the resulting effects on the forces and Moments. First of all, two different panel sizes were taken into account. One with 1194 submerged panels and one with 1618. This way, it could be ensured that the hull shape is approximated sufficiently well to make the resulting error small. However, it has to be mentioned that for both panel distributions, the chines don't always lie on panel edges. Therefore, the geometry of the chines was not captured entirely by the panel model. The finer panel distribution is shown in figure 10.

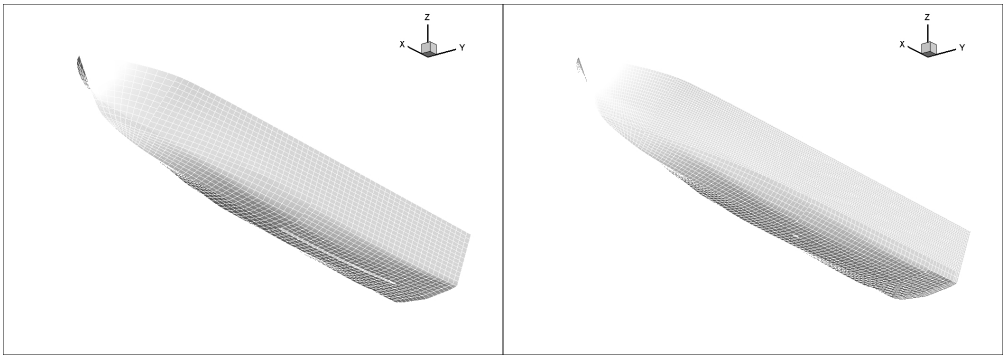

(a) Coarse panel distribution. (b) Fine panel distribution.

Figure 10: Panel distribution on model hull

The results of the two different panel distributions show a couple of differences. While for Y, Z, M and N the differences can be considered quite small, the longitudinal forces and especially the roll moment is off by more than 10%. Note that in this case surge forces and pitch moments can be directly compared, since there is no propulsion modelled. This leads to the conclusion that in the tested region of around 1500 submerged panels, the panel size is still a limiting factor for the quality of the results. However, it was not possible to use geometry files with significantly more panels because of the resulting memory consumption. For this reason, for the geometry file with 1618 submerged panels has been used for the following tests.

Wake sheets Another aspect of the panel distribution is the modelling of wake sheets behind lifting surfaces and the hull. The wake sheets are used to model vortexes introduced to the flow at the trailing edge of these lifting surfaces. However, these vortex sheets do not always model viscous flow vortexes accurately, leading to errors in the calculation of lift forces as well as numerically introduced high to extremely high pressure gradients on surfaces in close proximity of these vortex sheets. For the current hull, attention has to be put into the optional modelling of the wake sheet of the skeg. The close proximity of the stern section might lead to unrealistic flow and pressure calculations in the wake of the skeg. For that reason two approaches to the modelling of the skeg wake sheet will be taken into account. Both options are indicated

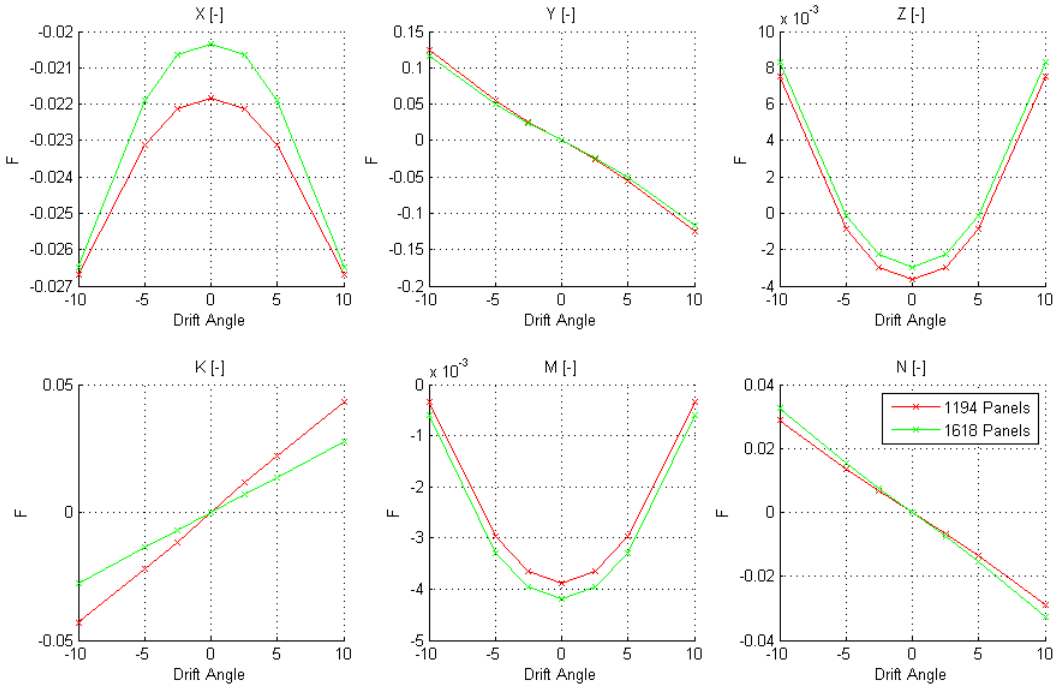

Figure 11: Forces and moments for two different panel sizes

in figure 12.

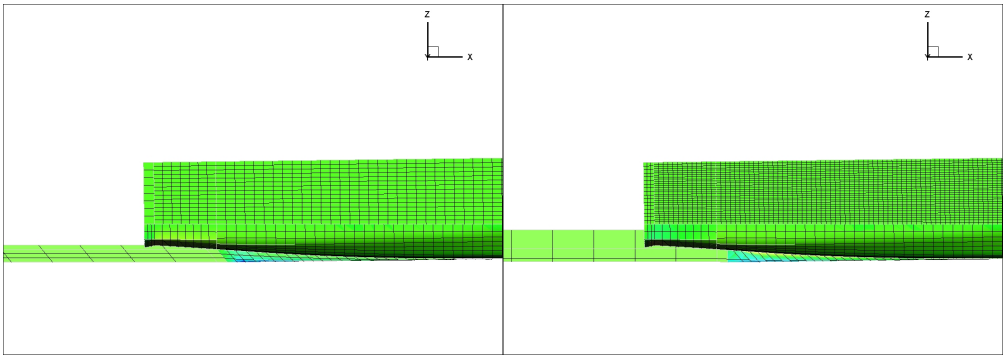

(a) Ending at the hull's surface. (b) Extended until the water surface.

Figure 12: Methods for modeling skeg wake sheet.

In one case, the wake sheet ends at the hull surface, while in the other case it is extended through the hull surface until the water surface. Experience with earlier panel code simulations suggests that extending the wake sheet to the water surface is required to calculate correct lifting forces. The effects of this can best be examined by looking at the flow and pressure distribution on the stern section of the vessel. These are shown in figure 13. The pictures were both taken at a 10 degree drift angle. Obviously, the geometry shown in **??** includes a wake sheet to model the transom flow, while the other uses empirical pressure reduction. The effect of the considered transom flow model can be assumed to be small compared to the effects of the two different wake sheets. When the wake sheet is not extended to the water surface, a large low pressure area behind the skeg is introduced as the flow skips from the high pressure side of the skeg to the low

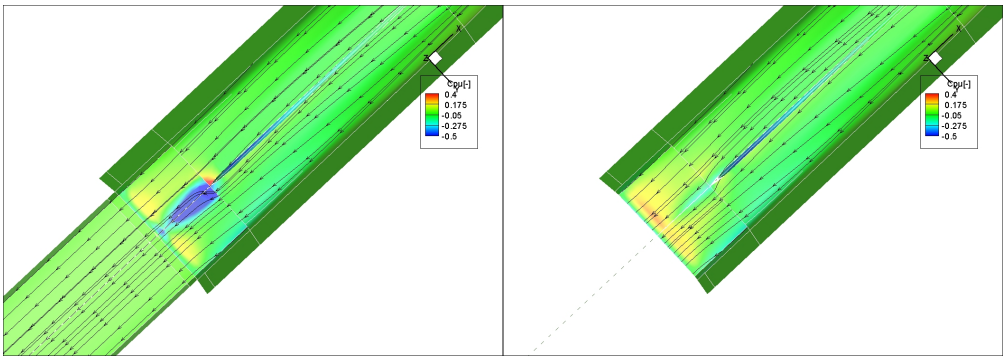

(a) Ending at the hull's surface. (b) Extended until the water surface.

Figure 13: Flow around stern section due to skeg wake sheet

pressure side. In combination with the locally very high pressure near the starboard trailing edge of the vessel, this is not a pressure distribution that one would expect in the wake of a lifting surface and indicates some numerical errors where the wake of the skeg crosses the hull panels.

Appendages Secondly, the hull has a skeg underneath the stern section and stabilising fins on the side. As mentioned in section 3.5 both fins and skeg can be modelled either with panels, including them in the hydrodynamic solution of the simulation, or as empirical lifting surfaces using lift and drag coefficients to predict the resulting forces. When it comes to the fins the choice has been made to model them empirically. This is because in the considered cases there are no roll motions and hence the lifting forces on the fins can be assumed to be small. Modelling them with panels and including necessary wake sheets would be unnecessarily time and memory consuming. For the skeg however, the situation is slightly different when drift angles are introduced. In that case the skeg might create a significant amount of transverse force. In order to investigate the differences in the simulations, both modelling options were tested and compared. Figure 10 shows panel distributions with the skeg included. The wake sheet is also included in the geometry file.

Figure 15 compares the results of both modelling methods. On the one hand, the empirical model is a lot simpler and does not take into account any details of the actual geometry used in this case. Only its position, the chord length and the maximum height are taken as input data. On the other hand, potential flow does not necessarily model the flow around a skeg correctly. The skeg in inclined flow is very likely to cause flow separation to some extend and vortices in it's wake. While these vortices are modelled to some extend by the wake sheet, the actual flow patterns introduced by this wake sheet are not very realistic. And since in this the wake sheet lies (partly) very close to the hull surface in the stern section, this might cause unrealistic pressure distributions in this area.

In order to get an idea of the potential flow around the modelled skeg, figure 14 shows pressure distributions on the hull surface behind near the wake sheet as well as streamlines and pressure distributions on both sides of the skeg. These pictures are from a test with a 10 degree yaw angle.

It can be concluded that even with the largest drift angle considered in this report, there are no very extreme phenomena occurring within the flow around the skeg. There are no high local pressure peaks, and the streamlines are all relatively smooth.

In this case, for all degrees of freedom, the difference can be described as small. Only X for larger drift angles some difference, however, compared to the overall resistance force this difference is less than 5%. For the lower speeds it is even smaller. Apparently, for these tests the simpler empirical model leads to good

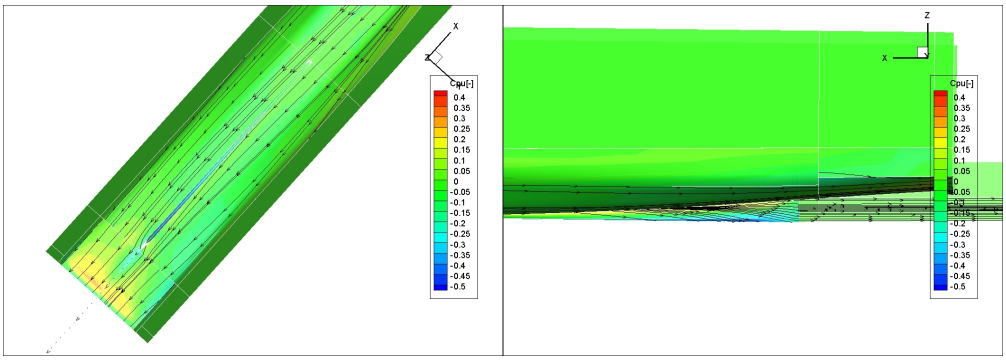

(a) Stern section.

(b) Port side pressure distribution.

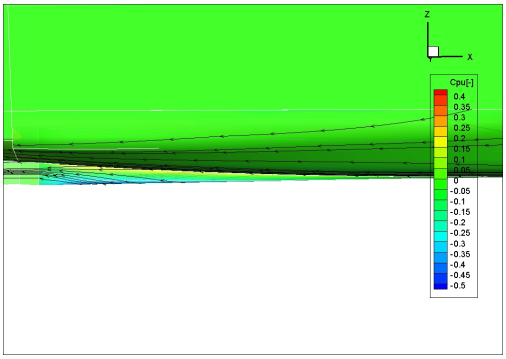

(c) Starboard pressure distribution.

Figure 14: Pressure and wave height measurements compared to photograph.

simulation results.

Transom Flow As mentioned in section 3.4.3, also the dry transom flow can be modelled either with a wake sheet or by applying an empirical pressure reduction near the stern. In order to obtain an idea of the resulting effects on the simulated flow, both options can be compared in figure 13. As can be expected, in both cases the pressure near the stern reduces to zero.

Free Surface Elevation Generally, since the free surface boundary condition is linearised, the Green's functions that determine the local potential only exist beneath the still water surface and there are no changes in the domain of these functions. As a result of that, the output of the hydrodynamic solution does not directly give a local wave height. Instead, only a pressure distribution on the still water free surface is known. Based on this pressure on the still water free surface, an estimate can be made for the local wave height. If that wave height is positive, a hydrostatic pressure on the hull that linearly increases from the estimated instantaneous free surface outside of the actual fluid domain to the calm water free surface can be added to the hull. If a wave trough is present, the calculated pressures up to a certain depth within the fluid domain will be negative (read: lower than atmospheric pressure). In this case, all negative pressures can be set to zero in order to model a wave trough. This simplified and linear way to model a wave elevation even within a simulation using linear free surface boundary conditions can greatly influence the over all forces on the hull. However, since there can be very high pressure gradients near the intersection of hull and still water free surface, and since due to numerical reasons explained in [24], an evaluation of the Green's functions exactly on the still water free surface is difficult, if not impossible, the exact location where the pressure is evaluated to make an estimate on the local wave hight is of great interest.

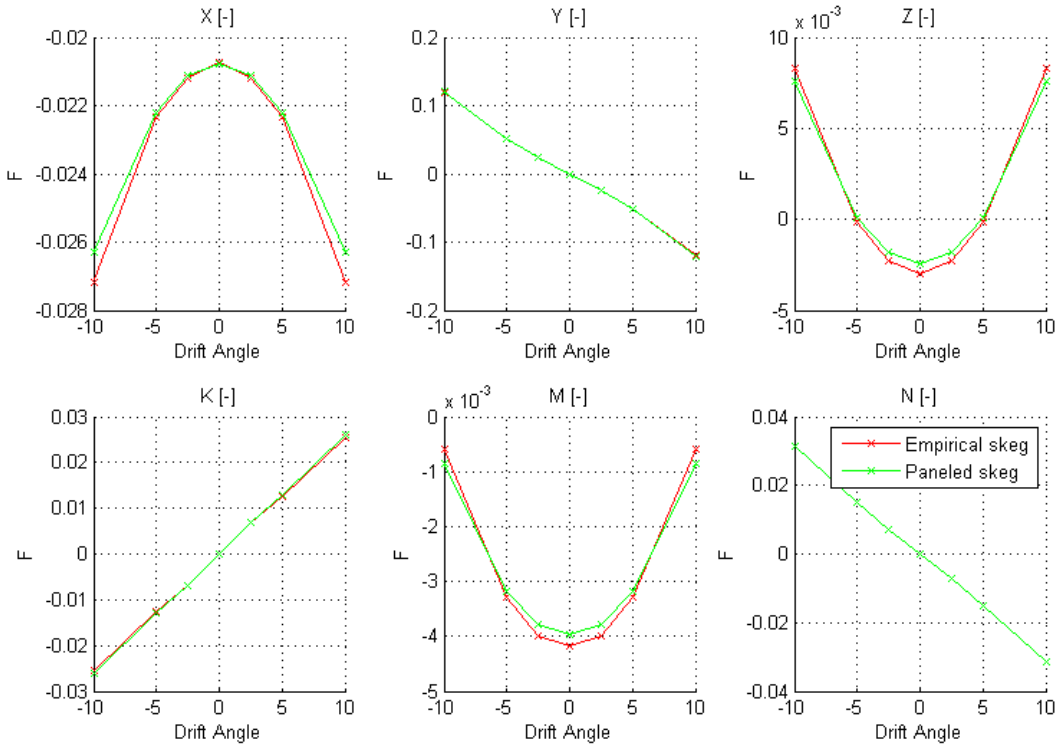

Figure 15: Forces and moments for two different skeg models

De Jong already put some effort into the comparison of different locations where the pressure can be evaluated. He therefore compared measurements made on a Wigley hull with results computed by Panship. The main conclusion being that up to a certain point the calculated wave elevation gets closer to model test results, the closer the point of evaluation of the Green's functions lies to the actual free surface and panel. However, at some point numerical errors take over and reduce the accuracy of the calculations again. This research lead to two three different options for calculating the wave elevation on the hull's surface that will be explored within the current validation:

Option 0 completely ignores the local wave height and only calculates the pressure within the computational domain of the Green's functions. In wave troughs, a negative pressure occurs near the still water water surface.

Option 1 evaluates the average pressure on the upper most row of hull panels. This pressure is then assumed to be equal to the hydrostatic pressure build from the wave top to the still water free surface and based on that the local, instantaneous wave elevation is calculated along the hull. Since the average pressure on the upper row of panels is used, the panel size can significantly affect the estimated wave elevation.

Option 2 uses a vertical offset from the water surface and a horizontal offset from the hull surface to determine the location at which the pressure will be evaluated. As de Jong mentions in in his PhD thesis [24], due to numerical reasons it is difficult to evaluate the pressure exactly on the intersection of hull and free surface. Here, a good compromise has to be found: The further the evaluation point moves away from the hull-waterline intersection, the smaller the numerical errors, but the larger the difference between evaluated pressure and actual pressure at the intersection.

To avoid giving these long descriptions of each option, every time it is mentioned within this report, the name of the input parameter 'IFSWAV' with the values 0, 1 or 2 that switches between the three options will in some cases be used to refer to the applied method. Physically spoken, close to the fluid domain boundaries of the hull and the free surface steep pressure gradients will occur with a peak pressure on the intersection of hull and free surface. Hence, the closer the pressure evaluation point lies to this intersection point, the higher the calculated wave height will be. In the simulation results it turns out that evaluating the pressure on the hull surface (option 1) consistently leads to higher waves. For illustration, the wave profiles for both options are shown in figure 16. For the figure, a run at 10 degree drift angle has been chosen leading to a large difference between starboard and portside profiles.

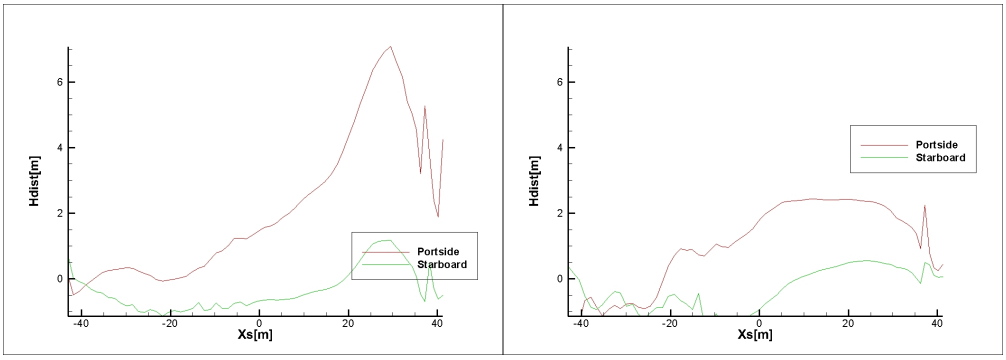

(a) IFSWAV 1 (b) IFSWAV 2

Figure 16: Wave profiles for two different pressure evaluation points.

In this case the differences between options 1 and 2 are quite extreme, with almost a factor 3 difference in peak wave height. While a high wave can be expected when moving at 42 knots with a 10 degree drift angle, for the current 87 meter hull, a 6 meter high bow wave as suggested by IFSWAV 1 is probably too extreme. In reality, viscous effects like wave breaking and spray will cause the wave to be significantly lower. However, the high pressures calculated in the simulation will have an effect on the calculated forces and moments. One other thing to notice are the very steep and unrealistic peaks right at the bow. These are obviously the consequence of very strongly oscillating pressures on the waterline. These oscillations are the result numerically evaluating certain integrals within the Green functions, as de Jong describes in [24]. Generally these peaks can be reduced by decreasing panel size and time step.

From the results, it is very obvious that the pressure distribution above the undisturbed free surface creates a significant difference in the over all forces and moments in all degrees of freedom. The high bow wave obtained when option 1 is used completely turns the sign of the obtained roll moment. Also, it causes the over all resistance to be almost twice as high compared to a simulation without any wave elevation (option 0). All in all, with the current relatively full hull shape of m8325 ($C_b = 0.52$) in high speeds with large a drift angle option 1 leads to a severe overestimation of the bow wave height and the resulting forces. The differences between having no wave elevation at all and option 2 are relatively small in comparison. In any case, it can be concluded that the linearisation of the free surface boundary condition significantly influences the resulting forces and moments calculated by the simulation, while the given options for eliminating resulting inaccuracies in the simulation results show a wide range of resulting forces and moments. Further investigation might be interesting to evaluate the options for correcting this linearisation.

Model Tests Generally, within this report the results of the model tests will be assumed to be the most accurate representation of the (full scale) reality. For this reason, simulation results closer to the actual model tests will in most cases be considered the more accurate results. Nevertheless it can be useful to have a look at the model tests separately to highlight some noteworthy details. Figure 18 shows the results of the

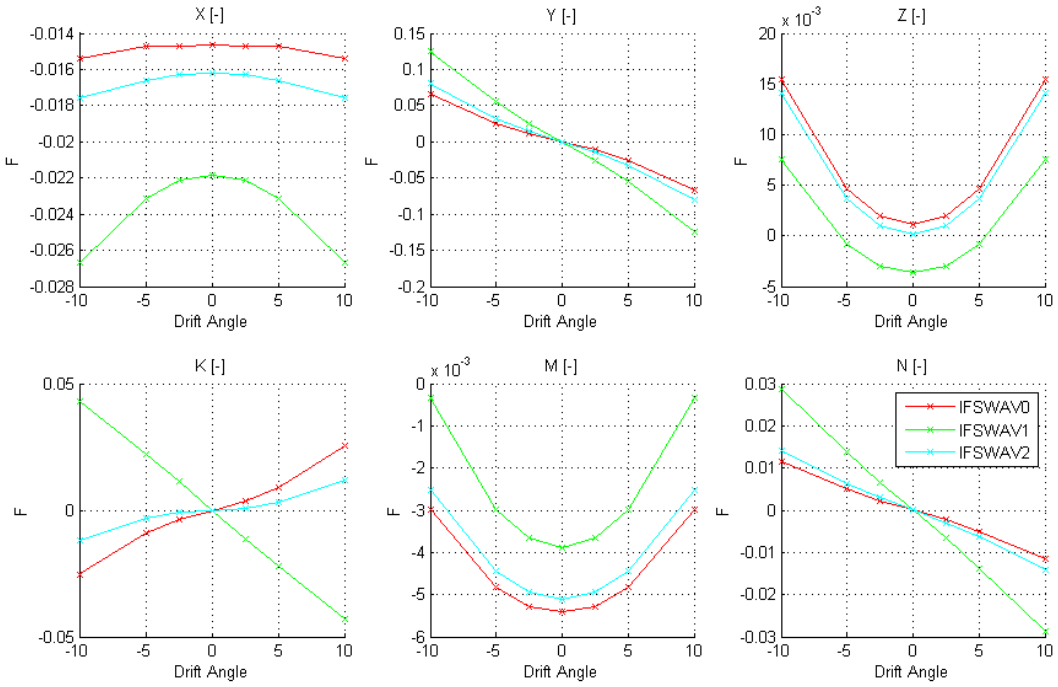

Figure 17: Forces and moments for three different choices of IFSWAV

model tests translated to dimensional full scale values for all speeds considered in this report.

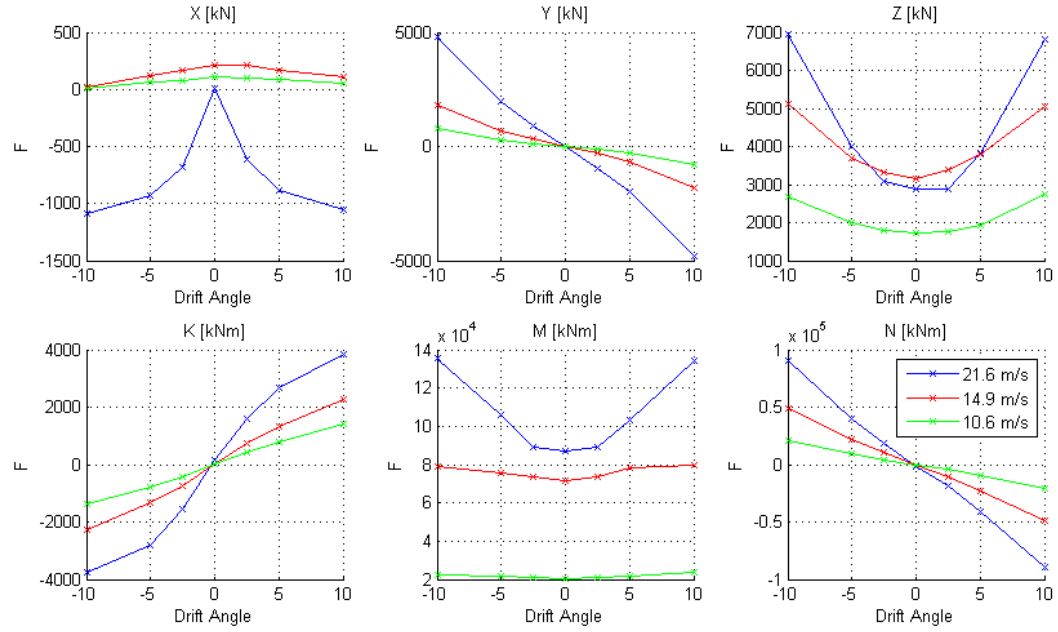

Figure 18: Forces and moments from the model tests.

Generally, the figures show approximately what can be expected. The Z-force is pointed downwards for

all tested speeds. However, one can see that for the highest speed tested, the suction force becomes smaller again as the hydrodynamic lift starts to increase. One aspect that does catch the eye is the x force at 21.6 m/s. While the value at zero drift angle is close to zero as one would expect for tests near self propulsion point, the increase of resistance is significantly steeper than for the other two speeds tested. This can be caused the applied waterjet propulsion. The model test report is not conclusive about how the applied rate of revolution was determined or whether it has been varied between runs at the same speed with different drift angles. For this reason, one should be very careful with drawing conclusions based on these measurement points.

Figure 19 compares the (non dimensional) model test results at 21.6 m/s to the simulation results. To get an idea about what input leads to the closest match, the three options for evaluating the free surface elevation are shown. The tests taken into account for this comparison are all run with the fine panel distribution and the skeg modeled with panels. The transom flow model is empirical for all runs except the last one with IFSWAV set to 2 (pressure for wave height evaluated with horizontal and vertical offset from the hull - free surface intersection). As mentioned in section 4.1.2, X and M can only be compared up to a constant. For Z, there is an error margin, independent of the drift angle, of 0.25% of the ships displacement due to a possible vertical component of the propulsion force. However, compared to the differences between all simulations results and the model test results, this can be neglected.

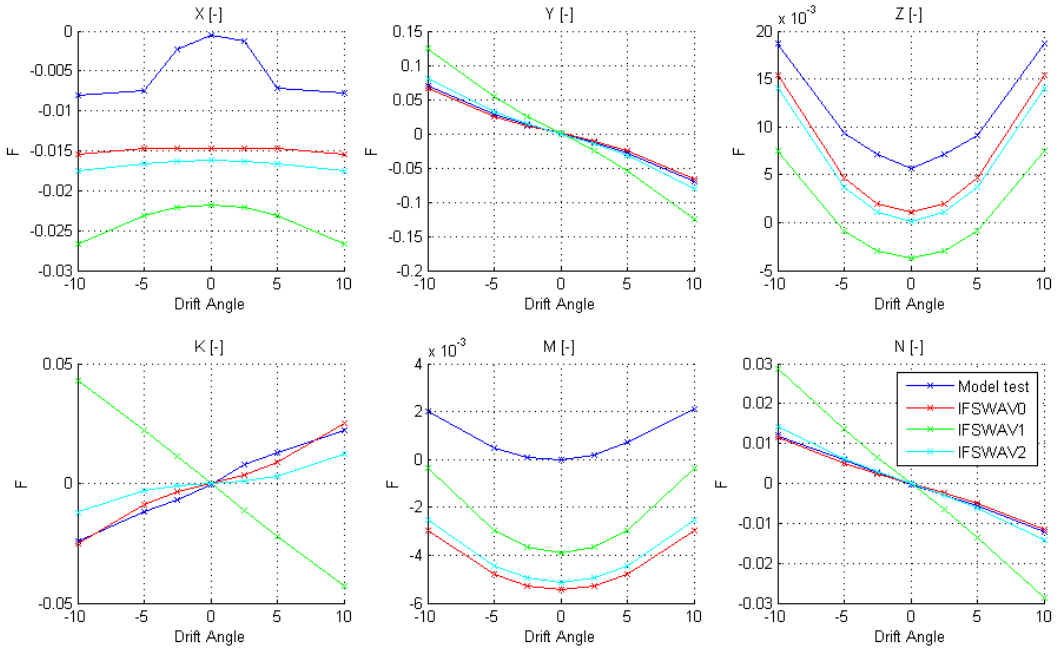

Figure 19: Forces and moments from the model tests compared to some simulation results.

Comparing the results of model tests and the different simulation outputs, first conclusions can be drawn to about the different input parameters used for the simulations. In all degrees of freedom IFSWAV 1 (pressure for wave height evaluated on the upper most submerged panel) leads to results relatively far from the other simulations, as well as from the model tests. A good explanation for this is the extremely high bow wave as shown in figure 16a. Especially for K, Y and N this leads to unrealistic results. Further more, applying the Kutta condition at the transom seems lead to reasonable results at zero drift angle, however Z-forces and as a result of that, the Pitching moments increase unrealistically fast for increasing drift angles.

As far as one can tell from these data, the simulation results obtained with no wave heights pressures

outside the fluid domain at all (IFSWAV 0), or with the lower waves obtained by evaluating the pressure with a horizontal and vertical offset from the hull - free surface intersection (IFSWAV 2) lead to the closest fit of the model test results. Nevertheless, there are still some details that should be highlighted. For sway forces and Yaw moments, the simulations fit the model tests quite accurately up to a few percent for all options of wave height calculation. For the roll moment, even the lower bow wave introduced by IFSWAV 2 already leads to a significant reduction of the roll moments due to a drift angle. Using no correction for the linear free surface (IFSWAV 0) matches the model results closer at least up to the currently considered 10 degree drift angle. Concerning the resistance and pitch moment, IFSWAV 0 and 2 lines lie pretty much parallel to each other, with 2, including some free surface elevation leading to a larger resistance and a slightly more bow up pitch moment. As noted before, the model test shows an unlikely development of the surge force. As shown in figures 20 and 21, at lower speeds, the model test and simulation results seem almost parallel.

The only systematical and large error that becomes obvious with these considered model tests is heave force. All considered simulation choices lead to a more upwards pointing heave force. This difference lies somewhere between 2% of the displacement at 10.6 m/s and 10% of the displacement at 21.6 m/s. The error seems to be approximately constant over all tested drift angles and exceeds by far the heave force that might be introduced by the waterjets in the model test.

Speed Variations Next to the design speed of 21.6 m/s, two other speeds (14.9 and 10.6 m/s) were tested during the model tests. These refer to Froude numbers of 0.51 and 0.36. While the results at the lower speeds roughly show the same effects and trends as the results at design speed, there are some details that should be pointed out.

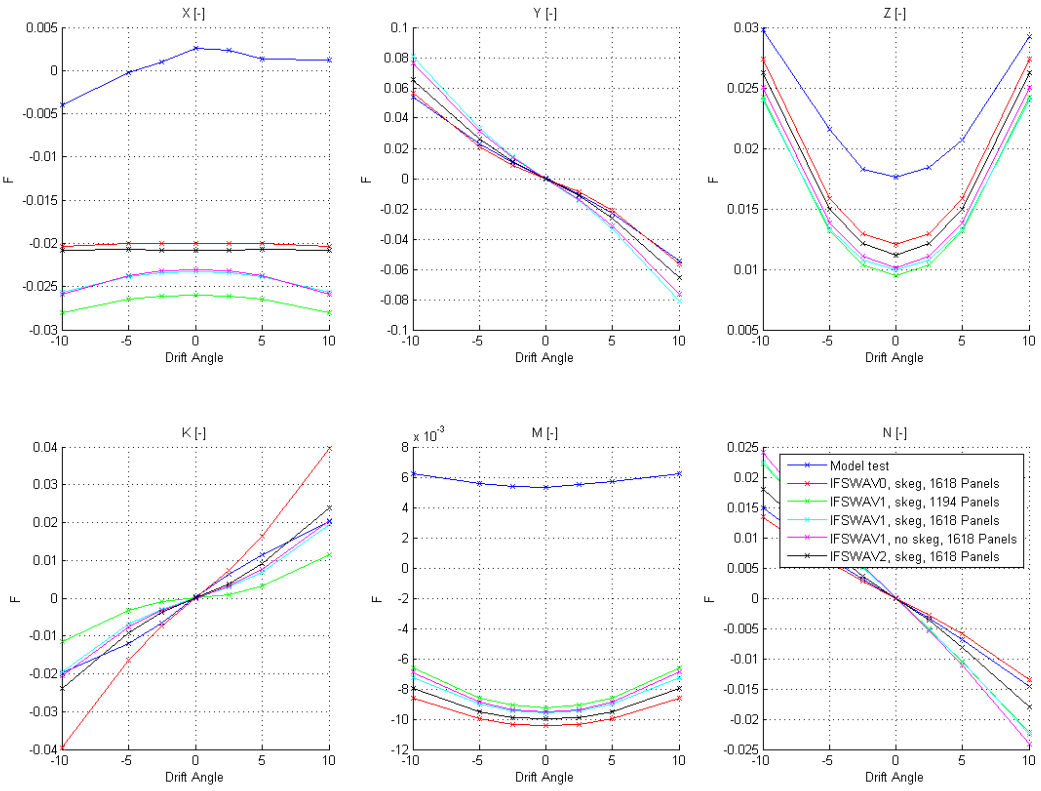

Figure 20: Forces and moments at 14.9 m/s.

Figure 20 shows the resulting forces and moments of the captive drift variation tests at 14.9 m/s. In order to limit the content of this chapter, all simulation choices that were tested have been put into one figure this time. One significant difference compared to the higher speed is that the model test results for the surge force now look more realistic. Although some asymmetry is introduced at 10 degree's drift angle, all in all the curve seems more continuous than before. Further more, the turning of the roll moment sign obtained at 21.6 m/s when evaluating the pressure for the wave height on the hull surface (IFSWAV 1) can not be found at lower speeds. Apparently, the pressure increase near the hull waterline intersection becomes significantly less at lower speeds. However, generally it seems that the roll moment is not predicted as accurate as sway forces and yaw moments.

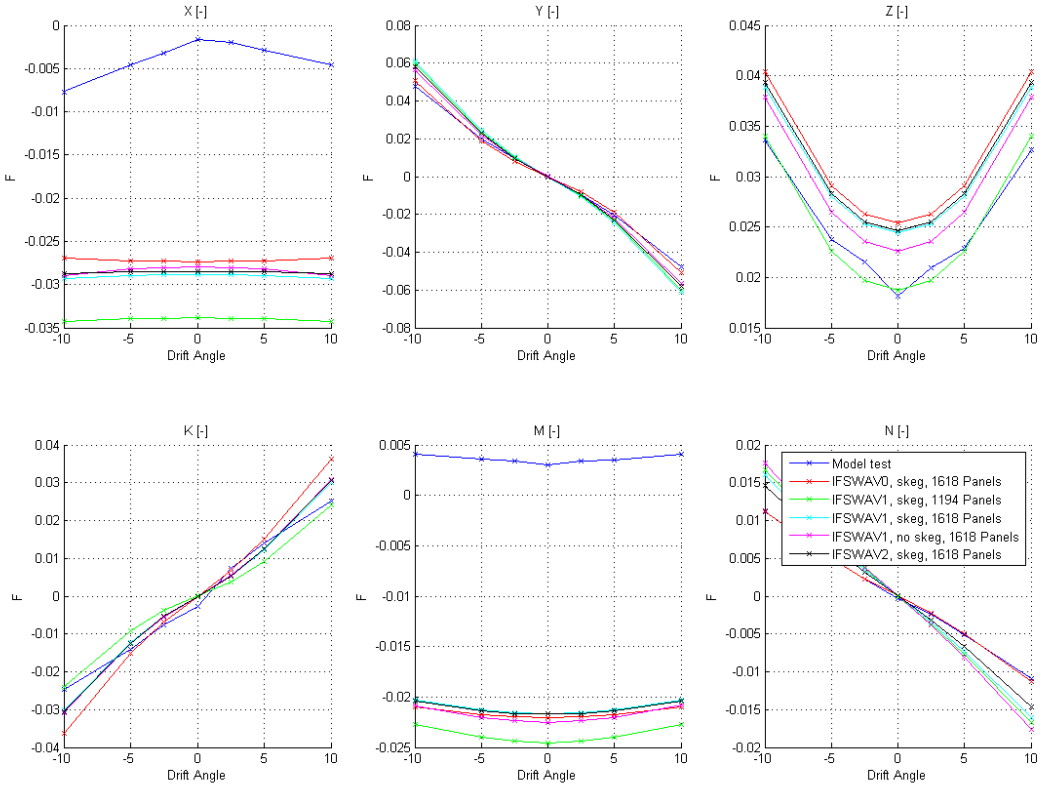

Figure 21: Forces and moments at 10.6 m/s.

Figure 21 shows the resulting forces and moments at 10.6 m/s. At this low speed, when taking no wave elevation at all into account (IFSWAV 0) or using the lower wave elevation when the pressure is evaluated with horizontal and vertical offset (IFSWAV 2) it seems that the resistance no longer increases with larger drift angle, but instead decreases. This trend can not be found in the model test results.

4.1.4 Conclusions

Generally, one should be careful drawing conclusions based on these captive tests. Although a lot of components that play a role in free sailing conditions with irregular waves were eliminated, still only the sum of several force/moment components can be measured, seemingly accurate/inaccurate results may be caused only by several errors cancelling each other out or amplifying each other randomly. However, by examining not only the resulting forces, but also details of the flow, like the flow around the skeg and the wave pro-

file along the hull, some educated opinions can be formed about causes and details leading to the final results.

These captive model tests were reproduced having two goals in mind. First, they are very well suited to verify different choices of simulation options and mathematical models, enabling well informed choices for the free sailing validation tests including and excluding waves. Secondly, the the potential flow solution and viscous components can be validated without unknown effects of the linearisation of the body boundary conditions. Any differences between simulation results and model tests found can be interpreted as the result of either the simplifications to the flow introduced by the potential flow model and the separately calculated viscous forces or neglecting free surface elevation around the hull.

Verification of Simulation options Part of the comparisons made were comparisons between potential flow solutions and empirical models derived from curve fittings on earlier measurements. Amongst these were the Skeg modelling and the transom flow model. For both cases the conclusion has to be made that the difference between both options were small. Apparantly, in this case with a relatively 'normal' hull shape, the simpler empirical formulations can be considered a good alternative for a more complex potential flow calculations.

The second group of input variations tested concerned the spacial discretisation, the panel distribution. Here two different numbers of underwater panels were tested as well as different options for the wake sheet of the skeg. In this case the effect on the flow surrounding the vessel as well as the resulting forces and moments is significant. In order to make sure that simulation results are reliable, the flow around the hull should be checked for obvious mistakes caused by some aspect of the simplifications made within potential flow. This holds especially in cases of complex geometries and vortex sheets.

Finally, several possibilities to deal with the linearised free surface boundary condition were tested in an attempt to reproduce model test results as accurate as possible. Here clearly the pressure above the water surface delivers a significant contribution to the over all results in all degrees of freedom. From the resulting forces and moments we can see that with increasing speed, but also with increasing drift angles, the contribution of above waterline pressure plays an increasingly large role. This is as one would expect, as the bow wave height increases as well. However, adding above waterline pressures on the hull by estimating a wave height based on the local pressure does not necessarily improve the simulation results.

Comparison between Simulations and Model Tests As a second step, the simulation results were compared to the model test results. When a suitable set of input options is chosen, a nice fit between forces and moments from the model tests and from the simulation can be obtained. However, this already shows one major problem. How this suitable set of simulation options (especially a suitable way to estimate wave height and above waterline pressures) has to be chosen strongly depends on the test conditions. Further investigation into the height of the bow wave and the pressure within the bow wave should give some clarity about detailed differences between simulations and model tests.

The only consistent significant difference in forces between simulations and model tests can be found in the heave force. For all tested speeds, drift angles and simulation options, the simulation overestimates the hydrodynamic heave forces by up to 10% of the ship's displacement. As with any difference found in these captive calm water tests, this can either a result of the potential flow, or of the linearised free surface boundary condition.

4.2 FDS

Similar to the captive simulations of the m8325 hull analysed in the previous section, captive simulations were carried out on the FDS hull. In contrast to the model tests carried out on the m8325 hull, for the FDS are no results for captive tests available. As such, a validation as shown in the previous section is not possible. Nevertheless, in order to evaluate and verify the effect of different simulation options, it can be

	Magnitude	Unit
L_{PP}	100	m
L_{WL}	99.982	m
B	12.502	m
T_F	3.125	m
T_A	3.125	m
C_b	0.401	-
Δ	1568.4	m^3
S	1212.3	m^2
GM	2.5	m

Table 3: Main particulars frigate.

interesting to look at simulation results of a second hull. In the conclusion of the previous section, especially calculation of the bow wave height based on local pressures near the hull - free surface intersection had a significant influence on the simulation results. Running captive simulations can show whether this influence can be qualitatively and/or quantitatively reproduced for the significantly more slender FDS hull. If this is the case, the free sailing model tests in calm water performed on the FDS hull that are discussed in section 5 and that include pressure and wave height measurements can be used to draw wider conclusions that are not limited to one hull shape. If this is not the case, the conclusion has to be made that the hull shape, probably the slenderness of the considered hull has significant influence in how the free surface elevation should be estimated in case of linearised free surface boundary conditions.

4.2.1 Hull Characteristics and Test Matrix

The FDS hull is a parent hull for a systematic frigate hull series. As such, a full scale vessel with this hull shape has never been built. The full scale values given within this report are chosen for a waterline length of 100 meters. A spreadsheet of the corresponding main particulars of the (full scale) hull that was used is given in table 3. During the tests, the hull was fitted with a twin propeller - twin rudder configuration. As shown in figures 22, next tho the rudders and propellers, two bilge keels and a skeg in the middle under the stern of the hull were added. In Panship, all appendages were modeled using empirical models instead of including them in the potential flow solution.

With a block coefficient of 0.4 and a L/B ration of 8, the FDS hull is significantly more slender compared to the m8325 hull. This might influence the flow around the hull when a drift angle is present. Viscous effects like flow separation might be modeled better by the strip theory cross flow drag model applied in Panship, since the 3D effects become less relevant.

The captive simulations will be carried out at two speeds that were also used for the free sailing model tests. The drift angles considered are kept identical to the simulations concerning the m8325 hull. This way, comparing results and is made easier and more conclusions can be drawn regarding the comparison of two hulls. Table 4 shows the resulting test matrix. Note that the considered speeds for the FDS are significantly slower than for the m8325. The fastest two considered speeds of the FDS can be approximately compared to the slowest two of m8325.

4.2.2 Modeling and Results

Taking into account the conclusions from the captive simulations on the m8325 hull, the number of input options tested could be fairly reduced. Only one panel distribution with 1600 submerged panels was used. In this geometry file, the hull is placed at design draft with zero trim, corresponding to a zero speed situation. Further more, as there is no need to compare simulation results to model tests, and different models that could be used for appendages resulted in no significant change of the simulation results, also the appendages

(a) Propeller configuration. (b) Bilge keel.

(c) Propeller shaft and skeg

Figure 22: Pressure and wave height measurements compared to photograph.

v[kn]	Fn[-]	drift angle[°]	heel angle[°]
Drift Variations			
17	0.28	-10, -5, -2.5, 0, 2.5, 5, 10	0
23	0.38	-10, -5, -2.5, 0, 2.5, 5, 10	0
35	0.57	-10, -5, -2.5, 0, 2.5, 5, 10	0

Table 4: Test matrix of captive tests.

were left out of the simulation.

What does remain is a comparison of different ways to handle the free surface elevation around the hull. The same three options as used for the model tests on the m8325 hull will be used: First there is no wave elevation taken into account at all (referred to as IFSWAV 0), secondly a wave elevation is calculated based on the pressure evaluated on the upper most submerged panel (IFSWAV 1) and thirdly, a wave elevation is calculated based on the pressure evaluated on a location with a certain horizontal and vertical offset from the hull - free surface intersection (IFSWAV 2). These three options had a significant effect on the simulation results, leading to different results depending on the speed considered. Especially for the highest Froude number, IFSWAV 1 lead to an over prediction of the bow wave height resulting in a wrong roll moment.

Flow Figure 23 shows a contour plot of the dynamic pressure including stream traces around the hull at a 10 degree drift angle. It can be very nicely observed that the potential flow does not separate around the sharp edge of the bow, creating a local area of very low pressure on the starboard side of the bow.

Free Surface Elevation Like with the m8325 hull, the IFSWAV parameter has been varied to observe the resulting height of the free surface elevation along the hull and show the effect on the over all forces and moments. Figure 24 shows the height of the contact line along the hull for the port and starboard side for 35 knots of speed at a 10 degree drift angle.

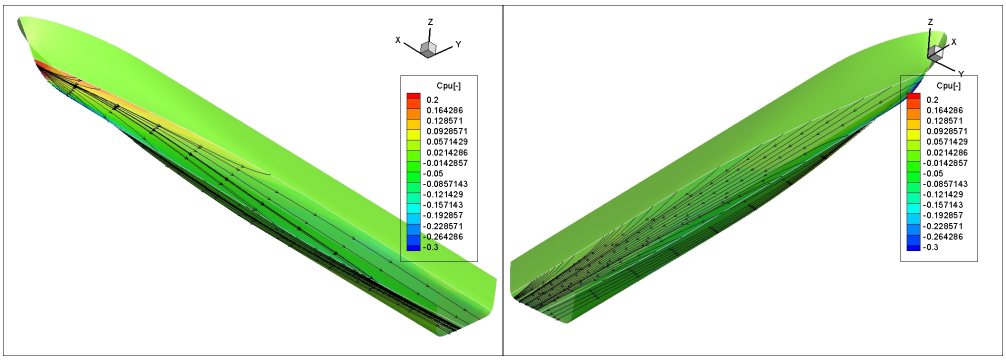

(a) Port side flow. (b) Starboard flow.

Figure 23: Dynamic pressure and stream traces on FDS hull.

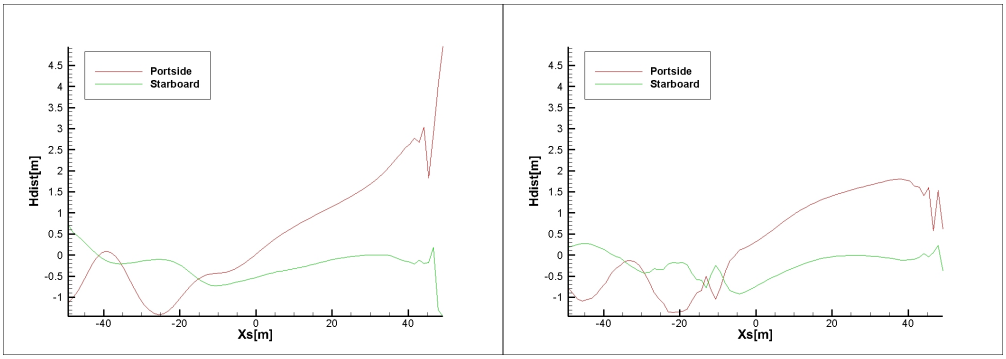

(a) IFSWAV 1 (b) IFSWAV 2

Figure 24: Wave profile on FDS hull.

Again calculating the local wave height based on the pressure on the upper most submerged panel (IFSWAV 1) shows an extremely high wave peak near the bow. It has to be noticed that in this case the wave hight less extreme than it was with the m8325 hull. This could be due to the fact that the considered Froude number is significantly lower (0.57 as opposed to 0.74). Also, again there are strong oscillations right behind the bow. All in all, the effect of the bow wave elevation on the more slender FDS hull seems quite similar to the effect on the more full m8325 hull.

Figure 25 shows the resulting forces and moments at 35 knots boat speed. As expected, IFSWAV 1 leads to more resistance and higher values for forces in all degrees of freedom. Because of the high pressure above the waterline, the centre of effort of the sway force shifts upwards, reducing the roll moment. Another effect that can be seen again is that at low speeds and IFSWAV 0, with increasing drift angles the resistance in Panship starts to decrease instead of increase. This effect could not be verified in the Model tests.

4.3 Conclusions

The captive steady tests described in this section were carried out with two main goals in mind. First of all, a verification was desired of several simulation options in oder to obtain a clear idea of what plays a significant role within the simulation results. Amongst others, variations in panel distribution, wake sheets and appendage models were tested. After evaluating all systematic changes, the conclusion can be made that the only tested variation that has a significant influence on the over all simulation results is the variation in the way the free surface elevation is calculated on the hull surface. Independent of the hull shape tested, the

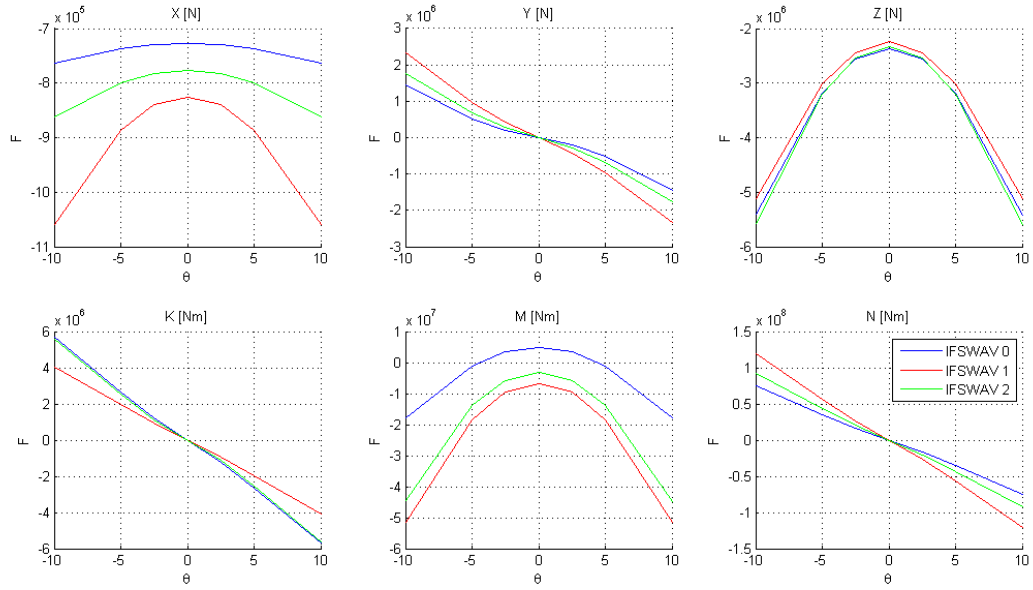

Figure 25: Forces and moments on FDS hull at 35 kn, IFSWAV variations.

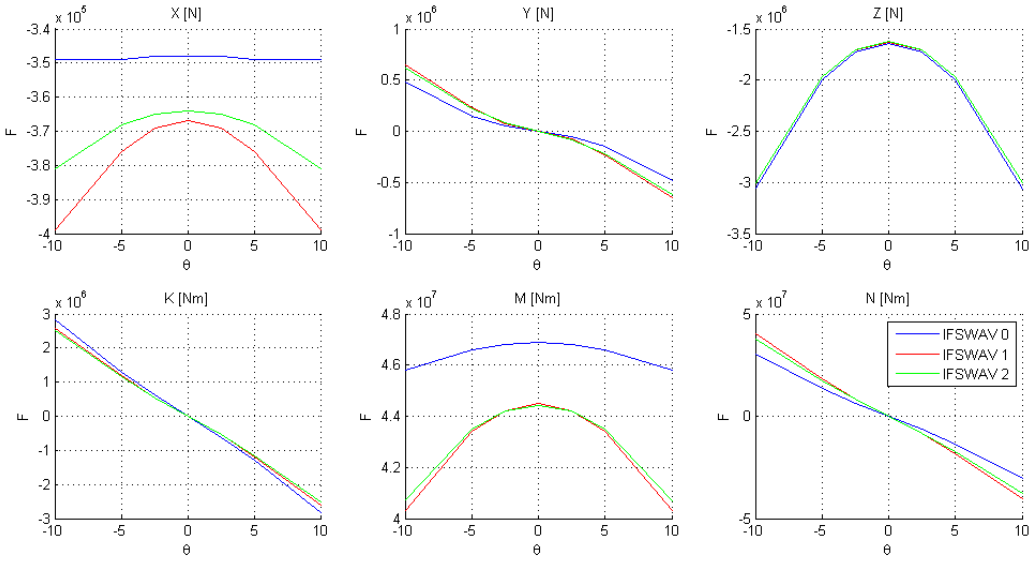

Figure 26: Forces and moments on FDS hull at 23 kn, IFSWAV variations.

difference between the two methods for estimating a local wave height, as well as neglecting all free surface elevation yielded significantly different simulation results. As can be expected, this difference increases as speed and drift angles increase (or in other words as the expected wave height increases).

Unfortunately however, it is not possible to give one option that leads to simulation results that fit the model test results best. At all times, evaluating the wave height based on the pressure on the upper most submerged panel row leads to the highest waves, while evaluating the pressure on a location further from the hull surface reduces this height significantly. With no wave height measurements available for the considered captive tests, it is impossible to tell with certainty which option fits the model tests the most accurate.

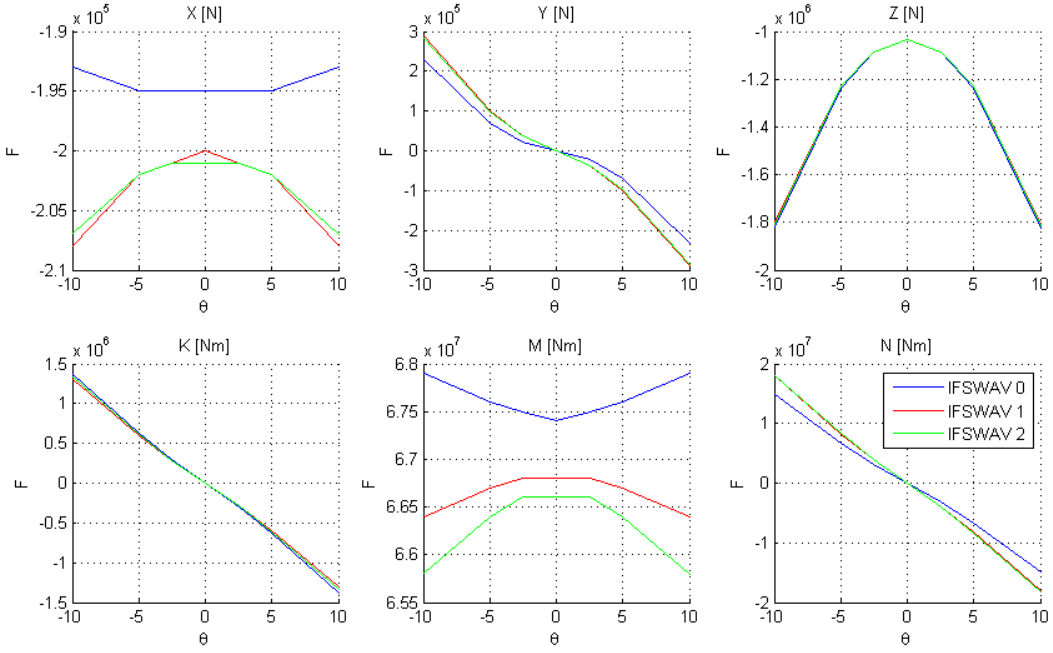

Figure 27: Forces and moments on FDS hull at 17 kn, IFSWAV variations.

However, based on the force and moment results that are available, it is reasonable to assume that there is not one option that always yields the best results. Instead it seems that when low wave heights are to be expected (at low speeds and without drift angles) the highest wave height option yields the closest fit while for higher speeds and higher drift angles the lower option or even completely excluding any surface elevation improves the simulation results.

The second objective of the validation of this captive steady tests was to eliminate a large number of force components and isolate and validate only the ones that are left. In this cases the force that is left to validate is a sum of the hydrodynamic solution and its viscous additions. Hence, any differences found between model tests and simulations are due to one of three components: the potential flow solution, calculated viscous forces or the effect of linearizing the free surface boundary condition. The only consistent difference between model tests and simulations that can be found is the hydrodynamic heave force. For all tested conditions, and for all tested simulation options the hydrodynamic heave force was overestimated significantly. The magnitude of this difference increases with the vessels speed, confirming that the cause is hydrodynamic in some way. However, looking at the three possible causes that were isolated beforehand, this does not help to further narrow down its cause. Further investigation will be necessary in order to accomplish that.

5 Free Sailing Tests

As a next step in the validation of the 3D time domain simulation for stern quartering waves, free sailing tests in calm water and in waves can be used. For this, a series of model tests on the FDS hull are available that do not only include measurements of the position of the vessel, but also measurements of pressure and wave height in the bow area. In two steps, these tests can be used to further investigate the consequences of the simplifications made in the simulation.

First, the free sailing tests in calm water will be used to verify the steady position of the vessel when sailing at a different speed. In contrast to the steady captive tests form the previous chapter, this time the effects of the body linear boundary condition are taken into account since the vessels actual trim and sinkage will be different from the ones used for the hydrodynamic solution. Moreover, from the captive tests we know that some attention should be given to the calculation and pressure distribution within the bow wave. Since during the calm water free sailing model tests pressure and wave height measurements were taken in the bow area, these will be used to validate further details of the bow wave and possibly give some ideas about how to properly approximate a bow wave within a simulation with a linear free surface condition.

Secondly, free sailing tests in irregular stern quartering waves will be validated. With the incident waves, a lot of extra components and complexity is added to the tests. In this context, one should not forget that the hydrostatic solution is fully non linear, giving Froude-Krilov forces from the calculated instantaneous position of the vessel. The differences between simulation and model test that are caused by incident waves will be mainly due to the hydrodynamic solution simulating the periodic movements of water particles in these incident waves. Nevertheless, in steep stern quartering waves, the body linear boundary condition in the hydrodynamic solution will have large effects on the solution since especially sway and yaw motions in stern quartering will exceed small values regularly. More over, in the hydrodynamic solution, due to the linear free surface condition, the incident waves are represented as horizontal movements of the water particles underneath the calm water free surface, causing another possible reason for differences between model tests and simulations. Even for the hydrostatic solution, the incident wave shape used within the simulation results in a sum of sinusoidal waves. This does not represent the situation during the model tests accurately. In viscous flow steep waves tend to get steeper on the front side, until finally breaking. In irregular waves it is inevitable that at some point waves become too steep and breaking occurs that will not be modeled in the simulation. Because of all these additional sources that will lead to inaccuracies in the simulation results, it will be difficult to pinpoint one cause for any inaccuracy that can be found. Nevertheless, from a purely practical standpoint, validating these complicated tests in steep stern quartering waves can be very useful. They can give an idea about the over all match between model test results and simulation results, providing a guide for future users of such a simulation method as to how much trust can be put into simulation results and in which conditions model tests should keep the preference when it comes to predicting the behaviour of a vessel.

The free sailing tests that are used for this project were carried out on the FDS hull described in section 4.2. The model has a scale of 1:15. Within the scope of the FAST project, these model tests were performed amongst others to validate a version of Panship with fully non linear boundary conditions. During the tests, the model was completely self propelled and free in all six degrees of freedom. During the runs, the only connection to the towing tank carriage are flexible cables for data transfer and power supply. The effect of these cables on the motions of the vessel should be negligible. The test setup is shown in figure 28. Tests in calm water, regular and irregular waves were carried out. A number of wave directions from bow to bow quartering, as well stern quartering were tested. The aft incoming wave directions were: 300 °, 315 °, 330 °, 345 °. The bow was fitted with 76 pressure sensors, creating a detailed picture of the pressures on the hull caused by the bow wave and incident waves. For capturing wave heights along the hull, five wave height sensors were installed in the bow area from station 16 onwards and one around station 7.

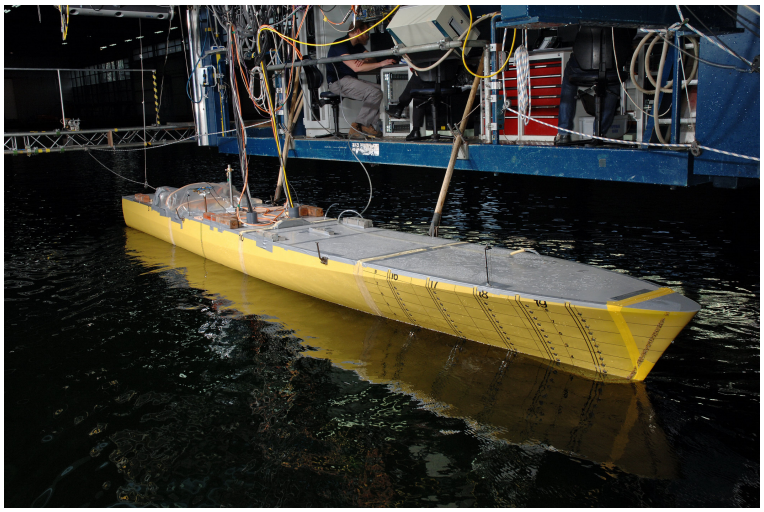

Figure 28: Test setup during free sailing tests of 100 meter frigate.

5.1 Calm water tests

As mentioned before, the free sailing tests will be used for two validating several aspects. First of all, the steady trim and sinkage calculated by the simulation will be compared to the measurements from the model tests. In addition to the conclusions about the hydrodynamic heave forces that could already be made after the captive tests, this will also allow conclusions about the hydrodynamic pitching moment. Secondly, withing the bow area wave height measurements were made on five locations. These can be used to give a comparison of the two different possibilities to estimate a wave height in a simulation with linear free surface condition described in section 4.1.3 with model test results. Finally, pressure measurements were taken in the bow area, creating the possibility to compare the pressures from the simulation with actual measurement results. From this, conclusions can be made about the pressure stretching that is used to estimate a pressure on the hull above the calm water free surface, but it may also enable to further isolate the reason for the overestimated hydrodynamic heave forces that was observed during the captive simulations.

During all free sailing tests in calm water, the pressure was measured in a total of 76 locations near the bow and the wave height was registered at 5 different x-coordinates near the bow. The locations of the pressure and wave height sensors in the bow are shown in figure 29. All coordinates in this chapter will be given in a ship fixed coordinate system with its origin at the intersection of the APP with the keel line. During all tests, all sensors took time series at 50 Hz (full scale time).

5.1.1 Model Test Measurements

During the test program, a total of seven runs were carried out with calm water and a speed of $F_n = 0.57$. For verification of the measurements, the results of these seven runs were compared. In figures 30a and 30b the pressure and wave height results of the first and the last run are shown with two main differences. First of all one pressure sensor obviously stopped working during the tests and, secondly, the bow seems to be submerged further in the last run. Results from all other runs lie somewhere between these two results, indicating a steady change during testing. This steady change in bow submersion turned out to caused by a bilge pump in the forward most compartment that was not working properly. At the end of the testing, about seven liters of water was found in this compartment. For this reason, during further analysis of the results, only the first run was used. The results of the pressure measurements of all runs care shown in appendix C.

In a first step to analyze these measurements, the time series of pressure measurements and wave height

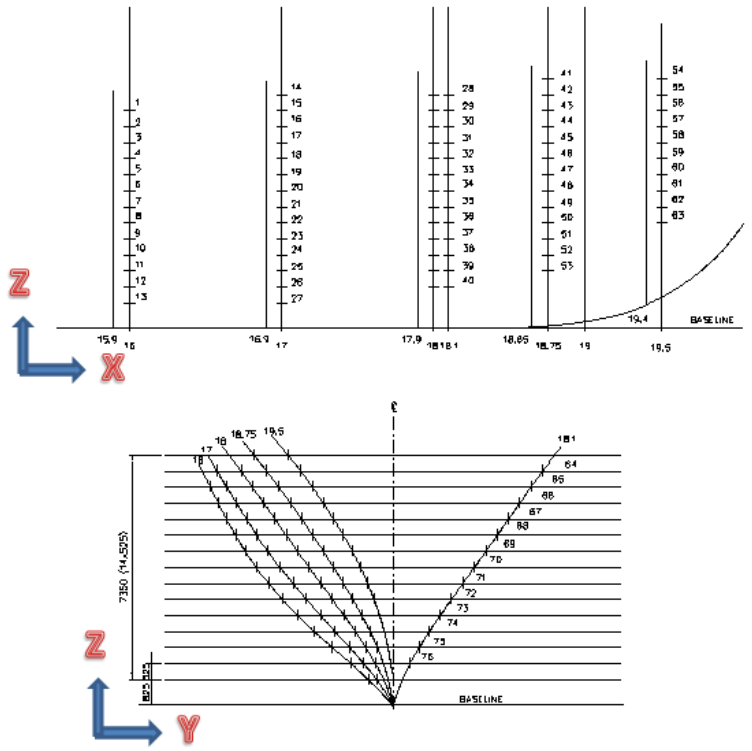

Figure 29: Loactions of pressure and wave height sensors in the bow.

measurements from the calm water tests were averaged, transforming the measured time traces into a steady pressure field and wave height for the entire bow area. To ensure proper calibration, before every run a baseline measurement with zero speed was taken. In figure 30, the resulting picture of the pressure on the starboard side of the bow is given and compared to a photo of the same run. This is a calm water run at $F_n = 0.57$.

In the plot of the measurements, a projection of the bow area on the x-z plane is shown. The red dots represent all locations of pressure sensors and the two red lines respectively show the still water waterline and the measured wave contact line. As one can see from the photo, the measured wave height matches quite well with the observations. From the pressure measurements, we see that, although the bow wave consists only of a quite thin sheet of water (as described in [10]) the pressure in this area seems to be considerably high and close to constant. For a closer look at the pressure distribution, figure 31 shows the pressure distribution per bulkhead.

Here, the pink lines represents the measured pressure, the green lines show the hydrostatic pressure from the measured wave height and the black line represents the still water waterline. It can be seen that the measured pressure goes to zero in a higher point than the actual wave height measurements. In most cases this can be explained by the fact that there was no pressure sensor on the waterline and the pink line interpolates linearly between the pressure sensors. For the measurements at $x = 93.75$ however, it can only be explained by a small measurement error in the wave height. This can be confirmed when we look at figure 30c. The contact line of the bow wave at the second row of pressure sensors seems to be only slightly lower than the four meter line. However, the measurement in figure 31 shows a measured bow wave contact line at about 3.4 meter.

Generally, figure 31 seems to confirm what figure 30 already suggested. Even though the bow wave only consists of a particularly thin sheet, the pressure is relatively high even very close to the contact line. Further

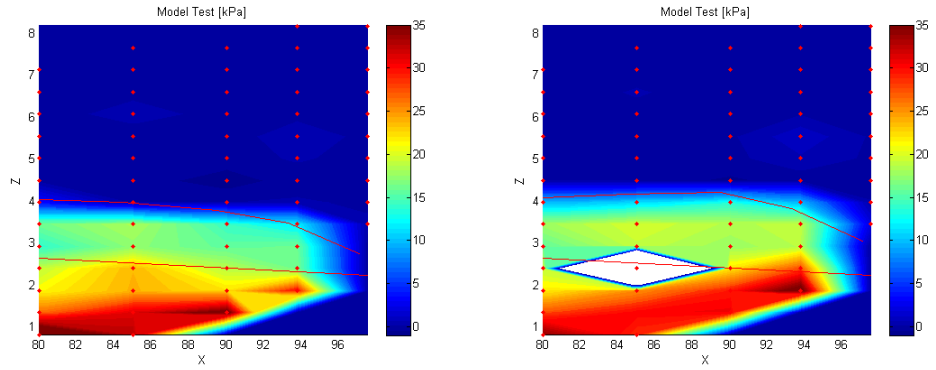

(a) Measurements first run

(b) Measurements last run

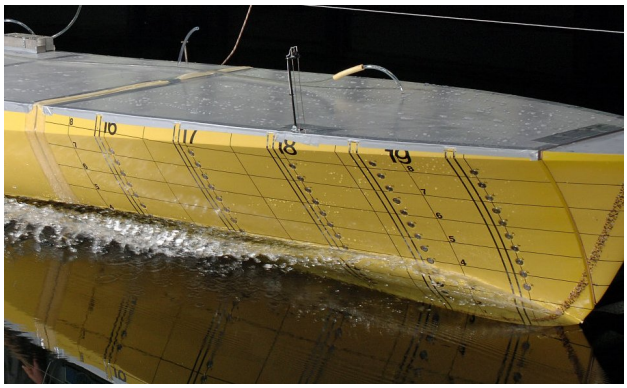

(c) Photo of the first run first run

Figure 30: Pressure and wave height measurements compared to photograph).

downwards the pressure increases slightly at a constant slope, that is smaller than the slope of the hydrostatic pressure. This is due to the effect of the water displacement by the bow that increases hydrodynamic pressure.

5.1.2 Simulation Results

The very same test that has been analysed as a model test in the previous subsection has also been simulated with a variety of input parameters. The pressures were interpolated at the same locations as where the pressure sensors were located during the model tests, but the wave height was registered for every panel along the waterline. This makes a direct comparison between the results of different simulation results with the measurements from the model test possible. From section 4, the most important simulation option to be varied proved to be the method for estimating the wave height on the hull surface.

Trim & Sinkage Since the model test was a free running self-propelled test, the exact trim and sinkage of the vessel at a speed of $F_n = 0.57$ can be measured. First, these will be compared to the trim and sinkage that the simulation calculates when the vessel is left free in all 6 DOF. The results are shown in the table 5. The table shows for both simulation and Model test the difference between trim and sinkage values at zero speed and at $F_n = 0.57$. So the values are entirely caused by the hydrodynamic forces on the hull.

Here, the z-axis is positive pointing upwards and the bow pointing downwards is a positive trim angle. An exact definition of the three options for dealing with the linearised boundary condition can be found in section 4.1.3. In short, IFSWAV 0 indicates that no free surface elevation at all is taken into account, while IFSWAV 1 and 2 refer to an estimated free surface elevation based on evaluation of the pressure near

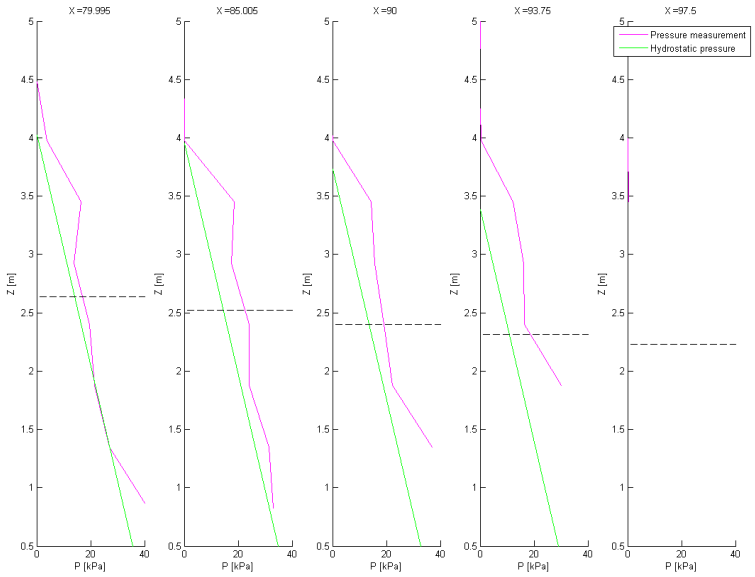

Figure 31: pressure measurements per bulkhead.

	Model test	IFSWAV 0	IFSWAV 1	IFSWAV 2
trim	$-1.3\,^\circ$	$-0.56\,^\circ$	$-0.69\,^\circ$	$-0.63\,^\circ$
sinkage	$-0.3m$	$-0.12m$	$-0.08m$	$-0.09m$

Table 5: Comparison trim and sinkage.

the hull - free surface intersection. The difference between IFSWAV 1 and 2 being the exact location that has been chosen for this pressure evaluation. Independent of method that is used to estimate a local wave height, we see that all simulations quite severely under estimate the change in trim and sinkage due to the forward speed. When looking at the difference in sinkage, the (average) difference between model test and simulation of 0.2 meter translates to a difference in hydrodynamic z-force of about 12% of the ships displacement. Simply put, at the given speed, the simulated vessel floats too high while less bow-up trim than should be expected according to the model tests.

One possible reason for this is the suction of the propellers underneath the aft ship. Just like with the waterjet propulsion used with hull m8325, a propeller does not only create a horizontal propulsion force, but also introduces a significant suction on the stern of the vessel. This effect is not modelled in the simulation and might possibly explain why the hydrodynamic heave relatively spoken is off more in this case than it was in the steady tests with hull m8325 at similar Froude numbers. However, the entire difference in trim and sinkage can not be explained by this effect. Hence, there still is a significant difference in dynamic heave between model tests and simulations that can not be explained. Moreover, with these tests on the FDS hull, it can be confirmed that this difference is not a consequence of the m8325 hull shape. Further more, in addition to the dynamic heave, also the dynamic trim is off in the simulations. Since the heave force also provides by far the largest component to the pitching moments, this can be translated to the conclusion that the heave force calculated by the simulation is off in magnitude and in centre of effort.

Pressure Distribution The next point of interest that was given for these calm water tests are the pressure measurements obtained from the bow area. While pressure distribution and wave elevation are closely linked, especially within simulations with linear free surface boundary conditions, it is worthwhile

looking at both separately. For a detailed explanation of how a wave elevation is estimated even in the simulations using linear free surface boundary conditions, one can refer to the paragraph about free surface elevation within section 4.1.3. For the purpose of this section, it is important to understand that when linear boundary conditions are used, the pressure on the calm water line can be used to estimate the local wave height. For the pressure distribution resulting from the simulations two separate aspects are of interest.

First, the pressure underneath the calm water free surface (that is a result of the hydrodynamic solution of the potential flow equations) can be compared between model tests and simulations, giving an idea about how close the potential flow solution with linear boundary condition comes to the actual viscous flow. Secondly, from the captive simulations described in section 4 we know that even solely the pressure above the waterline can have a significant influence on the over all forces on the vessel. Looking at the pressure measurements above the still water surface can indicate whether the linear pressure stretching from the pressure evaluated at the calm water surface to a zero pressure at the instantaneous water surface is actually an accurate representation of the pressures in a breaking bow wave occurring during the model test.

To be able to compare pressure and wave heights at identical trim and sinkage, separate captive simulations at the trim and sinkage measured during the model tests are necessary. The results of these captive simulations will be compared to the model tests described in section 5.1.1. The three linear Panship pressure distributions are compared to the model test measurements in figure 32.

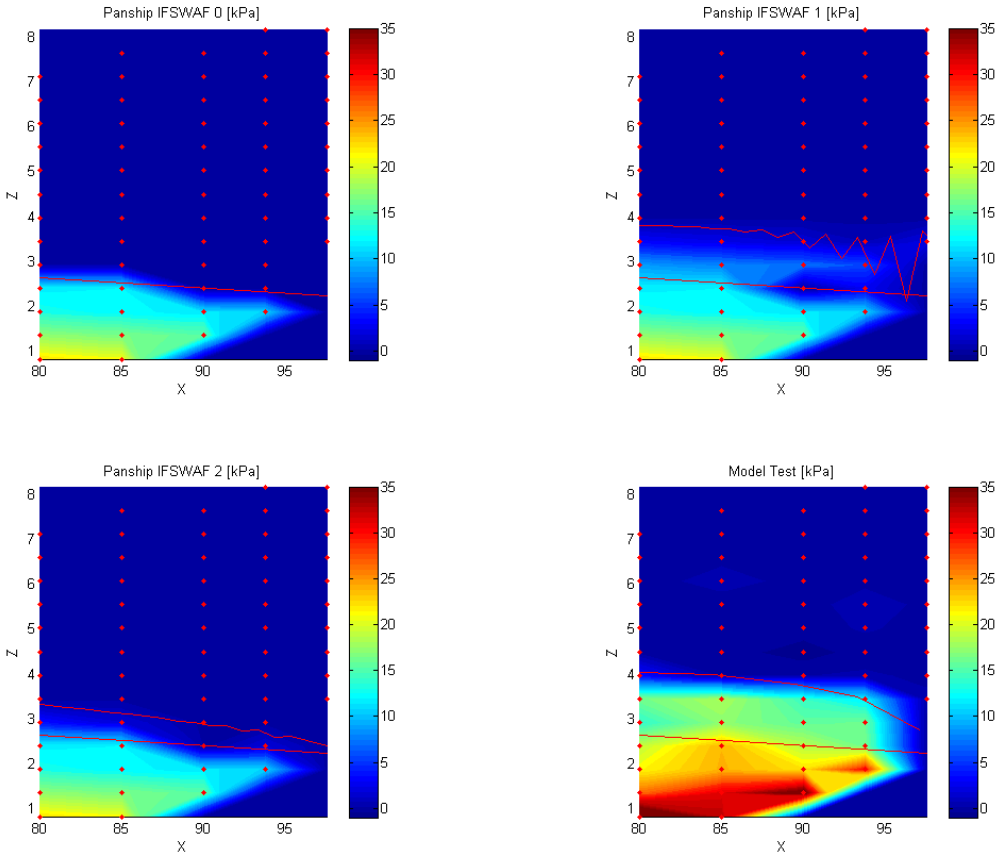

Figure 32: pressure distribution in linear Panship simulation compared to model test

Again, the figures show the pressure distribution in a projection of the bow area on the x-z plane. For orientation, all pressure measurement locations as well as the location of the calm water and the actual waterline are indicated as well. As expected, in the upper left figure there is no wave elevation since this option was turned off during the simulation (IFSWAV set to 0). For the other two simulation results, a wave elevation is present that in more or less extreme form shows some unexpected oscillations near close to the bow. As explained in [24], this is the effect a numerical evaluation of integrals within the Green function. A filter could be added to reduce the visibility of those numerical instabilities, however, this would not necessarily improve the simulation. For the purposes of this validation study, it is sufficient to assume that the effect of those instabilities have a negligible effect the vessel's motions and that to treat the calculated bow wave as if it would be an average between those oscillating points.

Clearly, the pressure in the bow area above, as well as under the still water surface is underestimated by all three Panship simulations. The difference goes up to around 15kPa in the lowest pressure sensors. This indicates, that the potential flow leads to lower pressures in the bow region compared to viscous flow and will certainly have an effect on trim and sinkage. Secondly, the linear pressure stretching above the waterline seems to under predict the pressure. The model tests show a pressure distribution that is more or less constant from the calm water free surface up to a point very close to the actual wave height, leading to high pressures even very close to the top of the breaking bow wave. A question that has to remain unanswered is whether this is the case only within a breaking wave, or if this can generally be observed.

Wave Elevation Finally, a last aspect of the simulation results that can be validated with these calm water tests is the wave profile along the hull. In addition to the two different wave profiles obtained with linear free surface boundary condition, the same simulation was also performed with non linear boundary conditions using Panship as well as Rapid, another nonlinear panel method code described in [7]. This creates an additional possibility to get an idea about which simplifications to the simulation method cause significant differences between model tests and simulation.

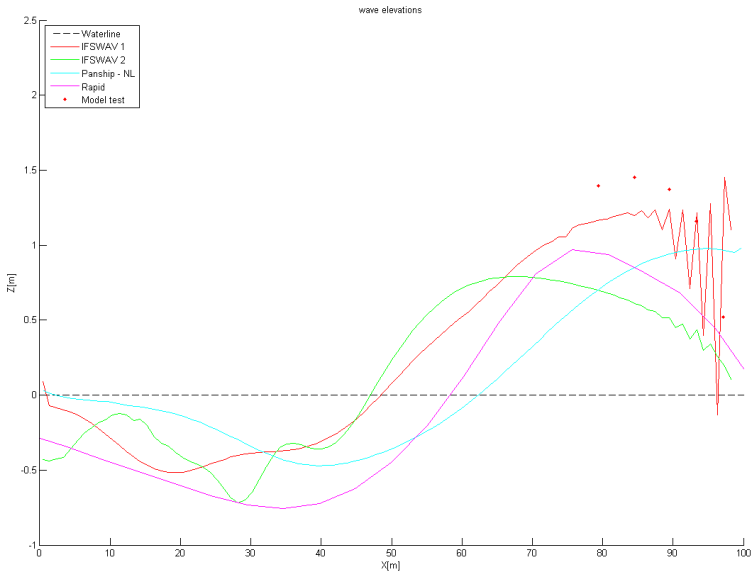

Figure 33: Free surface elevation along the side of the hull.

As a direct consequence of the pressure, also the wave elevation in the bow region is under predicted in all simulations compared to the model test measurements. Except for numerical instabilities near the bow, the

prediction of Panship with linear free surface boundary conditions and the wave elevation estimated based on the pressure on the upper most submerged panel row seems to be closest to the model test results in the bow region, even compared to simulations that use nonlinear boundary conditions.

Generally, the observations concerning the free surface elevation are coherent with the results for Wigley hulls obtained by de Jong in [24]. Like for the Wigley hull, for the current hull shape the linear version of Panship predicts a longer bow wave than the RAPID calculations. Panship with nonlinear boundary conditions predicts a very short bow wave. This is due to a mathematical filter that is applied that averages a number of wave elevations closer to the stern in order to suppress numerical instabilities. In the aft ship the two linear predictions lie in between the nonlinear simulations. Unfortunately, there are no usable measurements from the model test in this region.

The fact that all linear and non linear potential flow simulations show an under estimation of the wave height indicates that this is a general consequence of the potential flow model. Note that for the simulation with linear boundary conditions, in other conditions (hull m8325 at $F_n = 0.74$ with 10 degree drift angle) the simulation resulted in unrealistically high bow waves. So at least for the wave height based on the pressure on the calm water free surface, the quality of the bow wave prediction strongly depends on the tested conditions. As was already indicated in the conclusions of section 4, it seems that a lower bow wave in the model test leads to under prediction while a higher bow wave in the model test leads to over prediction.

5.1.3 Conclusions

For the free sailing tests in calm water there were three points of interest that should help validate simulation results. First the steady trim and sinkage of obtained in the simulation could be compared to the ones measured in model tests, giving an idea of the calculated hydrodynamic heave forces and pitch moments. Second, the pressure distribution in the bow area can already give a first hint towards the reason of discrepancies between heave and pitch in model tests and the pressure within the bow wave can be used to validate the pressure stretching between the instantaneous free surface and the calm water free surface. Finally, in the bow section the wave profile along the hull can be validated.

From the trim and sinkage results, it can be seen that the over predicted hydrodynamic heave force can again be found. Moreover it can be concluded that the in the simulations, the bow up trim due to forward speed is underestimated. The pressure distribution in the bow area certainly gives an indication about the cause of the difference in trim and sinkage between simulations and model tests. When the simulations would show an equally high pressure in the bow area, more bow up trim would without a doubt be the consequence. However, this would cause the dynamic heave forces to increase even more, resulting in an even larger difference in sinkage between model test and simulation. Hence, from these pictures of the pressure in the bow section we can conclude that there is an even larger difference in vertical forces caused by something else than the pressure in the bow area. First, it could be that in the model tests the pressure in the mid and/or aft section of the vessel is significantly lower than in the simulations, causing the vessel to sink in deeper and introducing a more bow up stern or, secondly, the additional downward force in the model tests is not caused by pressure, but by a vertical component of the viscous drag that is not included in the simulation.

From the results of the wave height measurements along the hull two conclusions can be made. First, all potential flow codes tested underestimate the bow wave height in the tested conditions indicating that generally in potential flow the pressure in the bow area is underestimated. Hence, the underestimation is not a consequence of the linear free surface boundary conditions. Secondly, when linear boundary conditions are used, the wave height is slightly under predicted in the conditions tested here, but significantly over predicted in conditions that lead to higher bow waves. This leads to the conclusion that the local wave height (at least in th case of a breaking bow wave) is not linearly dependent on the pressure on the calm water free surface.

test condition	number of heave maxima	H_S[m]	T_p[s]	heading[°]	v[knots]	number of runs
1	71	3.8	8.5	300	17	5
2	37	3.8	8.5	300	23	7
3	79	3.8	8.5	315	17	5
4	0	3.8	8.5	315	23	0
5	65	3.8	8.5	330	17	5
6	0	3.8	8.5	330	23	0
7	48	3.8	8.5	345	17	5
8	94	3.8	8.5	345	23	7

Table 6: Test matrix of stern quartering irregular waves.

5.2 Stern Quartering waves

Next to the runs in calm water, there were tests carried out in irregular stern quartering seas. The objective of these tests in stern quartering waves is mainly to give a practical indication of error margins of simulations in stern quartering waves. When waves are added the conditions become so much more complicated that it will be hard to pinpoint reasons for differences between model tests and simulations. Hence, for the goal of finding possible improvements to the simulation method, these tests will not contribute much. However, for the future use of the given potential flow code, it certainly is of great interest to given an idea of accuracy of ship motions in irregular stern quartering waves.

Therefore, the main difficulty while validating simulations in irregular stern quartering waves will be to find ways to accurately present and quantify differences found between model tests and simulations. For this, two different approaches will be used. First, a statistical analysis of the vessels motions will be given, and secondly, a deterministic approach is presented, comparing the vessels response to (nearly) identical wave train realizations in simulations and model tests.

It should be noted that the sea states tested in this chapter are relatively extreme. With a significant wave height of 3.8 meters, peak wave heights of over 6 meters were found. Even for a frigate of the given size, these conditions represent the boundary of what is sailable without encountering regular extreme broaches and capsizes. This can be concluded by the fact that initially the GM value was reduced from 2.5 to 1.5 meters to be able to observe more extreme broaches. However, after the model capsized in the first wave it encountered, the GM was increased again. Although no capsize was encountered in the runs that are presented in this report and the yaw angle never exceeded 25 degrees, it is save to say that conclusions can be drawn about the operational safety up to a point where it is definitely not safe anymore.

Test Matrix For these tests, a JONSWAP wave spectrum was used with 4 different incoming wave angles between 300 and 345 degrees. The characteristics of this spectrum (in full scale values) were a significant wave height of 3.8 meter and a peak wave period 8.5 seconds. All four headings were tested in two different speeds. The engines were then kept at the same RPM that was used before to obtain calm water speeds of respectively 17 and 23 knots (full scale) or $F_n = 0.28$ and $F_n = 0.38$. Of course, because of the stern quartering seas and resulting surf riding, a large variation in speed was observed during the tests. For each speed and each wave angle, a total of about 850 seconds of sailing was measured, which resulted in respectively 5 and 7 runs per wave angle and per speed. A total spread sheet of the tested conditions can be found in table 6. Unfortunately due to a lack of time, the runs at 23 knots with a wave direction of 315 and 330 degrees had to be canceled.

Propulsion and Steering Since the tests in stern quartering waves are free sailing tests including propulsion and autopilot, these are two additional aspects that have to be taken into account. In contrast to the

calm water tests, now the inflow velocity and angle on all appendages may vary in time, and the resulting propulsion/steering forces will depend on that. For this reason it is important to be aware of possible differences between model test and reality, and to try to minimise these. Especially since both propeller and rudder are modelled empirically in Panship, time dependent hydrodynamic effects might not always be included correctly.

In Panship, the time dependent propulsion force is based on the open water diagram of a Wageningen B-series propeller with the ship's time dependent speed in X-direction as inflow velocity. This means that, changes in the momentary speed due to for example surf-riding will be taken into account for the calculation of the propulsion force. However local velocities in waves are not taken into account, and moreover, since only the ship's velocity in X-direction is taken into account, larger yaw angles in the case of a broach will lead to significant inaccuracies in inflow velocities and thus propulsion force and resulting steering forces. For the rudder, two different ways of calculating the inflow velocity and direction will be tested.

First an empirical formulation to find the inflow direction and velocity. Basically , like with the propeller the instantaneous speed in x-direction is used, creating errors in case of larger yaw angles or local flow velocities due to waves or hull - appendage interaction. However, this option uses slightly less computational time. The second option includes the effect of waves and speed variations by evaluating the flow at the location of the rudder at the instantaneous location of the vessel. Especially when simulations in stern quartering waves are considered, this can vary significantly from the velocities obtained before. However, it comes at the cost of a slightly higher computational time.

Verification Since there are a couple of new aspects to these simulations in stern quartering seas, it is useful to perform a short verification of some input parameters that might be important in stern quartering seas. The new aspects to the modelling are mainly an effect of the introduced motions and the importance of course stability. In order to get those right, the exact appendage geometry, as well as the autopilot settings are of great importance. Due to the fact that 850 second simulation runs are very time consuming, one test condition was selected to compare different input variables. For this the run at 17 knots with a wave heading of 330 degrees was chosen, since initially, these lead to a broach in the simulation, but not during the model test. The parameters that were tested are:

Rudder inflow direction and velocity: As explained in section 5.2, one can choose to use the actual flow velocity at the time step at the location of the rudder instead of simply the forward speed of the vessel. In the case of stern quartering waves, there might be a significant difference in direction and magnitude between these two velocities. However, using the local flow velocity comes at the cost of a slightly higher calculation time

Viscosity: While up until now, for all tests the viscosity of the full scale vessel was used for all simulation, this might not be entirely accurate for the runs in stern quartering waves. When model viscosity is used, the total drag of the vessel is increased, leading to a higher rate of revolution for the propeller, which again leads to a higher incoming flow velocity on the rudder and to higher lifting forces. Thus, using the model viscosity might lead to improved directional stability and prevent the vessel from broaching.

Appendage geometry: Generally, implementing the exact geometry off all appendages that are not included in the panel distribution is hard to do. They are included in the simulation by means of empirical formulations and simple analytical models based on their position and some dimensions. These necessary dimensions are not always given in the technical drawings, and even if they are, extraordinary shapes and appendage-appendage or hull-appendage interaction are never taken into account. Amongst others, some attention has been put into correctly modeling propeller shafts and bilge keels. The propeller shaft diameter and the chord length of the skeg were increased to better fit the technical drawings.

Autopilot settings: During the simulation, as well as during model tests an autopilot has been used to keep the vessel on its course. These autopilots regulate the rudder angle based on the instantaneous rate of turn, yaw angle and sway position, with a maximum excitation and angular velocity given. Especially

maximum rudder angle	δ_{MAX}	35	deg
rudder angle per degree course deviation	C_Φ	3	deg/deg
rudder angle per deg/s rate of turn	B_Φ	11.62	deg/(deg/s)
rudder angle per m transverse course deviation	C_Y	0.7	deg/m
maximum rudder rate of application	$\dot{\delta}$	10.33	deg/s

Table 7: Autopilot settings.

the rudder angle based on the transverse position has been varied with great effect on simulation results. Very significantly, when this parameter was decreased, the number of capsizes significantly increased. The autopilot settings that were used in model test as well as in the presented simulation results are shown in table 7.

Additionally, because in the calm water simulations the pressure distribution above the calm water free surface proved to have a very significant effect on the over all forces and moments on the hull, Both options for estimating a wave height based on the pressure near the hull-free surface interaction were tested for all simulation conditions.

In figure 34, the Y position, heel and yaw angles during several simulations are plotted against the time. All these simulations were taken in the same wave spectrum with identical initial random seeds. This means that the resulting wave pattern is identical for all pictures. Only as time passes, the vessel's position in the waves will vary due to different motions resulting from different input. The bow waves were calculated based on the pressure on the upper most row of submerged panels. The most important conclusion from these time traces is that while initially the ship did broach severely, this is reduced significantly by only minor changes to the simulation input. During the statistical analysis, these differences between the time traces have a very large effect on mean values and standard deviations. Basically, one broach that occurs during only one of both the model test or the simulation makes the statistical data incomparable. Another phenomenon that was observed not only in this condition, but every time a severe broach occurred in the simulation, is that instead of going back to a zero yaw angle immediately, the ship makes a complete 360 degree turn before advancing. This is clearly an error in the simulation, since in reality there would be no reason for an autopilot to make such a turn. This error might be caused by an extreme violation of assumption that a straight course is sailed, that is used in the evaluation of the Green functions.

As one can see, except from varying the inflow velocity on the rudder, any of these changes prevents the simulation from broaching in this case. Still, switching on the more exact calculation of the rudder inflow velocity reduces the maximum yaw angle in the broach to about 50 degrees. All in all, each of these little changes has a very significant effect on the output, stressing the importance of getting every detail of the simulation input right. On the other hand, this might show that the simulation is over sensitive to little changes, and that results can be tuned into any direction, within the given accuracy of the input parameters and geometry. In order be sure if this is the case, several model tests with the same minor geometry changes would have to be carried out, to see if these indeed have a dramatic effect on the ship's motions.

An example of the input files used is given in appendix D. This example file implements test condition 1 with 17 knots of boat speed, wave angle of 300 degree's and a testing period 850 seconds. Next to the main input file, in this case there has to be also a rudder control input file to set the correct settings for the autopilot. These settings are kept identical in the model test and the Panship simulation. Table 7 shows the values that were used.

5.2.1 Statistical Validation

As a first method of comparison between model test results and simulations, the statistical properties of measured and calculated ship motions can be analyzed. When the number of wave encounters is large enough, the statistical properties of a ship operating in the same wave spectrum should be independent of

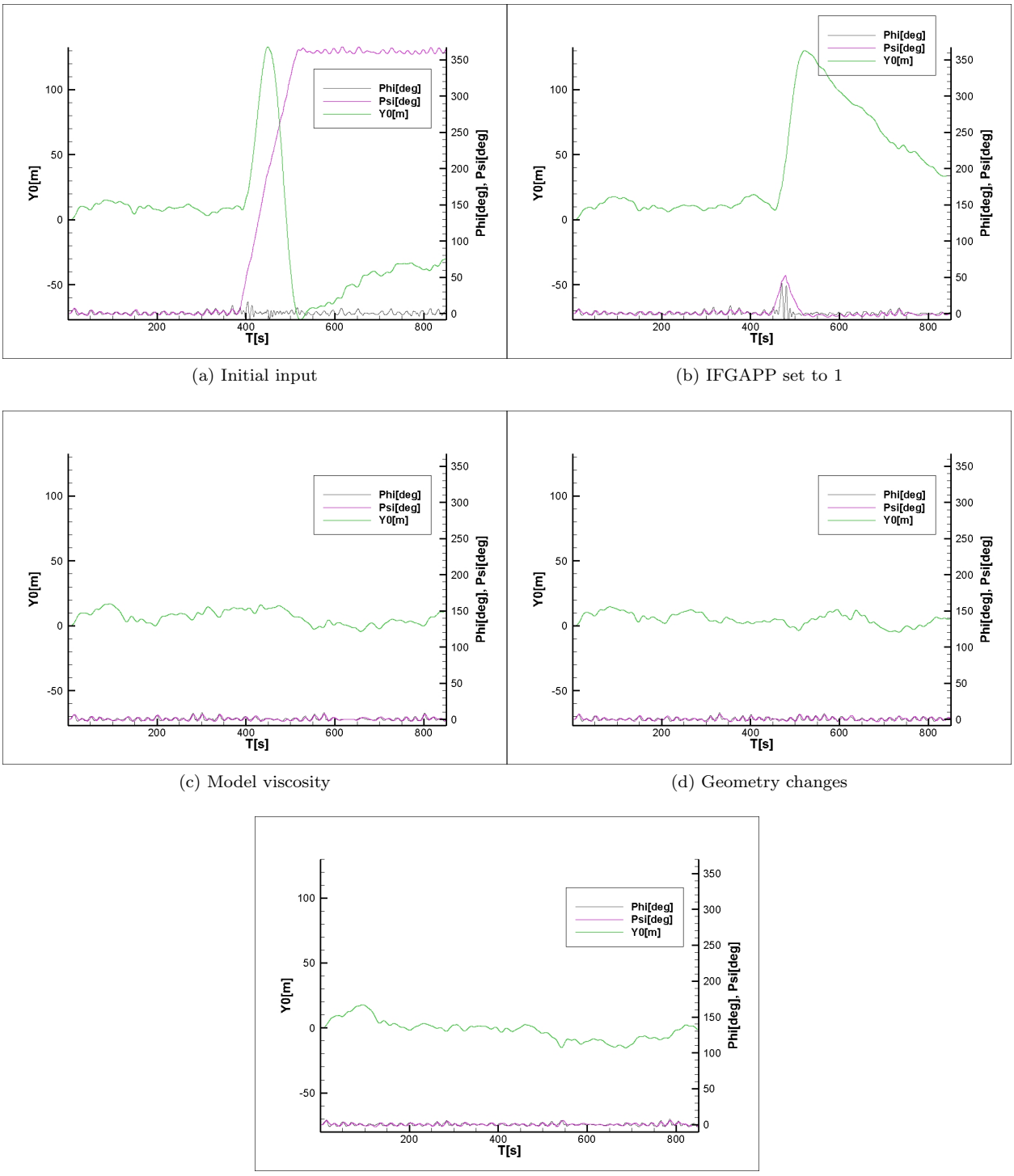

(a) Initial input

(b) IFGAPP set to 1

(c) Model viscosity

(d) Geometry changes

(e) all changes combined

Figure 34: Time traces of Y position, heel angle(Phi) and Yaw angle (Psi)

the actual wave train that was realized. This makes it easy to compare the measured data from the model tests to predictions made by a simulation.

One important question however is how large the tested time span should be in order to obtain statistically representative data. As mentioned before, adding all model test runs in identical conditions, the available time that has been measured is about 850 seconds. As mentioned in table 6, this leads to somewhere between 40 and 80 maxima in the heave motions of the vessel. Usually, in order to be statistically significant the number of wave encounters should be at least around 200. However, by comparing a number of simulations of 850 seconds with different realizations of the wave train, a good impression can be obtained about the dependence of the data on the wave train realization. For this, 10 different random seeds were used for the simulation wave train. The initial seeds that were used can be found in appendix F.

Another aspect that proved to be of significance is the occurrence of extreme broaches and capsizes when varying the autopilot settings. During the model tests no extreme broaches occurred and the maximum yaw angle did not exceed 25 degrees. During simulations with identical autopilot settings, some extreme broaches took place up to yaw angles exceeding 50 degrees and even one capsize occurred when sailing at 17 knots in waves from 300 degrees. However, the chances of a broach or capsize occurring seem similar in simulations and model tests. In sharp contrast to that, when the rudder angle per meter transverse course deviation was decreased, the chances of severe broaches and capsizes increased significantly. In the most extreme case 7 out of 10 of the tested random seeds lead to a capsize when the vessel was sailing at 17 knots in waves from 300 degrees.

To keep the amount of data in this report limited, one representative test condition will be examined closely. The figures of all other conditions can be found in appendix E. For 17 knots average speed and a wave heading of 330 degrees, the statistical results are shown in figures 35 to 37. Here IFSWAV 1 represents data from simulations where the bow wave height was estimated based on the pressure evaluated on the upper most row of submerged panels, while in the case of IFSWAV 2 this was done based on a pressure evaluation in a location with a certain horizontal offset from the hull.

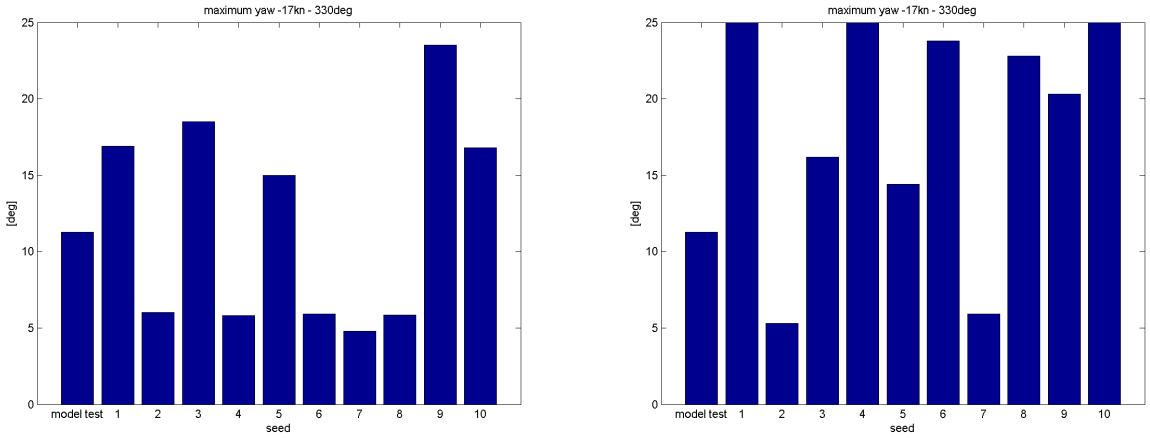

(a) IFSWAV 1

(b) IFSWAV 2

Figure 35: Maximum encountered yaw angles, for IFSWAV 1 and IFSWAV 2, for 17 knots, 330 degrees wave angle

Maximum Yaw Angles First, the maximum encountered yaw angles are compared between the model test (left most bar), and the 10 random seeds. This gives an approximate measure of the severeness of the most extreme broach that occurred during the run. In these conditions, all random seeds resulted in usable simulation results. One thing that can be observed immediately, is that there are very significant differences between the wave train realizations. The largest encountered yaw angle varies between about 5 and almost 30 degrees. Even between IFSWAV 1 and 2 there seem to be large differences in some cases. However, since

small differences in the ship's yaw angle accumulate during a run, this can just be the effect of the vessel encountering different waves towards the end of the simulations.

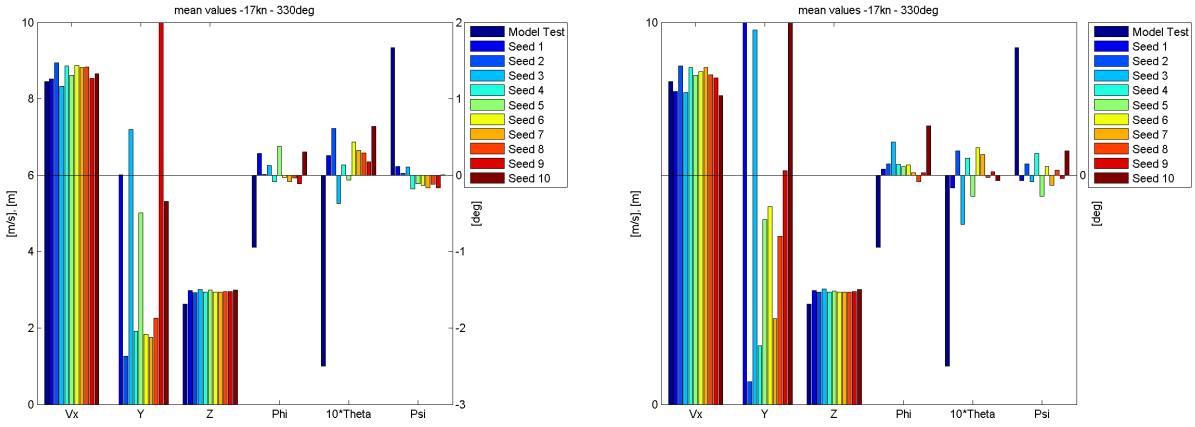

(a) IFSWAV 1

(b) IFSWAV 2

Figure 36: Mean values in all six degrees of freedom, for IFSWAV 1 and IFSWAV 2, for 17 knots, 330 degrees wave angle

Mean Values Next, the mean values in all six degrees of freedom are shown in figure 36 (notice that in x-direction the speed has been chosen instead of the position, this is to ensure meaningful results). Notice that the variations in θ were very small, so that the values have been multiplied by 10. Another point to notice is that the mean Y value has been set to zero for the model test. For the Panship runs, Y=0 is kept at the initial position of the vessel. This means that the mean values in Y-direction can not be compared between model test and Panship based on this figure. However, since the standard deviation is independent from the mean value, these can still be compared in figure 37.

The mean value of time traces gives one indication about the similarity of two random signals. However, it has no information at all about contained frequencies and, what is more important in this case, systematical errors are not filtered out. Moreover, from the time trace of the Y-position in figure 34b we can already see that one single random event (in this case a broach) can completely spoil the mean Y-value. Therefore it is safe to assume that 850 seconds is not enough to come to statistically significant values for the mean Y-position and Yaw angle. Nevertheless, for all other degrees of freedom, some conclusions can surely be drawn based upon these mean values.

When it comes to the results, one thing that is obvious immediately is the huge variation between mean Y-positions. Where the variation in speed in x-direction and the z-position is small, the Y-position differs up to more than 10 meters per run. One look at the time traces shown in figure 34 shows that this is because even small broaches already have huge consequences for the motions in Y-direction. Nevertheless, for this vessel, 10 meters is still only a little less than a ship's width. Next, one thing that can be observed is that the mean Z-position in the model test is slightly lower than in all all and the trim angle θ is about 0.2 degrees smaller. This is consistent through most tested conditions and reflects the conclusions on trim and sinkage made in section 5.1.2: Simulations consistently underestimate the bow up trim and overestimate the rise due to forward speed. One new, but obvious difference between model test and Panship results is that mean heel angle. Though not always as clear as in the presented case, this is in most conditions significantly smaller in the model test and often of opposite sign. Concluding, it should be noted that for a vessel in a wave heights of about 4 meters, the differences between model tests and simulations seem relatively small.

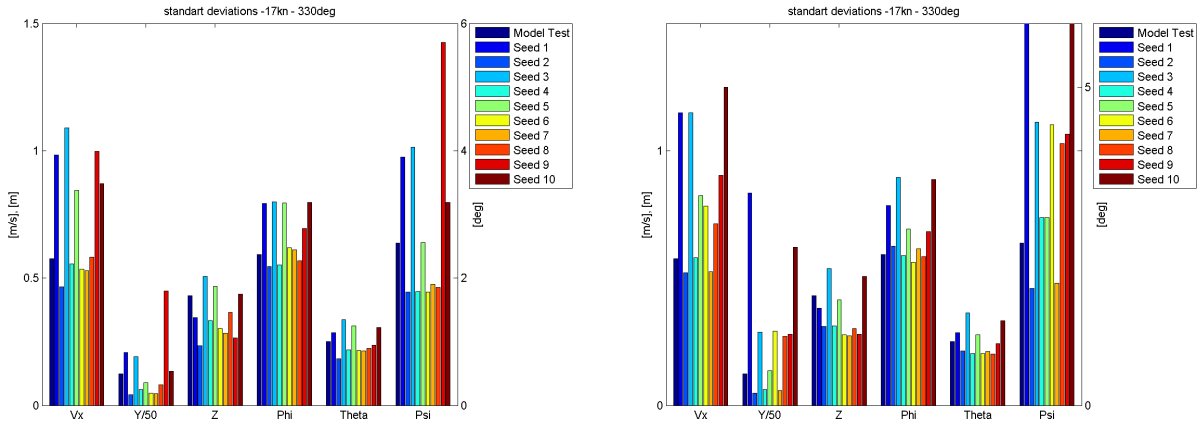

(a) IFSWAV 1

(b) IFSWAV 2

Figure 37: Standard deviations in all six degrees of freedom, for IFSWAV 1 and IFSWAV 2, for 17 knots, 330 degrees wave angle

Standard Deviations Next to the mean values, in figure 37, the standard deviation is a good measure of the similarity of two random signals. In contrast to the mean value, the standard deviation gives information about the deviation from the mean value. Especially for the ship motions in waves this can be an interesting parameter, since it gives an idea about the amplitude of motions that can be expected. Moreover, since it is independent of the mean value, systematical errors are filtered out and signals can still be compared.

For the standard deviations, the different random seeds seem to lead to smaller variations. However, take into account that the Y-values are divided by 50 in order to fit into the graph. Nevertheless, for all degrees of freedom, all random seeds used for simulations remain within the same order of magnitude, and independent of which location has been chosen to evaluate the pressure for the wave height (IFSWAV 1 or 2), the simulation results and the model test results seem quite similar. At least within the possible range caused by different wave train realizations. When comparing IFSWAV 1 and 2, it seems that in the presented case IFSWAV 2 results in slightly more extreme values: The spread between different random seeds is becomes larger when this option is chosen. However, compared to the large impact that the pressure evaluation location had in the calm water and captive tests, the difference in these situations is remarkably small. Also, when the same simulations were run with a smaller rudder angle per transverse course deviation in the autopilot settings the effects of IFSWAV 1 and 2 were inversed.

Probability of Exceedance One last tool to evaluate the similarity of model test and simulation time traces is a probability of exceedance curve. For the yaw and heel angles these plots were made for all six conditions where model tests were available. these plots give more detailed information about the random signals that in these cases represent time traces of the vessel. Again, to get an idea of the spread that is to be expected between several runs of 850 seconds each, the 10 different wave train realizations that were simulated are shown as separate lines. All plots can be found in appendage G, two extreme cases will be presented in figures 38 and 39. One with waves from 345 degrees and relatively small motion amplitudes and one in waves from 300 degrees with relatively large amplitude motions.

For both roll and yaw motions it is obvious that waves that come in further from the side the spread in encountered angles becomes larger.It is interesting to see that for even in the simulations where waves came in from 345 degrees, there seem to be two wave train realizations that lead to at least one extreme broach to more than 25 degrees of yaw, while all other wave trains show similar behaviour. Further more, there are two characteristic differences between model tests and simulations that could be found in most of the tested

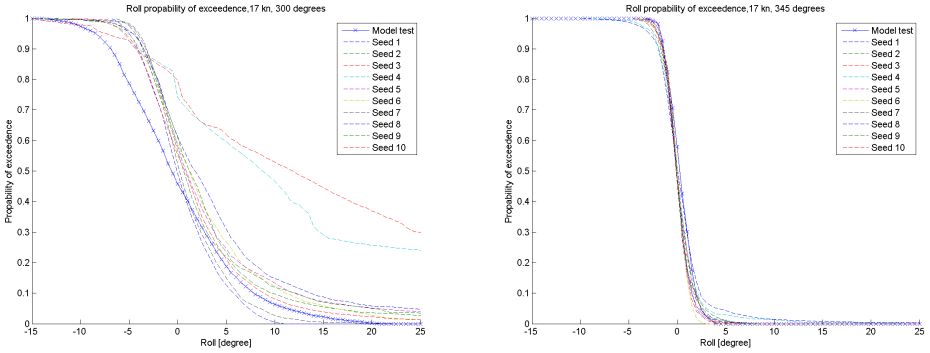

(a) 17 knots, 300 degrees

(b) 17 knots, 345 degrees

Figure 38: Probability of exceedance curve of roll motions for two different wave directions.

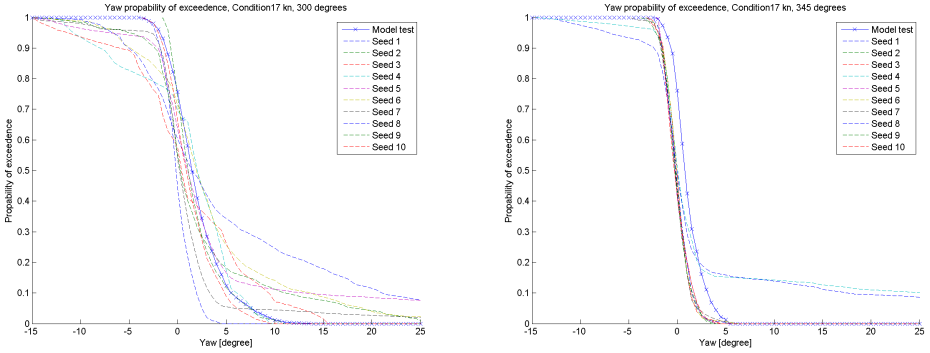

(a) 17 knots, 300 degrees

(b) 17 knots, 345 degrees

Figure 39: Probability of exceedance curve of yaw motions for two different wave directions.

conditions. First, as can be seen in figure 38a, for the roll motions the probability of negative roll motions often is larger for the model test than for all simulated wave trains. This matches very well the difference in mean values observed in figure 36. However, for positive heel angles the simulations match the model test results quite well. Secondly, for the yaw probability of exceedance, in some cases the model test curve lies significantly further to the right of the plot as can be seen in figure 39b. Except for this constant difference, the model test results and the simulations seem to show parallel curves.

Conclusions Based on the statistical analysis of the vessel's motions in all six degree's of freedom, it can be said that generally the simulation results and the model tests match well. Differences that do exist are small, in any case not creating or preventing a 'dangerous' situation and largely depending on the situation that has been tested.

Another conclusion is that, while the location at which the pressure for the wave height is evaluated had a very severe impact on the forces on the hull during clamped drift variations, this is largely reduced in the simulations for aft in coming waves. If anything, the spread between different wave trains is slightly larger when the pressure is evaluated with a horizontal offset from the hull. However, this seems to be a random effect that is non existent or even inverses when different autopilot settings are used. This confirms the idea that the pressures above the calm water free surface become significantly more important at Froude numbers higher than 0.5.

The last, but a very important conclusion from this statistical analysis is that very close attention has to be put to the simulation input. Very small differences in input often do result in large differences in simulation results. A question that has to be raised is without doubt is whether this sensibility is realistic or not. Since only one series of model tests has been made, this can not be answered with certainty. What can be said is that for all four input variations tested in this section, the closer the simulation input matched the situation in the model tests, the closer also the simulation results matched the model tests. In relation to this, it might also be worth further investigating the effect of autopilot settings on the risk of capsizing, as results obtained during this project indicate a strong correlation.

5.2.2 Deterministic Validation

Another option to compare results of simulations and model tests in irregular stern quartering waves is to reproduce the exact wave train from the model test in the simulation and compare the resulting motions of the vessel. This approach is referred to as the deterministic approach. The advantage of this approach is that it is not necessary to perform long model tests with a sufficiently large number of wave encounters. Instead, short runs of ± 10 wave encounters can be used to compare the response of the vessel in the model test to the simulation results. The downside however is that for the exact reproduction of the wave train additional wave measurements during the model tests are necessary, and the correct state and position of the vessel at the start of the simulation, provides additional difficulties during the modelling process.

A second aspect of this deterministic approach is the vessel's position in the wave train after a certain simulation time has passed. It is safe to assume that there will be small differences - in the recreated wave trains as well as in the forces on the vessel arising from these wave trains - between model tests and simulations. However, over time these small differences in forces will lead to differences in the position of the vessel in the waves. The focus of this validation is not to see how fast the position of the vessel in a simulation deviates from its position in the model test. Rather the objective is to give a reasonable estimation of the quality of the simulations prediction of the vessel's motions due to a known position in the waves. Therefore, the increasing deviance in the vessels position in the wave between model tests and simulations should be prevented. This can be done by taking the measured position and rotation of the vessel during the model test as a the base for force calculations during the simulations.

For this deterministic analysis of the model tests in stern quartering waves, separate runs in all tested wave conditions were chosen based on the observed realisations of the wave trains. The objective was to choose one run with high waves and one run with relatively calm waves for each wave condition. In the end, it was not always possible to reproduce the measured wave trains, so that a total of 9 runs could be used for this deterministic validation. The details of these runs can be found in table 8.

Run number	Speed [kn]	Wave direction [deg]
704002	17	345
704003	17	345
704006	17	345
706003	17	330
707001	17	315
707005	17	315
708004	17	300
708005	17	300
709003	23	300

Table 8: Runs that were used for deterministic validation.

Recreating Wave Trains During the model tests the wave trains were measured in three positions around the vessel. One measurement in front of the bow, one behind the stern and one on port side, the side where the waves come in. In the end, the measurements on the port side of the vessel were used to recreate the wave trains in the simulations, since these were the measurements closest to the actual hull.

In order to be able to use the wave measurements in simulations, they were transformed into frequency domain. The resulting spectrum was in turn used as input for the simulations. Due to a discrete spectrum, and a limited frequency band that has been taken into account, during this transformation small changes in the wave height might occur. All comparisons between simulation and model test wave trains can be found in appendix H. The similarity between the wave trains varied, but to get an idea, two extreme cases are presented in figure 40.

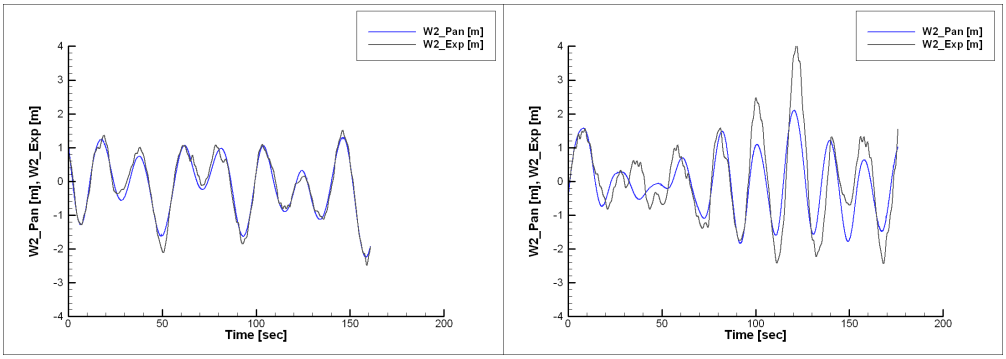

(a) Run 704002 (b) Run 706003

Figure 40: Wave trains reproduced in simulations compared to measurements during model tests.

Generally, the wave trains can be produced well in the simulations. In steep waves the exact amplitude of the wave is not always predicted well. Further more, in the towing tank small high frequency waves can be observed that probably are reflections from the sides of the basin. These frequencies lie outside of the band that is reproduced, so they can not be found in the simulations either.

Comparing Wave Forces As mentioned earlier, the objective of these deterministic validations is to validate the forces on the hull based on a known position of the vessel in the wave. This objective can be met best if the forces on the hull are calculated based on the position measured from the model test instead of based on the actually predicted position. This way, the deviation in vessel position between model test and simulation does not necessarily increase over time, and the full time of each run can be used to compare the forces in the model tests and the simulations.

Note that this concerns mainly the hydrostatic Froude Krilov forces, since for the hydrodynamic solution a body linear boundary condition is used. The hydrodynamic forces are still calculated based on the vessel sailing a straight line at the average speed. For this reason it will be interesting to see whether is a certain value for sway or surge motions beyond which the simulation accuracy will drop significantly.

Starting Position One additional factor that might play a significant roll is the start of the simulation. During model tests, first waves are started, then the vessel accelerates, and finally when it is sailing in steady conditions, the measurements are started. For the simulation, the vessel is placed at the location where the measurements started and instantly accelerated to the chosen speed. In the first seconds of the simulation, there are no free surface memory effects present, that would normally influence the positioning of the

vessel. Only after a progression of several boat lengths, accurate results can be expected from the simulation.

To deal with this issue, a couple of options have been tested. The simplest option is to create a switch on period in which the waves are slowly increased from zero to the desired wave spectrum. Of course this will lead to less severe motions of the vessel in these first seconds. However, it might be that in the end these motions are more realistic than what would be calculated without any memory terms present.

Secondly, it is possible to obtain the values of the free surface memory terms from a previous run in calm water. Physically spoken, this represents the vessel sailing in calm water up until the simulation start when the wave state at that point in time is added. Of course, for this option two simulation runs are necessary, one in calm water and the actual simulation in deterministic waves.

Finally, an option that is slightly more difficult to implement into the simulation code, but that most probably will lead to good results is to hold the vessel captive on the course that has been measured during the model test for the first seconds. This way, the memory terms can be established in these seconds based on the actual position of the vessel as obtained from the model test. At the start of the validation period, the vessel not only has the exact position in the wave that has been measured during the model test, but only the free surface memory effects that result from the course that the vessel sailed during the model test.

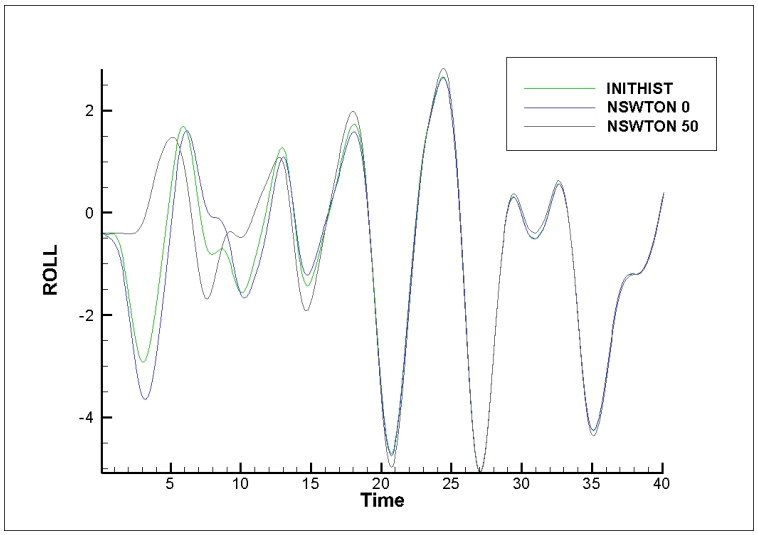

Figure 41: Simulation results resulting from different approaches to the switch on period.

Figure 41 shows pitch and roll motions for the first three tested options for one run. Obviously, changing this options has a significant effect on the position of the vessel during the simulation especially during the first seconds of the simulations. Especially using a switch on period of 50 time steps (as indicated by NSWTON 50) leads do different results during the first 25 seconds. Later during the simulation, in the three time traces come closer again, however, they never merge completely. For this reason, for the validations shown in the next paragraph, the option to keep the vessel captive on the measured course from the model tests for the first 30 seconds has been implemented in the simulation code. This way, the most accurate results can be obtained.

Results Of course, the results from the simulations depend on the wave train that is used as input, and as described earlier, the similarity between simulation wave train and mode test wave train varies. For this reason the two runs of which already the wave trains are shown in figure 40 will be examined in this paragraph. The time traces of all degrees of freedom of all other runs can be found in appendix H.

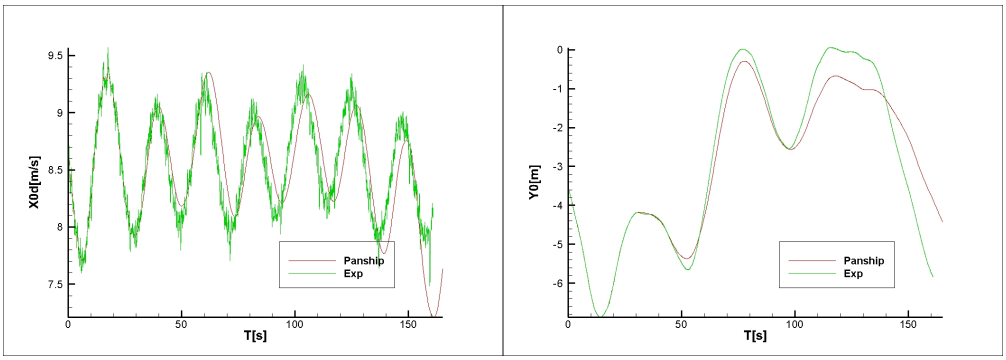

(a) Speed

(b) Sway

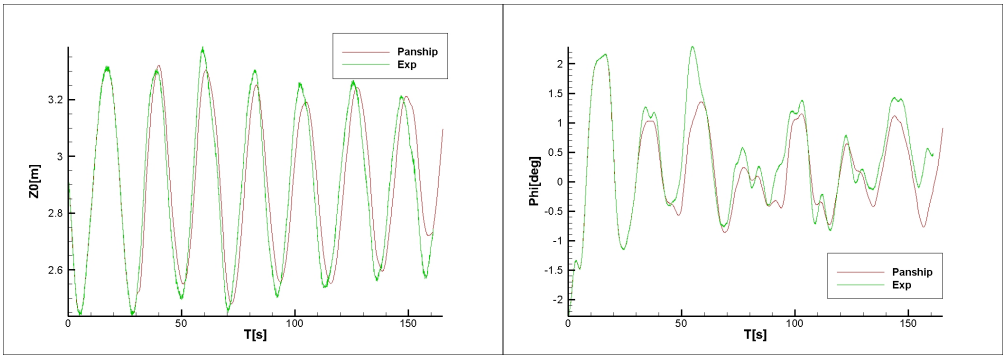

(c) Heave

(d) Roll

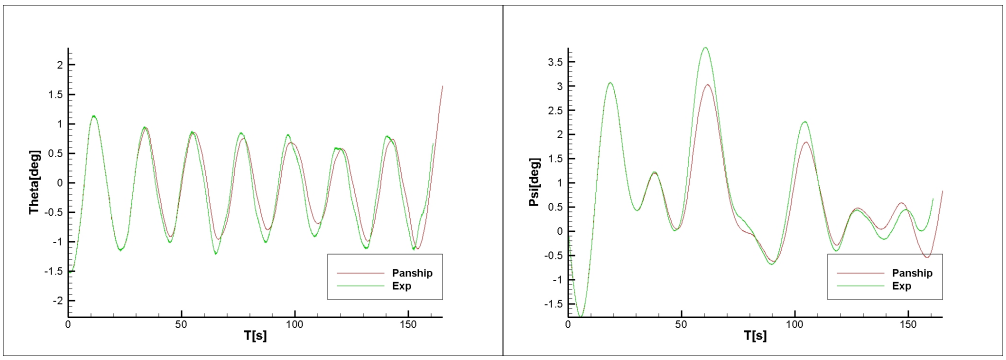

(e) Pitch

(f) Yaw

Figure 42: Time traces of model test and Panship for run 704002.

The results presented in figures 75 and 78 represent well the general findings in other runs. First of all, similarity of the vessels motions does strongly depend on the similarity of the wave trains. The switch on period of 30 seconds is clearly visible, in which the vessel is kept captive on the course measured during the model tests. After that differences between model test and simulation start to emerge. Looking at the sway motions, large discrepancies tend to develop over time. Apparently, the restoring spring term for sway motions that is introduced with the autopilot is small compared to the exciting terms introduced by waves.

Like with the wave trains, the most significant differences that can be seen in the vessels motions are the motion amplitudes and the high frequency response. Especially for the latter, it is reasonable to assume that it is a consequence of the high frequencies missing in the simulation wave train. Concerning the amplitude motions, especially the roll motions amplitudes seem hard to predict. While the motion amplitudes tends

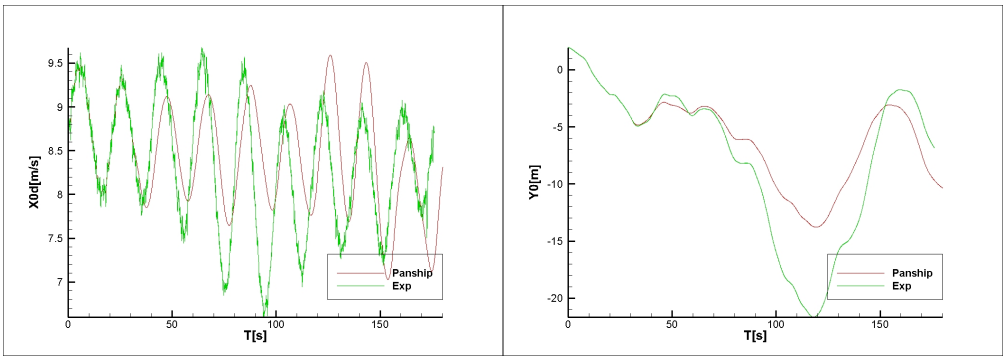

(a) Speed

(b) Sway

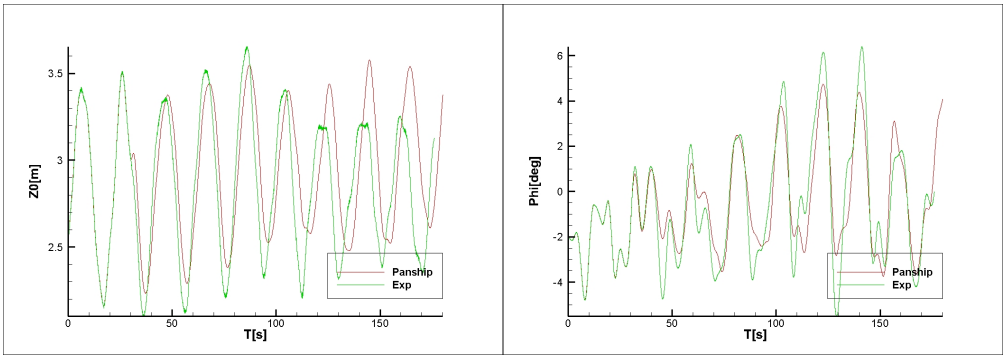

(c) Heave

(d) Roll

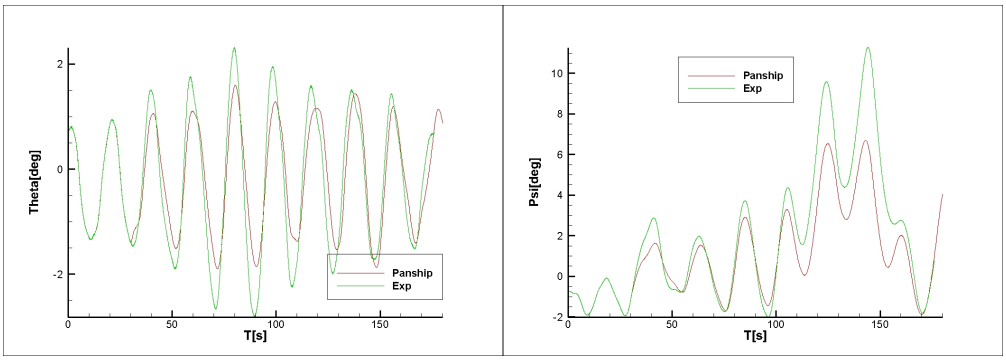

(e) Pitch

(f) Yaw

Figure 43: Time traces of model test and Panship for run 706003.

to differ between model tests and simulations, there is no consistent trend of the simulation over or under predicting the motions. In some cases the simulated amplitudes are higher, while in other cases the model test amplitudes are higher.

During some of the tested runs sway motions of up to about one ship length were encountered. In this situation the body linear hydrodynamic solution does not represent the reality very well any more, since the hull actually is in a significantly different position with respect to the waves. Nevertheless, it is not visible that large sway motions always lead to a decreasing similarity between simulation and model test results.

Conclusions The deterministic validation confirms the impression that the presented simulation method provides a good estimate of the motions that can be expected in reality. The fact that the similarity between simulation results and model test results strongly depends on match of the wave trains indicates that the differences between wave trains might be an important cause of differences between model tests and simulations. Nevertheless, these differences in wave trains certainly do not explain all of these differences.

From the obtained time traces, it can not be concluded that the accuracy of the simulation's prediction drops significantly when a certain sway or surge is exceeded. Although the odd linear hydrodynamic solution can not deliver any accurate results anymore, the simulation still delivers a reasonable output. This indicates that in stern quartering seas the hydrostatic Froude-Krilov forces deliver the larger part of the forces on the hull.

5.3 Conclusions

This section described all free sailing tests that were validated during this project. These free sailing tests were reproduced with a number of goals in mind. First of all, the calm water free sailing tests can further help to understand the consequences of the choices made within the presented simulation method. The model test measurements can be used to validate the dynamic trim and sinkage, as well as the wave elevation and pressure distribution in the bow area. Secondly, the model tests in steep stern quartering waves can be used to obtain a general idea about how well the risk for dangerous situations (broaches, capsizes) in a given sea state is predicted by the simulations.

The free sailing tests in calm water confirm the findings during captive tests, that the dynamic heave is over predicted by the simulation method. Since in these free sailing tests also the dynamic trim can be compared between model tests and simulation, conclusions can also be made about the dynamic trimming moment. The results show that the vessel in simulations is consistently trimmed less bow up than in the model tests. A clue to the differences in dynamic heave and trim can be found in the pressure measurements in the bow. In the simulation, the pressure in the entire bow area, but especially in the bow wave is significantly lower. Finding an option to increase the pressure in the bow area would certainly lead to more bow up trim. However, to also improve the dynamic heave predictions, the pressure further aft on the hull would have to decrease significantly.

Next, the bow wave elevation was compared between several potential flow simulation methods and the model tests. Combined with the pressure measurements in the bow, a complete picture of the differences between simulated and actual bow waves can be obtained. An interesting finding is that all potential flow codes under estimate the bow wave height, regardless whether linear or non linear free surface conditions were used. For the tested simulation method with linear free surface condition, independent of the method used to estimate a wave height, it is under estimated. In combination with the captive tests at higher Froude number, the conclusion has to be made that result of both methods used to estimate a wave height to strongly varying results depending on the test conditions. It seems that higher Froude numbers lead to an over prediction of the wave height, while lower Froude numbers lead to an under prediction.

When it comes to the free sailing tests in stern quartering waves, the idea is to show how well simulations can predict the occurrence of dangerous situations in severe irregular waves. It could be shown that the vessel indeed ended up broaching significantly or capsizing when only small changes in autopilot settings, simulation input or center of gravity of the model were made. Hence, the tested conditions were close to the limit of safe sailing conditions and although no capsize occurred during the model tests, it is safe to assume that conclusions can be made for stern quartering sea states up to a point where operation can not be classified as safe anymore.

One very important conclusion that has to be stressed after these validation tests is that the course stability in simulations can be critically influenced by very small changes to the appendage geometry or input options. However, the fact that a closer imitation of the model test always resulted in a higher similarity

between model test and simulation results indicates that this sensibility might be an accurate representation of reality. Further investigation into this topic might be worthwhile when trying to make vessels safer for severe stern quartering sea states.

From the deterministic validation, the most important conclusion is that there is no clear maximum value of the vessels motions after which the simulation's accuracy decreases significantly. Even if the linear hydrodynamic solution can not be accurate anymore, the non linear hydrostatic solutions seems so dominant that it keeps the simulation results reasonably accurate.

Generally, in the statistical as well as the deterministic validation, the impression is that the vessel's motions are predicted well. The statistical values of the vessels motions in all six degrees of freedom, as well as the extreme values are similar. For application of the simulation method in an early design state, the obtained accuracy is sufficient to get a good idea of its operability in a severe sea state. The risk of dangerous situations and even capsizing occurring is well modeled by the chosen simulation method.

6 Dynamic Trim and Sinkage

During the model tests that were carried out to validate a time domain potential flow code, one main difference between simulation results and model tests was found to be the trim and sinkage due to forward speed. For this reason, a decision was made to further investigate possible reasons for those differences and possibly improve the simulation's predictions in this perspective. This section is used to describe the results of this investigation and will help to better understand why potential flow leads to different results than model tests.

Generally, for fast vessels trim and sinkage change as a result of forward speed. For all tested conditions in Froude numbers up to 0.74, in the model tests suction dominated, leading to an increase of sinkage and a slight bow up trim. This suction is the result of a low pressure area behind the bow wave. During the simulations, this suction was present as well, but it's magnitude was significantly smaller. The reasons for this difference surely has to be found in the simplifications made to the flow in order to make simulations possible. From the model tests performed in the previous chapters it is already possible to exclude the body linear boundary condition as a reason since differences were found not only in free sailing simulations, but (in the form of the heave forces) also in captive tests. Further more, a hint at possible differences in the pressure resulting from the potential flow model could be obtained from the pressure measurements in the bow area during free sailing tests. Nevertheless, there are some ideas of additional factors that might play a role that are worth looking into in further detail.

First, for fast vessels with dry transom sterns, at least in a simplified 2D picture, flow first meets the hull at the bow-waterline intersection but leaves it at the transom edge. Hence, it leaves the hull at a lower point and this induces a downwards pointing vertical component of the viscous resistance.

Secondly, the linear free surface boundary condition and the estimation of the bow wave height certainly do have an effect on trim and sinkage. If the bow wave height and the pressure above the calm water free surface could be estimated more accurate, this might lead to a more accurate predition of the dynamic trim and sinkage.

6.1 Viscous Drag

As described in section 3, in the presented simulations the viscous drag was calculated in x-direction with the drag coefficient derived from the ITTC formula from 1957, based on the the Reynolds number. In y-direction, a crossflow-drag method as described in [11] is used to calculate the viscous drag of several hull components. In z-direction, there is assumed to be no viscous drag component.

This last assumption, while naturally acceptable for slow ships, might be inaccurate or fast ships when the stern is ventilated. When water particles "attach" to the hull in a higher spot than leaving the hull, there in fact is a vertical downwards pointing component to the viscous drag. On the other hand, when looking over the entire hull, there might also be streamlines (for example in the bow wave) that cause an upwards pointing viscous force. The question is if there is a significant vertical component to the viscous forces, and if there is, in which direction it might point. In order to get an idea of the magnitude of this vertical component, it would be necessary to know the local viscous drag force vector on every location of the hull. A summation of all those vectors would give the total magnitude and direction of the total viscous drag.

6.1.1 Formulations for Local Drag Coefficients

The idea is to implement a different way to estimate viscous forces on the hull. Instead of calculating the viscous resistance globally over (parts of) the hull, the viscous forces can be calculated for every panel separately. Since the flow direction and velocity, as well as the area are known for each panel, the magnitude and direction of the viscous drag can be calculated at each panel.

The fact that most fast ships operate with ventilated sterns and have quite simple hull forms helps with this approach. At least as long as there is no drift angle, there are no larger areas of flow separation at the stern, and generally the flow along the hull follows reasonably straight lines. Instead of a global drag coefficient for the entire hull, local drag coefficients C_τ for each hull panel have to be obtained. This coefficient can be found by differentiating the flat plate resistance derived with the ITTC formula in x-direction.

$$\begin{aligned}\tau = \quad \frac{d}{dL}\left(\frac{1}{2}C_F\rho V^2 L\right) \quad &= \frac{d}{dL}\left(\frac{0.0375\rho V^2 L}{(log(R_n)-2)^2}\right) \\ &= 0.0375\rho V^2 \frac{log(R_n)-4}{(log(R_n)-2)^3}\end{aligned}$$

This leads to the following expression for the local drag coefficient:

$$\begin{aligned}C_\tau \quad &= \frac{\tau}{\frac{1}{2}\rho V^2} \\ &= \frac{0.075(log(R_n)-4)}{(log(R_n)-2)^3}\end{aligned}$$

Next to the ITTC formula there are also other expressions derived from curve fitting measurement results. In [1], there are several formulas given, most of them derived from pipe flow. The only one that holds for $R_n > 10^9$ and is actually derived from tests on a flat plate is the Schulz-Grunow formula:

$$C_\tau = \frac{0.37}{log(R_n)^{2.58}}$$

Here, the length that will be used to calculate the local Reynolds number should actually be the length of the local stream trace over the hull. However, for reasons of simplicity, during the simulations this is approximated by the distance of the panel center to the bow.

Both formulas shown here as well as setting the viscous drag to zero will be tested for captive drift variations on hull m8325 and compared to the results from section 4. This way it will be possible to get a general idea of the effect of viscous drag on the forces and moments in all degrees of freedom. It should be noted however, that in y direction, the crossflow drag method used in the simulations does not only account for viscous drag, bot also to a significant extend for flow separations that will take place in case of non zero drift angles. This effect is not taken into account with the local drag coefficients. Therefore, it can be expected that sway forces and roll moments in case of non zero drift angles will not be represented accurately when these coefficients are used. This does not affect the objective to find the vertical component of the viscous drag.

6.1.2 Results

The resulting heave and surge forces from the different methods that are tried to calculate the viscous resistance are presented in figure 44. The resulting forces for other degrees of freedom can be found in appendix I. These results were obtained from simulations using the m8325 hull (87 meter patrol boat concept) at 21.6 m/s or $F_n = 0.74$.

The surge force results can be used to verify that the given expressions for viscous resistance. When comparing zero viscous drag and the original simulation results (indicated as ifswav 2 without skeg) with the results based on local drag coefficients, we can see that the viscous component calculated with the local drag coefficients is $\frac{1}{3}$ smaller compared to the original simulation results. This might be due to the simplified method to calculate the local Reynolds number. However, when looking at the results in heave force, a difference of this order of magnitude in the viscous force component will not lead to different conclusions about the vertical component of the viscous drag. One can conclude that the viscous resistance in z-direction for both of the expressions that use local drag coefficients negligible is. If anything, there is a very small upwards pointing component for larger drift angles. However, since with those drift angles a significant amount of

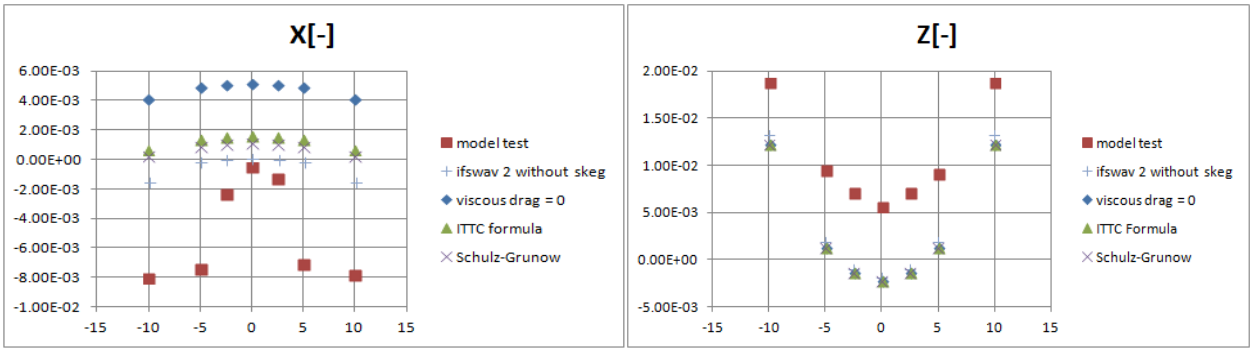

(a) Surge forces

(b) Heave forces

Figure 44: Forces and moments measured in model tests and calculated with simulations including different viscous drag calculations

flow separation takes place in viscous flow, the obtained local flow direction and velocity in potential flow are not realistic anymore. Hence, conclusions should not be drawn based on this small differences with these large drift angles. Concluding this section it is safe to tell that the effect of the viscous resistance on the hydrodynamic lift forces is negligible.

6.2 Bow Waves

In sections 5 and 4, a number of model tests were compared with (as far as possible) identical simulations. After the results were compared, the conclusion was that heave and pitch forces/moments were a point of interest, since their predictions were off and since the resulting trim and sinkage have an important impact on the ship's motions in all degree's of freedom. One element that certainly has an effect on the heave and pitch are the radiated waves, and the resulting pressure fluctuations under the calm water waterline, caused by hull movements. During normal operation, the dominant part of these radiated waves is the (in almost all fast sailing ships) breaking bow wave. This section will focus on some ideas to alter, and possibly improve the simulation predictions of wave height and pressure distribution due to forward speed.

During simulations, it is very important to estimate the wave elevation along the hull correctly. In the simulation code used in this report, the free surface conditions are linearised, essentially estimating zero wave elevation at all times and locations. However, to improve the simulations, the calculated pressure on the (calm) free surface can be used to estimate a local wave height on the hull. This leads to additional pressures and forces on the hull. From the results of the section 4 tests we can see that these forces have a significant effect on the overall simulation results, including the forces in z-direction. It seems that calculating the wave height from the pressure in the middle of the upper most row of panels on the hull leads to a severe overestimation if the dynamic lift forces, while using a horizontal offset from the hull leads to approximately the same results as taking no wave elevation at all into account.

Since the forces in z-direction are one of the main concerns when it comes to the overall accuracy of the presented simulation method, it is very reasonable to have a second look at the calculation of the wave elevation and pressures. In [24], de Jong already put some effort into comparing the Panship results to experiment data on Wigley hulls, experimenting with different locations to evaluate the pressure used for the free surface elevation. His conclusion is that the elevation is reasonably well predicted, although the maximum wave height of the bow wave was always under predicted. Further, the wave height is predicted more accurate, the closer the pressure elevation is taken to the hull. However, in most cases this also leads to numerical instabilities.

In this report the measurements of pressure and wave height in the bow region, gathered during the

model tests described in 5 will be analysed and compared to simulation results. Afterwards, some options for an empirical calculation of the bow wave height will be analysed, as well as, possibilities to improve the pressure stretching that is used to obtain pressures between the instantaneous free surface and the calm water free surface. The hull that was used for all considered runs was the FDS hull at a hull scale speed of 35 knots or $F_n = 0.57$.

6.2.1 Free Surface Elevation

One important aspect of the bow wave is the contact line between hull and water surface. When trying to accurately simulate the forces on a vessel due to the bow wave, at least it's height and steepness have to be reasonable accurate. From the results of section 5 we know that generally all tested numerical simulations underestimate the height of the contact line in the bow area. Unfortunately, there are no measurements further aft for this particular hull form and we can still see a pretty wide spread between the four tested numerical methods. For this reason, the only option for this paper is to ignore the wave elevation in the aft part of the hull and fully focus on the prediction of the bow wave.

Empirical Wave Height and Location A completely different approach to the prediction of a bow wave height are empirical expressions developed on the base of measurements on systematical test series. Most of these empirical approaches use formulations to calculate the location (in x and z direction) of the highest point of the contact line and scale the numerical results to match these calculations. As described in section 2, there were a number of formula's developed in the past to calculate the location of this highest point of the bow wave based on several hull form parameters.

For empirical formulations of wave height and location we will have a look at the formulations of Waniewski[10], Noblesse[14] and Maxeiner[20]. As we can see in section 2 these papers all provide empirical formulations for the z and x location of the highest point of the bow wave contact line. While Maxeiner and Waniewski limit themselves to simple (mostly) wedge like bow shapes and non dimensional formulations for bow wave height, Noblesse's paper [14] is the only one to provide actual values for the non dimensional wave height and steepness. Moreover, it's results are partly based on the measurement results from Waniewski [10], but also including a large number of other papers and some Wigley and series 60 hulls.

Nevertheless, all formulations as shown in section 2 are essentially quite similar. The main difference is the power of the Froude number in the equation. While this is constant for the equations given by Maxeiner (at 1.33) and Waniewski (at 1.5), leading to an unbounded wave height in the limits $T \to 0$ and $T \to \infty$, Noblesse solved this problem by letting the Froude number power increase from 1 to 2. This way at least the boundary conditions for the extreme values are realistic. It also means that for realistic values of the draft somewhere between these extremes, the values predicted by these three expressions can be expected to be quite similar.

$$Z_b = C^W \cdot d \cdot \frac{F_n^2}{1 + F_n} \cdot \frac{\tan\theta}{\cos\theta} \tag{6.1}$$

$$X_b = C^X \cdot d \cdot \frac{F_n^2}{1 + F_n} \tag{6.2}$$

For these reasons, the results of Noblesse's formulations 6.1 and 6.2 will be compared to the measurements and simulations done for this paper. The question thereby is whether the non dimensional wave height C^W and wave length C^X are in deed (approximately) constant for a large range of planing hulls. Noblesse shows that for wedge shaped hulls this is the case. However, the spreading of measurements increases significantly for Wigley hulls and series 60 hulls. For a possibility to predict these values for any "normal" planing hull, a necessary premise is that they are approximately constant within this range of hull forms. Since the series 60

hulls are in fact planing hulls, C^W and C^X for the tested frigate would have to be close to C^W and C^X for the series 60 hull shapes tested by Noblesse. Noblesse measured average non dimensional bow wave heights C^W of 2.2, and bow wave lengths C^X of 1.67. Figure 45 shows the resulting location of the highest point of the bow wave compared to measurements and simulations.

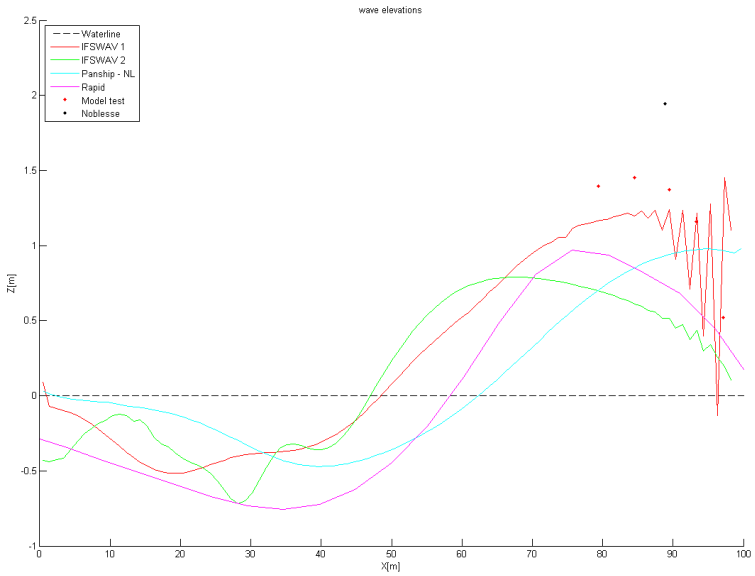

Figure 45: Free surface elevation along the side of the hull.

As one can see in figure 45, this empirical calculation results in a much higher and steeper bow wave than actually measured. In order to approximate the test results, the non dimensional bow wave height has to be set to 1.7, while the non dimensional bow wave length has to be 2.3. These values lie respectively 22% and 35% in contradicting directions off the values given by Noblesse for series 60 hulls. Even after varying the used draft d and half entrance angle θ to fit effective values suggested by Noblesse, the numerical solution of the linear version of Panship with the IFSWAV parameter set to 1 remains the most accurate prediction, apart from the numerical wiggles near the bow.

To conclude this paragraph, one can say that apparently, even within the range of "normal" planing hull shapes, the range of non dimensional bow wave heights and lengths is too large too make reasonably accurate predictions for new and untested hulls. A better guess at the bow wave dimensions will be given by the results of numerical simulations with a well chosen input. The most accurate prediction in this case is given by Panship with the wave height calculated based on the pressure on the upper most row of submerged hull panels (IFSWAV 1). However, as already mentioned by de Jong in [24], this method proves to be sensitive to numerical instabilities. Therefore, applying a suitable filter to the calculated wave elevations might further improve the predictions.

Pressure extrapolation towards free surface As explained in section **??**, when using IFSWAV 1, the pressure that is used to estimate the local wave height around the hull is taken from the upper most row of submerged panels. However, as is shown in figure 46, especially in the bow area there are very steep pressure gradients near the calm water free surface. Therefore, extrapolating the pressures of the upper most row of panels towards an estimated value on the calm water free surface might lead to a higher and more accurate estimate of the bow wave height. Since the pressures are extrapolated from the existing panels, there is no need for extra evaluation points.

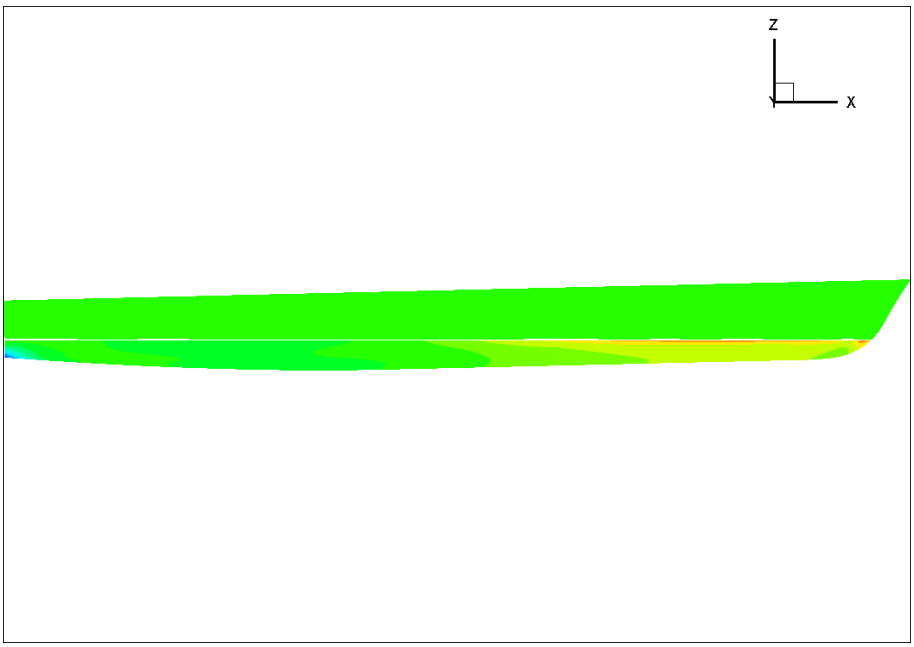

Figure 46: Dynamic pressure distribution underneath the still water free surface (with IFSWAV set to 0)

This extrapolation is done by looking at the two upper panel rows and extrapolating the average values in the middel of these panel rows linearly towards the water surface. This way, the occurring steep pressure gradients in the bow area near the water surface can be taken into account more accurately. Further aft, as pressure gradients are less steep, the calculated wave height will be affected in a less significant way.

As one can see in figure 47, the new wave height in the bow region is indeed significantly higher than before. Further aft and in the wave trough, the difference becomes smaller. This coincides with the expectations based on the local pressure gradients in the bow area and further aft of the hull. However, one can also see that the numerical errors near the bow are amplified as well. All in all, at least aft of the numerical errors, the new predictions lie very close to the measured values, suggesting a closer fit to the actual radiated waves.

One next thing to investigate is the effect of this new wave height on the pressure distribution and the over all trim and sinkage. Since the main difference is the increased wave height in the bow area, one would expect slightly more bow up trim and maybe a little more dynamic rise. However, because the pressures underneath the waterline remain unchanged, these effects will be small. Only above the waterline the pressures should increase proportionally to the wave height.

In figure 48 one can clearly see that the new and higher wave causes higher pressures above the waterline and, that as expected under the waterline there are no changes. However, the effect of these slightly higher pressures in the bow area is negligible when it comes to the over all trim and sinkage that is calculated for free sailing conditions.

6.2.2 Pressure distribution

As mentioned before, when linear free surface and body boundary conditions are used, the pressures on these surfaces are evaluated at their mean position rather than at their actual positions. However, these pressures on the still water waterline and hull can still be used to calculate a local wave height and ship motions and thus pressures on the hull outside of the still water submerged surfaces. The question however is, how to

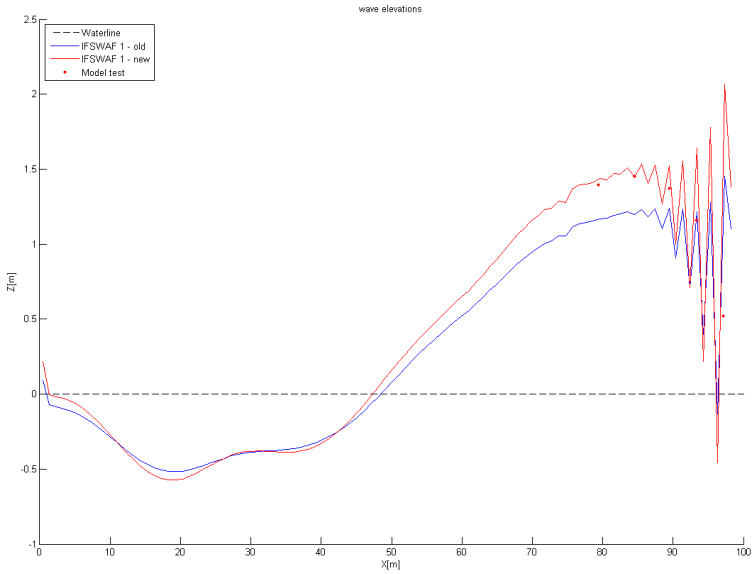

Figure 47: Free surface elevation along the side of the hull when the pressure is extrapolated.

calculate these pressures on panels above the still water waterline. Since they lie outside the fluid domain, the potential flow equations will not provide an answer.

Old Pressure Stretching Method The simulation solves this problem by stretching the pressure from the still water free surface to the calculated actual free surface in a way that de Jong described in [18]. Basically, the dynamic pressure p_d on the waterline is interpreted as the static pressure p_s from the wave, leading to a linear increase of pressure from wave crest to still water waterline as shown in figure 49 from [18].

However, as can be seen in figure 31, at least in the breaking bow wave, this does not match very well with the measurements in the free sailing model tests. Figure 50 shows that the pressure in the bow wave is significantly higher in the experiments than predicted by simulations for all input options tested.

Figure 50 shows, as one would expect, that all simulations with linear free surface boundary conditions have identical solutions underneath the still water waterline. Above this line the pressures should decrease linearly to the actual water surface. While we can confirm this for the bulkheads at 80 and 85 meter, we see that at 90 and 93.75 meter this is not the case. This can be due to a combination of linear interpolation between panels and pressure sensor locations and the significant numerical instabilities that we can see in figure 45 for the given x-positions.

As discussed in section 5.1, the measured pressure in the bow wave, from right underneath the actual water surface seems to be significantly high. This is the case even when the bow wave only consists of a thin sheet shortly before breaking. On top of that, even under the still water waterline, the actually measured pressure seems to be higher than the simulation results suggest. All in all, it seems that a correction approximately constant over the height, applied to the simulation results would lead to better coherence with the model tests.

Hydrostatic Pressure Currently, the hydrostatic pressure is calculated from the still water surface downwards. In reality, however we know that the hydrostatic pressure starts to build from the actual free surface.

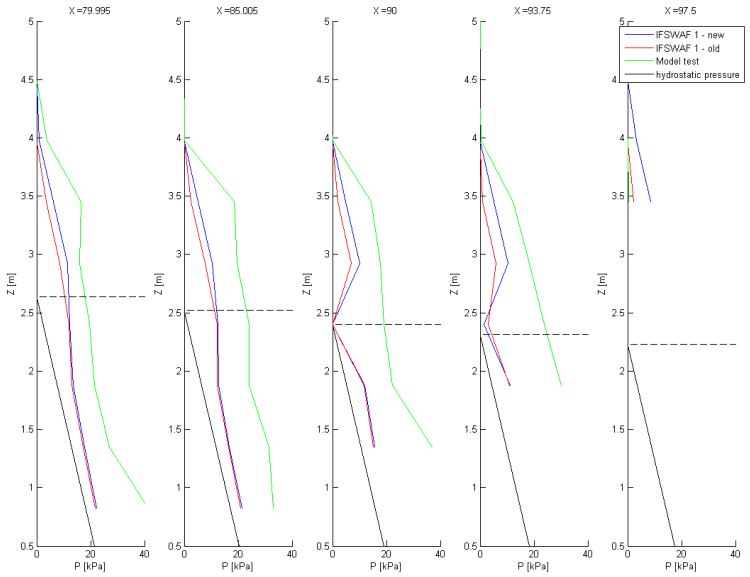

Figure 48: Comparison between pressures based on new and old wave height.

A possibly more realistic alternative would therefore be to use the actual water surface to calculate the hydrostatic pressure. This would lead, at least under the still water surface, to a correction on the currently calculated pressure that is independent of the height.

Obviously, since in the current approach the hydrodynamic pressure is considered to be zero above the still water surface, this leads to a pressure jump at the still water surface, which is clearly not realistic. Therefore, a suitable approximation for the hydrodynamic pressure is necessary. Realistically, this should be some distribution that leads a total pressure somewhere along the dashed red line (a pressure distribution without jumps or kinks). Further, from the model experiments we know that the pressure in the bow wave is actually quite high almost up to the actual water surface. A first very simple solution might therefore be to assume a constant dynamic pressure up to the actual water surface. Of course, this only transfers the pressure jump from the still water surface to the actual surface, but since that is where we know that

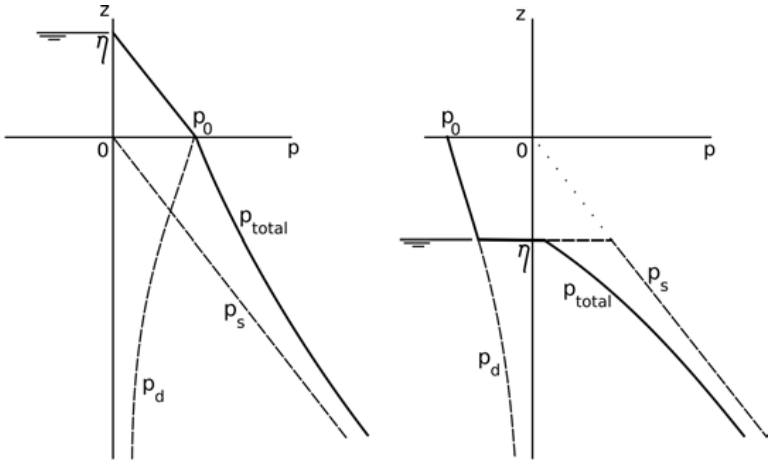

Figure 49: pressure stretched for wave crests and troughs.

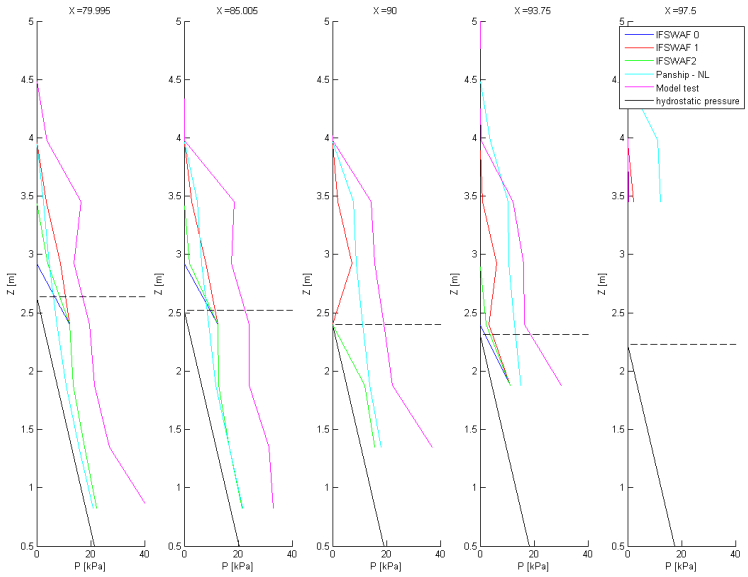

Figure 50: pressure measurements and predictions per bulkhead.

the pressure gradient is indeed steep, this might lead to a better approximation of reality. The resulting schematic pressure distribution is shown in figure 51. In the future it might be interesting to look at alternative hydrodynamic pressure distributions that do not cause a pressure jump at the actual free surface, while still remaining a steep pressure gradient right underneath the actual free surface.

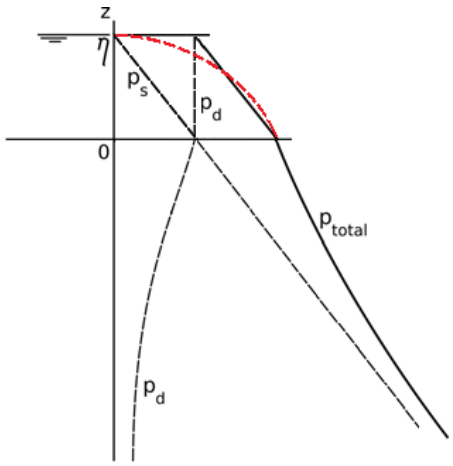

Figure 51: pressure stretched for wave crests.

In the wave trough, it will lead to negative pressures even under the calculated actual free surface, which is of course not realistic. This is indicated in figure 52. Obviously, to agree with reality, a correction to the total pressure would be necessary for it to approach zero at the actual free surface (as indicated by the red dotted line). Unfortunately, since there are currently no pressure measurements available in a wave trough, any formulation for a correction would be pure guessing. Therefore, currently the best solution is to just set any negative pressures to zero and hereby, just like at the wave crests, knowingly introduce a small inaccuracy. It is then up to future research to find more accurate solutions.

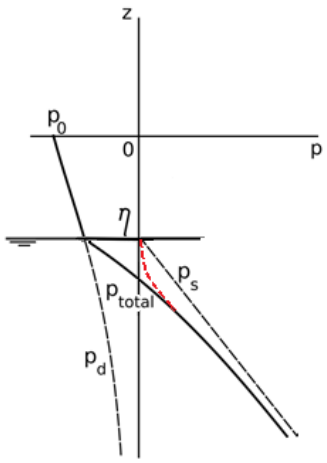

Figure 52: pressure stretched for wave troughs.

	Model test	IFSWAV 1 old	IFSWAV 1 new	IFSWAV 2 old	IFSWAV 2 new
trim	$-1.3\,^\circ$	$-0.56\,^\circ$	$-1.78\,^\circ$	$-0.63\,^\circ$	$-1.72\,^\circ$
sinkage	$-0.3m$	$-0.12m$	$0.23m$	$-0.09m$	$0.13m$

Table 9: Comparison trim and sinkage.

New Pressure Stretching method Since the results of this new pressure calculation method seem promising, it is implemented in the simulation to look at the pressures and overall forces and moments on the entire hull. Just like before, tests were carried out in calm water at a speed of $F_n = 0.57$. First, the vessel will be free in heave and pitch, to see if these values due to forward speed are predicted better than before. Afterwards, the ship will be clamped at the heave and pitch value measured in the model tests, so that the bow wave contact line and pressure distribution can be compared. In table 9, dynamic trim and sinkage calculated by the updated simulation method is compared to the old values and the values of the model test. Clearly we can see that, for both pressure evaluation locations (IFSWAV 1 and 2), the new pressure calculation leads to an over prediction of the dynamic trim as well as a very severe over prediction of the dynamic rise. Apparently, aft of the bow wave, the new pressure calculation method leads to an over prediction of the pressure on the hull.

Figure 53 shows the pressure calculations using the new pressure stretching method (with IFSWAV set to 1) for free sailing and clamped conditions. Also, these results are compared to the old IFSWAV 1 results and the model tests. Clearly, for the clamped simulation, we can see that interpolation and numerical instabilities still lead to an almost zero pressure close to the waterline at the bulkheads at 90 and 93.75 meters. Apart from that however, the pressures are predicted more accurately than before. In any case, they show much closer resemblance to the model tests as the old results.

Conclusions From the new simulation results we can conclude that the new method of extrapolating the pressure above the water surface leads to more accurate results for the bow area (above as well as below the waterline). Apart from numerical errors, the the pressure calculations seem to be as accurate as one can reasonably expect from a potential flow method. However, since there only are measurements up to bulkhead number 16, only results within the region of the breaking bow wave are examined. Further aft, the results might very well differ. Looking at the dynamic rise and trim (and thus, the dynamic heave force and pitch moments) the new results do not look very promising. The rise is over predicted by about half a meter, and the trim is over predicted about half a degree. Especially the large difference in rise will have significant effects on the vessels manoeuvring and seakeeping behaviour. Therefore the new method of pressure extrapolation probably will show no improvement when it comes to any predictions of ship's

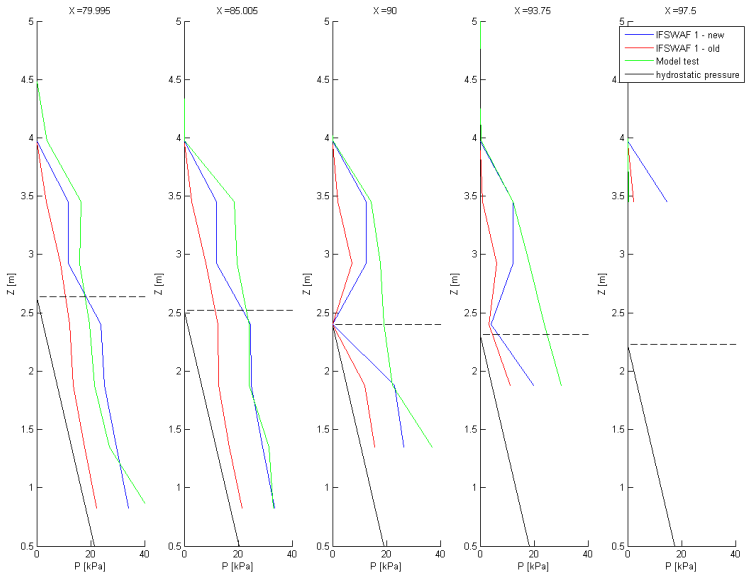

Figure 53: pressure measurements and predictions per bulkhead as calculated by the new pressure stretching method.

motions in free sailing simulations.

6.3 Conclusions

The goal of this section was to have a closer look at possible reasons for the differences in trim and sinkage between potential flow simulations and model tests. Two main aspects were investigated closer to see if they have an effect on the dynamic trim and sinkage. First of all, a detailed look has been given to the viscous drag on fast vessels. Due to the ventilated stern, there might be vertical component to the viscous drag vector. Secondly, the height, as well as the pressure due to the bow wave has been examined, and alternatives for these calculations have been given.

In order to get a good idea of the direction of the viscous resistance, it has been evaluated on every hull panel separately. While this way the effect of flow separation in case of a drift angle is knowingly neglected, a possible vertical component to the viscous drag should be visible in the results. However, from examining the resulting heave forces, it is safe to tell that is such a component exists, it is negligibly small.

When it comes to the wave elevation in the bow wave, for the conditions examined in this chapter, a significant improvement could be made to the estimated bow wave height. By extrapolating the pressure up to the location of the calm water free surface, a more accurate match with the bow wave in the model test could be obtained. However, the effect of this change on the dynamic trim and sinkage is negligible as the simulated pressure underneath the calm water free surface remains identical. Moreover, simulations in higher Froude numbers and on a full hull shape that are presented in section 4 indicate a significant over prediction of the bow wave height even with the pressure evaluated in the middle of the upper most row of hull panels. Hence, a relevant question is whether the obtained changes are an improvement in general, or only for slender hull shapes in Froude numbers around 0.57 and without any drift or heel angle. Further investigation will be necessary to be able to answer this question.

Finally, the pressure in the bow area was closely examined. For the given test conditions, the pressure in the bow wave as well as below the calm water free surface was lower in the simulation than in the model

tests. In an attempt to minimise that difference, the hydrostatic pressure was obtained from the actual free surface instead of the calm water free surface, thus increasing the local pressure in the bow area by the height of the bow wave, and decreasing the local pressure in wave troughs further aft in the vessel. While the resulting pressure distribution in the bow area seems promising, dynamic trim and sinkage certainly are not. The conclusion has to be that with the new pressure stretching method, further aft on the hull the pressures are significantly over predicted, so that the dynamic rise of the vessel i over predicted as well. Further investigation and if possible model tests with pressure measurements over the entire hull should be carried out to get a better idea of what might lead to better simulations in this respect.

7 Conclusions and Recommendations

The goal of this project was to provide a thorough validation of a 3D time domain potential flow simulation method for stern quartering waves. This has been done basically in three steps. First, captive and free sailing tests in calm water have been carried out in order to verify simulation input and try to divide the complicated problem of simulating a vessel in stern quartering waves int multiple smaller problems that can be analysed separately. Secondly, an effort was made to further isolate the reason for the main differences that were found during the calm water tests. This has been done by looking at pressure and (bow) wave height measurements, as well as altering the way the viscous drag is taken into account during the simulation. Finally some model tests in irregular stern quartering waves were validated. Next to the validation of details and forces that has been given by validating calm water tests, during the tests in stern quartering waves, conditions were as close as possible to an actual vessel in severe sea state. Validation of the simulations in those conditions are very useful to give an estimation about the ability of a simulation to predict the chance of a vessel capsizing or broaching due to a given sea state. As such, for the application of the simulation method in a design proces, these validations show the area of applicability and draw attention details that are important for a valid immolation output. During this project, two methods have been used to show the similarity between model tests and simulations. First, long model tests have been used to validate simulations in identical wave spectra on a statistical bases, and secondly, for shorter runs, the wave train from the model test has been reproduced in simulations, to validate them on a deterministic base.

Calm Water Simulations During the calm water simulations, a several different simulation input options were tested and numerical refinement studies were carried out. From the refinement studies, a maximum time step as well as a minimum number of memory time steps that has to be taken into account could be obtained. For the panel distribution on the hull, an ideal value could not be found since up to the point where a modern desktop pc does not provide sufficient resources anymore, simulation results were improving with increasing number of panels. Mainly the resistance of a vessel seams to be dependent on the number of panels used. During following validations of the simulation method it should be kept in mind that the number of panels was limited by the computational resources.

A second point of interest that showed during these verifications was the calculation of the bow wave elevation and the pressure inside the bow wave. From the calm water tests, it was clear that differences in this calculations resulted in significant differences in over all forces and moments on the hull. In the simulation method that was used, initially no wave elevation at all has been taken into account, since a linear free surface boundary condition was used. However to correct for this simplification in the hydrodynamic solution, a possibility to estimate a wave height based on the pressure near the free surface-hull intersection has been tested. Within the wave obtained by that method, only a hydrostatic pressure building up from the instantaneous free surface to the calm water free surface is assumed. This is referred to as pressure stretching. However, because of steep pressure gradients near the hull-free surface intersection, the exact location for the pressure evaluation to obtain the instantaneous wave height is very important. For this, two options were examined, one using the pressure on the middle of the upper most submerged panel row, and one using a certain horizontal and vertical offset from the hull-free surface intersection. While in all tested conditions the first option lead to the highest bow wave and the highest resulting forces, depending on the test conditions any of the two methods to estimate a wave elevation, as well as taking no wave elevation at all into account could lead to the best match of the model tests. From the tests carried out during this project only a trend can be observer that higher wave heights during model tests (tests at high speeds with a full hull shape and at large drift angles) seem to lead to an over prediction of the wave height, while lower speeds, more slender hull shapes and zero drift angles lead to an under estimation of the bow wave height.

When it comes to the validation of calm water simulation results against model tests, captive and free sailing tests in calm water were carried out. For the captive tests, a validation of forces and moments could be given, while the free sailing tests lead to a validation of dynamic trim and sinkage. Both these validations lead to similar conclusions, that the dynamic heave force is over predicted, and the bow up trim is under predicted in the simulations. This conclusion can be made for all tested conditions and both tested hull

shapes.

Dynamic Trim and Sinkage In an effort to isolate the reason the observed differences in dynamic trim and sinkage between model tests and simulations, some small variations in the simulation method were tested out. First, a variation in the calculation of the viscous drag was made in order to not only obtain the magnitude of the viscous resistance, but also its direction. The idea is that for fast vessels with a transom stern the viscous resistance may have a downwards pointing vertical component. Secondly, for one case on a slender hull the bow wave was examined closer. The bow wave elevation of the given Panship simulation code was compared to other potential flow simulation methods, as well as to empirical expressions for the peak wave height and location. Finally, pressure measurements in the bow area were compared to simulation results for the same case that was used for the bow wave elevation. To obtain a better fit for the pressure in the bow area, a different way for pressure stretching was tried out in which the hydrostatic pressure was based on the distance on the instantaneous wave height instead of the calm water free surface.

As a conclusion from these variations on the simulation method, it can be stated that the difference in dynamic heave and trim is most probably a result from differences in the pressures obtained from potential flow and actual viscous flow. The viscous resistance did not lead to any significant vertical component, even if the direction of the flow on each panel was taken into account. Through a change in the way that the pressure for the bow wave height was evaluated, a good match of the model test bow wave could be obtained. However, the difference in trim and sinkage to the old simulations was negligible. The new approach to the pressure stretching however lead to a significantly better match of the pressures in the bow between measurements and simulations. While this seems promising, the over all free sailing dynamic trim and sinkage are not improved. Here a recommendation has to be made for further research and maybe model tests with pressure and wave height sensors further aft in the vessel. This way, when trying to find methods for better matching pressure measurements, the entire hull can be taken into account instead of only the bow section. From the combination of pressure measurements and dynamic trim and sinkage data obtained within this project, the conclusion is that the given simulation method under estimates the pressure in the bow area, while over predicting the pressure in the midship section and again under predicting it in the stern section. One possible interpretation of this is that the pressure fluctuation due to the bow wave system is under predicted.

Stern Quartering Waves Finally, a number of validations of model tests in steep stern quartering waves were carried out in order to give a comparison of the resulting motions of the vessel. For these validations a given spectrum of irregular waves was used in tests with two speeds and 4 incoming wave directions. The selected sea state is close to the maximum that the given vessel could handle without regularly capsizing. Again, first a verification of simulation was used to get an idea of the significance of several input parameters. Afterwards, two methods for the comparison between the vessels motions were used. First, the time traces of the vessel's motions were interpreted as random signals, and statistical properties of those time traces were compared. Secondly, the vessel's response to a given wave train could be compared.

From the input verification, it can be concluded that all tested variations in the simulation input had a significant impact on the simulation output. Even details as an increased propeller shaft diameter could prevent a broach of the vessel. Even more important parameters were the viscosity used and the settings of the autopilot. This extreme sensitivity of the simulation to its input leads to the question if the simulation output is a merely random result of small variations in the input. However, for all variations tested during this project, the closest match between model test and simulation in the input always lead to the closest match in the output. In turn this leads to the question if the model test results - and to take it even further, the operational safety of a full scale vessel - are as sensitive to little changes in autopilot settings or appendage geometry. Further more, if the simulation results are realistic, then the additional drag due to the higher viscosity in the model test significantly increases the directional stability of the vessel in stern quartering waves. Further research into this topic might lead to interesting new insight about operational safety of a vessel in stern quartering seas.

For the statistical comparison presented in this report, model tests of about 850 seconds with about 40 to 80 wave encounters were available. To get a good idea of the similarity of the motions in model test and simulation, mean values, standard deviations, maximum values and probability of exceedance curves were compared. Because the given 850 seconds of model tests in one condition were not enough to obtain statistically significant data, multiple 850 second simulations were carried out for each condition. This way, the spread of the compared statistical data between the simulations with different wave train realisations could be interpreted as a region within which the model test results should fall. Generally, the conclusions from this statistical validations is that the vessel's motions in the simulations is quite similar to the motions measured during model tests. While there are some differences for one or two degrees of freedom per test condition, there is no consistent error that shows in the simulation results. The conclusion that has to be made is that for a given wave spectrum, the validated simulation method provides a good way to estimate the resulting motions of a vessel as well as the probability of dangerous situations like broaches or capsizes.

This conclusion can be confirmed with the deterministic validations that were carried out. In this case, shorter time traces of only about 150 seconds were compared. On top of the confirmation of the statistical results, the deterministic validation could be used to see if the simulation results become less accurate in case of large sway or surge motions. This might be the case since the hydrodynamic forces in the simulation are calculated with a body linear boundary condition. In case of large motions, the vessel's instantaneous position can vary significantly from the position that is used for the hydrodynamic solution. However, from the simulation results no such limit of motions could be found. even though sway motions up to about one ship length occurred during the runs, a significant reduction of the simulation accuracy could not be found. This indicates that in stern quartering waves the hydrostatic forces are dominant compared to the hydrodynamic forces. For the simulation method, this leads to the conclusion that simulations can still be expected to yield reasonable results, even if large motions occur.

List of Tables

List of Figures

References

[1] S. F. Hoerner - *Fluid-Dynamic Drag*. Great Britain, 1965.

[2] M. R. Renilson, A.Discrollt - *Broaching - an investigation into the loss of Directional Control in Severe Following Seas*. Royal Institution of Naval Architects, 1981.

[3] M. R. Renilson - *An Investigation into the Factors Affecting the Likelyhood of Broaching-to in Following Seas*. Glasgow University, United Kingdom, 1982.

[4] O. Rutgersson, P. Ottosson - *Model Tests and Computer SimulationsAn Effective Combination for Investigation of Broaching Phenomena*. The Society of Naval Architects and Marine Engineers, New Jersey, 1987.

[5] J. O. de Kat - *The Simulation of Ship Motions and Capsizing in Severe Seas*. The Society of Naval Architects and Marine Engineers, New Jersey, 1989.

[6] M. R. Renilson, A.J. Tuite - *Broaching Simulation of Small Vessels in Severe Following Seas*. Int. Symp. on Ship Stab. in a Seaway, 1995.

[7] H. C. Raven - *A Solution Method for the Nonlinear Ship Wave Resistance Problem*. PhD Thesis, Delft University of Technology 1996.

[8] Kostas J. Spyrou - *The Nonlinear Dynamics of Broaching*. The annals of Marie Curie Fellowships, Vol. 1, pp. 62-69, 2000.

[9] F. van Walree - *Development, validation and application of a time domain seakeeping method for high speed craft with a ride control system.* 24th Symposium on Naval Hydrodynamics, Fukuoka, Japan 2002.

[10] T. E. Waniewski, C.E. Brennen, F.Raichlen - *Bow Wave Dynamics*. Journal of Ship Research, Vol. 46, pp. 1-15, 2002.

[11] O. M. Faltinson - *Hydrodynamics of High-Speed Marine Vehicles*. Cambridge University Press, 2005.

[12] F. Noblesse, D. Hendrix, L. Faul, J. Slutsky - *Bow-Wave Height and Location*. 5th International Offshore and Polar Engineering Conference, Seoul, Korea, 2005.

[13] K. Garme - *Improved time domain simulation of planing hulls in waves by correction of the near-transom lift*. International Shipbuilding Progress, 52(3):201-230, 2005.

[14] F. Noblesse, D. Hendrix, L. Faul, J. Slutsky - *Simple Analytical Expressions for the Height, Location, and Steepness of a Ship Bow Wave*. Journal of Ship Research, Vol. 50, pp. 360-370, 2006.

[15] N. Umeda, M. Hori and H. Hashimoto - *Theoretical prediction of broaching in the light of local and global bifurcation analysis*. STAB, 2006.

[16] E. Jacquin, P.-E. Guillerm, A. Drouet, P.Perdon - *Simulation of unsteady ship manoeuvring using free-surface RANS solver*. 26th Symposium on Naval Hydrodynamics, Rome, Italy, 2006.

[17] N.W.H. Bulten - *Numerical Analysis of a Waterjet Propulsion System*. PhD Thesis, Eindhoven University of Technology, 2006.

[18] P. de Jong, F. van Walree, A. Keuning, R. H. M. Huijsmans - *Evaluation of the Free Surface Elevation in a Time-Domain Panel Method for the Seakeeping of High Speed Ships*. Delft University of Technology, Marin, the Netherlands, 2007.

[19] P. Ferrant, L.Gentaz, R. Luquet, G. Ducrozet, B. Alessandrini, E. Jacquin, A. Drouet - *Recent Advances Towards the Viscous Flow Simulation of Ships manoeuvring in Waves*. France, 2008.

[20] E. Maxeiner - *Physics of Breaking Bow Waves: A Parametric Investigation using a 2D+T Wave Maker*. PhD Thesis, University of Maryland, 2009.

[21] T. G. Yen, S. Zhang, K. Weems W. M. Lin - *Development and Validation of Numerical Simulations for Ship manoeuvring in Calm Water and in Waves.* 28th Symposium on Naval Hydrodynamics, Pasadena, California 2010.

[22] F.van Walree - *Validation of Time Domain Seakeeping Codes for a Destroyer Hull Form Operating in Steep Stern-quartering Seas.* ITTC Workshop on Seakeeping, Seoul, Korea 2010.

[23] F.van Walree, P. de Jong - *Validation of Time Domain Panel Code for High Speed Craft Operating in Stern Quartering Seas.* 11th International Conference on Fast Sea Transportation, Honolulu, USA 2011.

[24] P. de Jong - *Seakeeping Behaviour of High Speed Ships - An Experimental and Numerical Study.* PhD Thesis, Delft University of Technology 2011.

[25] P. de Jong, M. R. Renilson, F. van Walree - *The Broaching of a Fast Rescue Craft in Following Seas.* Delft University of Technology, University of Tasmania, Maritime Research Institute Netherlands, 2013.

[26] V. Barthelemy - *Validating Panship for Maneuvring Predictions of High Speed Vessels.* 2013.

A Panship Input Table

SIMULATION	NTIME [-]	NHIST [-]	NHISTW [-]	DTIME [s]	NSWTON [-]	ISKIP [-]	UVEL [m/s]	VVEL [m/s]
GEOMETRY	GEONAM(1) Char(10)	GEONAM(2) Char(10)	RLENGTH [m]					
MASSPROP	RMASS [kg]	Kxx [m]	Kyy [m]	Kzz [m]	COG-x [m]	COG-z [m]		
OPTIONS1	IFLGFIL (0/1/2)	ILINSP (0/1)	IFSWAV (0/1/2)	ISGOUT (0/1)	ICAVOP (0/1)	FGNAM(1) Char(10)	FGNAM(2) Char(10)	IFGAPP [-]
OPTIONS2	IVTK (0/1)	IPRES (0/1)	INITHST (0/1)	IBATCH (0/1)	IAMASS [-]	IMTRM [-]	IRPMTH (0/1)	
CONSTANTS	RHOW [kg/m^3]	CSIGVB [-]	FSWAVM [-]	FAKWTE [-]	ZFGMIN [m]	ALFGF [-]	TIMGF [s]	NUMTHR [-]
OSCIL	IMODE (0/1)	OMEGAM [rad/s]	AMPLIM [m, deg]					
CFVISC	CLV [-]	CDV [-]	VISC [m^2/s]					
CONTROL	ICONTRLS (0/1)	IDELAY [–]						
TRIMFLAP	XTRMFLAP [m]	YTRMFLAP [m]	ZTRMFLAP [m]	STRMFLAP [m^2]	DELTRM [deg]			
INTERCEPT	XINTCPT [m]	YINTCPT [m]	ZINTCPT [m]	WINTCPT [m]	DELINT [deg]			
WATERJET1	XWJET [m]	YWJET [m]	ZWJET [m]	BINTPWJ [m]	DNOZWJ [m]	DIMPWJ [m]	RPMWJ [1/min]	
WATERJET2	CQFLW [-]	RLIWJT [m]	DELWJT [deg]					
RUDDER	XRUD [m]	YRUD [m]	ZRUD [m]	CHRUD [m]	BRRUD [m]	DIHEDRUD [deg]	IRUDPRP [-]	WAKRUD [-]
PROPELLER1	XPROP [m]	YPROP [m]	ZPROP [m]	DIAMPRP [m]	PDRPRP [-]	RPMPRP [1/min]		
PROPELLER2	NBLPRP [-]	BARPRP [-]	THDPRP [-]	WAKPRP [-]	IPRPOD (0/1)			
PROPSHAFT	XSHAFT(1) [m]	YSHAFT(1) [m]	ZSHAFT(1) [m]	XSHAFT(2) [m]	YSHAFT(2) [m]	ZSHAFT(2) [m]	DSHAFT [m]	
WAVESPEC	IWAVE (1-8)	HWAV [m]	TWAV [s]	PSIW [deg]	GAMWV [-]	NFREQ [-]	IRANDM [-]	
EXTNLFOR	FEXT(1) [N]	FEXT(2) [N]	FEXT(3) [N]	FEXT(4) [Nm]	FEXT(5) [Nm]	FEXT(6) [Nm]		
MODE-OFF	JMODE(1) (0/1)	JMODE(2) (0/1)	JMODE(3) (0/1)	JMODE(4) (0/1)	JMODE(5) (0/1)	JMODE(6) (0/1)		
INITPOS	XPOSIN(1) [m]	XPOSIN(2) [m]	XPOSIN(3) [m]	XPOSIN(4) [deg]	XPOSIN(5) [deg]	XPOSIN(6) [deg]		
INITVEL	XDPOSIN(1) [m/s]	XDPOSIN(2) [m/s]	XDPOSIN(3) [m/s]	XDPOSIN(4) [deg/s]	XDPOSIN(5) [deg/s]	XDPOSIN(6) [deg/s]		
SLAMPOS	XSLAM [m]	YSLAM [m]	ZSLAM [m]					
ACCPOS	XACC [m]	YACC [m]	ZACC [m]					
INTLOADS	NTCT [-]	NLCT [-]	ILDNAM(1) Char(10)	ILDNAM(2) Char(10)				
FSGRID1	IFGFSFIL (0/1)	FGFSNAM(1) Char(10)	FGFSNAM(2) Char(10)					
FSGRID2	FSLENA [m]	FSLENF [m]	FSLENS [m]	NXGRID [-]	NYGRID [-]	ZFSGRD [-]		
ROLLDAMP	IROLD (0/1/2/3)	ILIFRD (0/1)	LINFACT [-]	QUADFACT [-]	B44L [kgm^2s]	B44Q [kgm^2]	BETAE [deg]	
BILGEKEEL	XBILKL [m]	YBILKL [m]	ZBILKL [m]	HBILKL [m]	PHIBILKL [deg]			
MOORSPRING	CMRX0 (N/m)	CMRY0 (N/m)	CMRYAW (Nm/rad)					
COMMENT	Arbitrary	User	Comment					

Figure 54: Complete panship input table.

B Potential Flow Equations

For all gas and fluid flow, the governing equations are the so called Navier-Stokes equations. This set of differential equations could be used to simulate any flow. The solution of these equations is a velocity field ($\vec{v}$), a function describing the fluid velocity in any direction at any given position within the domain. However, to be able to obtain a numerical solution for these equations, an excessive amount of computer power is needed. This is the reason that in the past a number of simplifications have been developed that lead to reasonable results, but with only a fraction of the computational effort needed. One of these simplified flow models is potential flow. This Appendix will describe the simplification from the (incompressible) Navier-Stokes equations to the potential flow equation.

B.1 Conservation of Mass

The first equation that has to be satisfied within any fluid domain is the conservation of mass. This simply means that, within the fluid there can be no production or destruction of particles. Hence the sum of all inflow around the domain boundaries ($S(t)$) has to be equal to the change in mass within the domain($V(t)$).

$$\frac{d}{dt}\int_{V(t)} \rho dV + \int_{S(t)} \rho\vec{v}\cdot\vec{n}dS = 0 \tag{B.1}$$

Using the Gauss' divergence theorem, the integral over the domain boundary can be transformed into a volume integral. After pulling together both integrals we get the following:

$$\int_{V(t)} (\frac{d}{dt}\rho + \nabla\cdot\rho\vec{v})dV = 0 \tag{B.2}$$

Here, the first simplification takes place. For flow speeds under mach 0.3, it can safely be assumed that the fluid will act like an incompressible fluid. This means that ρ can be assumed to be constant.

$$\int_{V(t)} (\nabla\cdot\vec{v})dV = 0 \tag{B.3}$$

This is the mass conservation equation for the incompressible Navier-Stokes equations

B.2 Conservation of Momentum

The conservation of momentum within a fluid domain is basically the fluid mechanics version of $F = m\cdot a$. Unfortunately, since the fluid can be moving freely within the domain and even over the domain boundaries, this equation becomes a little more complicated.

$$\frac{d}{dt}\int_{V(t)} \rho\vec{v}dV + \int_{S(t)} \rho\vec{v}(\vec{v}\cdot\vec{n})dS = \sum\vec{F} \tag{B.4}$$

Here, the first integral represents the momentum that is present within the domain, and the second integral represents the momentum that is flowing in and out of the domain with the fluid particles crossing the boundaries.

Again, the Gauss' divergence theorem can be used to eliminate turn the surface integral into a volume integral.

$$\int_{V(t)} \vec{v}(\frac{\partial\rho}{\partial t} + \nabla\cdot\rho\vec{v}) + \rho(\frac{\partial\vec{v}}{\partial t} + \vec{v}\cdot\nabla\vec{v})dV = \sum\vec{F} \tag{B.5}$$

Now here we can substitute (B.2) in order to eliminate the term within the first brackets. Secondly, let's have a look at the right side of the equation. All external forces that act on a fluid domain are gravity, pressure and viscous drag. Here, the second simplification is made to the equations. Since Potential flow assumes an inviscid flow, only pressure and gravity remain.

$$\sum\vec{F} = -\int_{S(t)} p\vec{n}dS + \int_{V(t)} \rho g dV = \int_{V(t)} (\rho g - \nabla p)dV \tag{B.6}$$

Again, the surface integral has been transformed into a volume integral. After this, the entire equation looks as follows:

$$\int_{V(t)} \rho(\frac{\partial \vec{v}}{\partial t} + \vec{v} \cdot \nabla \vec{v}) dV = \int_{V(t)} (\rho g - \nabla p) dV \tag{B.7}$$

At this point, the third assumption used for potential flow has to be made. This is that the flow is irrotational, which means that the curl of the velocity field, $\nabla \times \vec{v}$ is zero. Notice that the second term of the left hand integral can be rewritten using the definition of the curl of a vector:

$$\vec{v} \cdot \nabla \vec{v} = \nabla(\frac{1}{2} V^2) + \nabla \times \vec{v} \tag{B.8}$$

Here, V represents the local flow velocity $\sqrt{u^2 + v^2 + w^2}$. Since the last part is assumed to be zero, the final equation for the conservation of momentum can be given as:

$$\int_{V(t)} \rho(\frac{\partial \vec{v}}{\partial t} + \nabla(\frac{1}{2} V^2)) dV = \int_{V(t)} (\rho g - \nabla p) dV \tag{B.9}$$

B.3 Velocity Potential

A vector that has zero curl has to be the gradient of a scalar function. This scalar function is commonly known as the velocity potential and is defined as follows:

$$\vec{v} = \nabla \Psi \tag{B.10}$$

Substituting this potential into (B.9) (and differentiating both sides of the equation to eliminate the integrals) gives us the Bernoulli equation for potential flow.

$$\frac{p}{\rho} + \frac{\partial \Psi}{\partial t} + \frac{1}{2} \nabla \Psi \cdot \nabla \Psi - gz = C \tag{B.11}$$

Substituting (B.9) into the conservation of mass (B.3) gives the continuity equation for potential flow:

$$\nabla^2 \Psi = 0 \tag{B.12}$$

C Pressure Measurements in Seven calm water runs

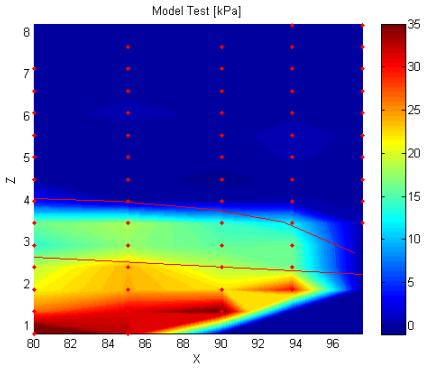

Figure 55: Pressure and wave height measurements 1st run.

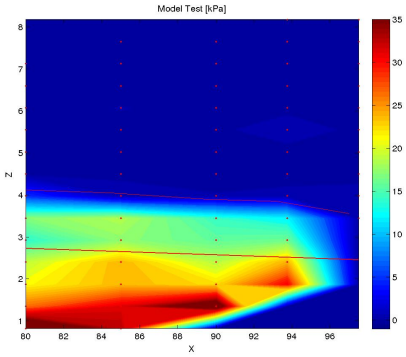

Figure 56: Pressure and wave height measurements 2nd run.

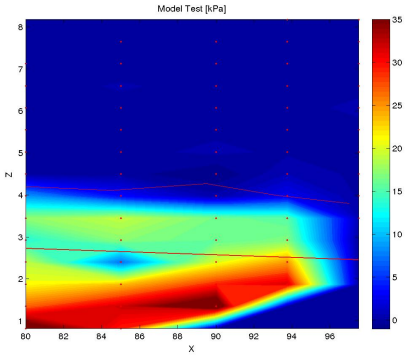

Figure 57: Pressure and wave height measurements 3rd run.

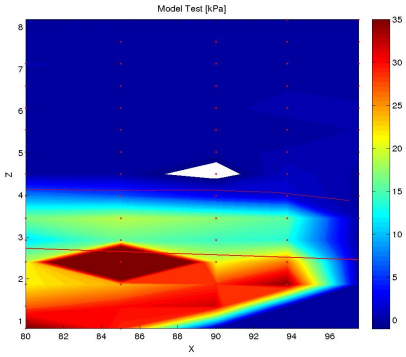

Figure 58: Pressure and wave height measurements 4th run.

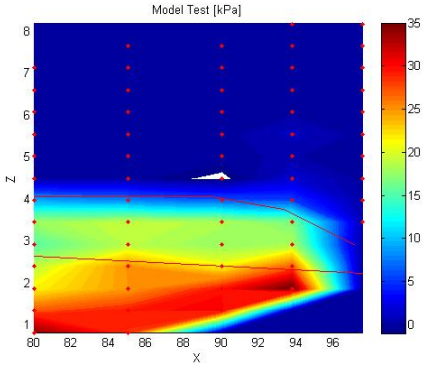

Figure 59: Pressure and wave height measurements 5th run.

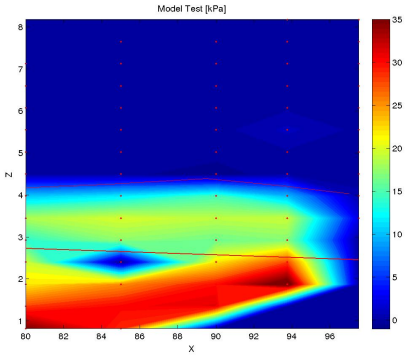

Figure 60: Pressure and wave height measurements 6th run.

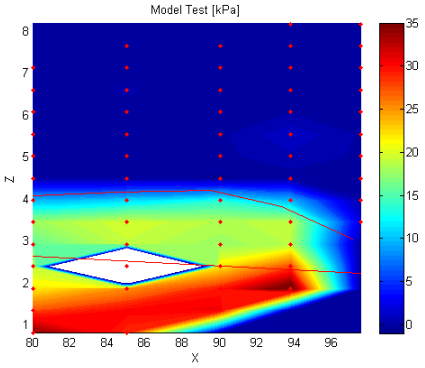

Figure 61: Pressure and wave height measurements 7th run.

D Example input file irregular stern quartering waves

```
SIMULATION8500      150       0         0.100     50        10        11.832
GEOMETRY  FDS_23.psh          100.0
MASSPROP  1607000.  5.00      25.0      25.0      44.71     6.10
OPTIONS1  1         1         1         0         0         GfFDS.dat
OPTIONS2  0         2         0         0         0         0         0
CONSTANTS 1025.0    1.0       5         0.25      0.75                          6
OSCIL     0         1.25      0.5
CFVISC    0.0       1.0       1.2E-06
MODE-OFF  1         1         1         1         1         1
WAVESPEC  5         3.8       7.1       345       3.30      80        847235
CONTROL   0         0         0
ROLLDAMP  1         1         1.0       1.0                           20.0
COMMENT   Skeg
RUDDER    17.5      0         1         12.5      0.9       0
COMMENT   Portside
RUDDER    1.803     1.950     1.2       1.618     2.183     103       1
BILGEKEEL 30        4.25      1.75      0.044     110
BILGEKEEL 30.11     4.25      1.75      0.044     110
BILGEKEEL 49.89     4.25      1.75      0.044     110
BILGEKEEL 50        4.25      1.75      0.044     110
PROPSHAFT 3.777     1.950     0.2       20        1.95      1.12      0.1
PROPELLER13.382     1.950     0.2       2.666     0.671     431.5
PROPELLER24         0.607
COMMENT   Starboard
RUDDER    1.803     -1.950    1.2       1.618     2.183     77        2
BILGEKEEL 30        -4.25     1.75      0.044     70
BILGEKEEL 30.11     -4.25     1.75      0.044     70
BILGEKEEL 49.89     -4.25     1.75      0.044     70
BILGEKEEL 50        -4.25     1.75      0.044     70
PROPSHAFT 3.777     -1.950    0.2       20        -1.95     1.12      0.1
PROPELLER13.382     -1.950    0.2       2.666     0.671     431.5
PROPELLER24         0.607
SLAMPOS   79.995    6.018     7.125
SLAMPOS   79.995    5.7525    6.6
SLAMPOS   79.995    5.4765    6.075
SLAMPOS   79.995    5.1855    5.55
SLAMPOS   79.995    4.8675    5.025
SLAMPOS   79.995    4.5105    4.5
SLAMPOS   79.995    4.101     3.975
SLAMPOS   79.995    3.648     3.45
SLAMPOS   79.995    3.15      2.925
SLAMPOS   79.995    2.5995    2.4
SLAMPOS   79.995    2.001     1.875
SLAMPOS   79.995    1.395     1.35
SLAMPOS   79.995    0.828     0.825
SLAMPOS   85.005    5.793     7.65
SLAMPOS   85.005    5.472     7.125
SLAMPOS   85.005    5.1495    6.6
SLAMPOS   85.005    4.824     6.075
SLAMPOS   85.005    4.4865    5.55
SLAMPOS   85.005    4.122     5.025
SLAMPOS   85.005    3.7245    4.5
SLAMPOS   85.005    3.2985    3.975
SLAMPOS   85.005    2.853     3.45
SLAMPOS   85.005    2.391     2.925
SLAMPOS   85.005    1.914     2.4
SLAMPOS   85.005    1.4325    1.875
```

```
SLAMPOS   85.005    0.9705    1.35
SLAMPOS   85.005    0.555     0.825
SLAMPOS   90        5.004     7.65
SLAMPOS   90        4.626     7.125
SLAMPOS   90        4.257     6.6
SLAMPOS   90        3.8925    6.075
SLAMPOS   90        3.5235    5.55
SLAMPOS   90        3.15      5.025
SLAMPOS   90        2.7675    4.5
SLAMPOS   90        2.382     3.975
SLAMPOS   90        1.9965    3.45
SLAMPOS   90        1.6155    2.925
SLAMPOS   90        1.2465    2.4
SLAMPOS   90        0.9       1.875
SLAMPOS   90        0.588     1.35
SLAMPOS   93.75     4.5795    8.175
SLAMPOS   93.75     4.1625    7.65
SLAMPOS   93.75     3.7635    7.125
SLAMPOS   93.75     3.3825    6.6
SLAMPOS   93.75     3.012     6.075
SLAMPOS   93.75     2.6505    5.55
SLAMPOS   93.75     2.3025    5.025
SLAMPOS   93.75     1.965     4.5
SLAMPOS   93.75     1.641     3.975
SLAMPOS   93.75     1.329     3.45
SLAMPOS   93.75     1.035     2.925
SLAMPOS   93.75     0.765     2.4
SLAMPOS   93.75     0.525     1.875
SLAMPOS   97.5      3.453     8.175
SLAMPOS   97.5      3.0405    7.65
SLAMPOS   97.5      2.661     7.125
SLAMPOS   97.5      2.304     6.6
SLAMPOS   97.5      1.9635    6.075
SLAMPOS   97.5      1.6425    5.55
SLAMPOS   97.5      1.3485    5.025
SLAMPOS   97.5      1.0815    4.5
SLAMPOS   97.5      0.8445    3.975
SLAMPOS   97.5      0.633     3.45
```

E Stern quartering waves, statistics

E.1 IFSWAV 1

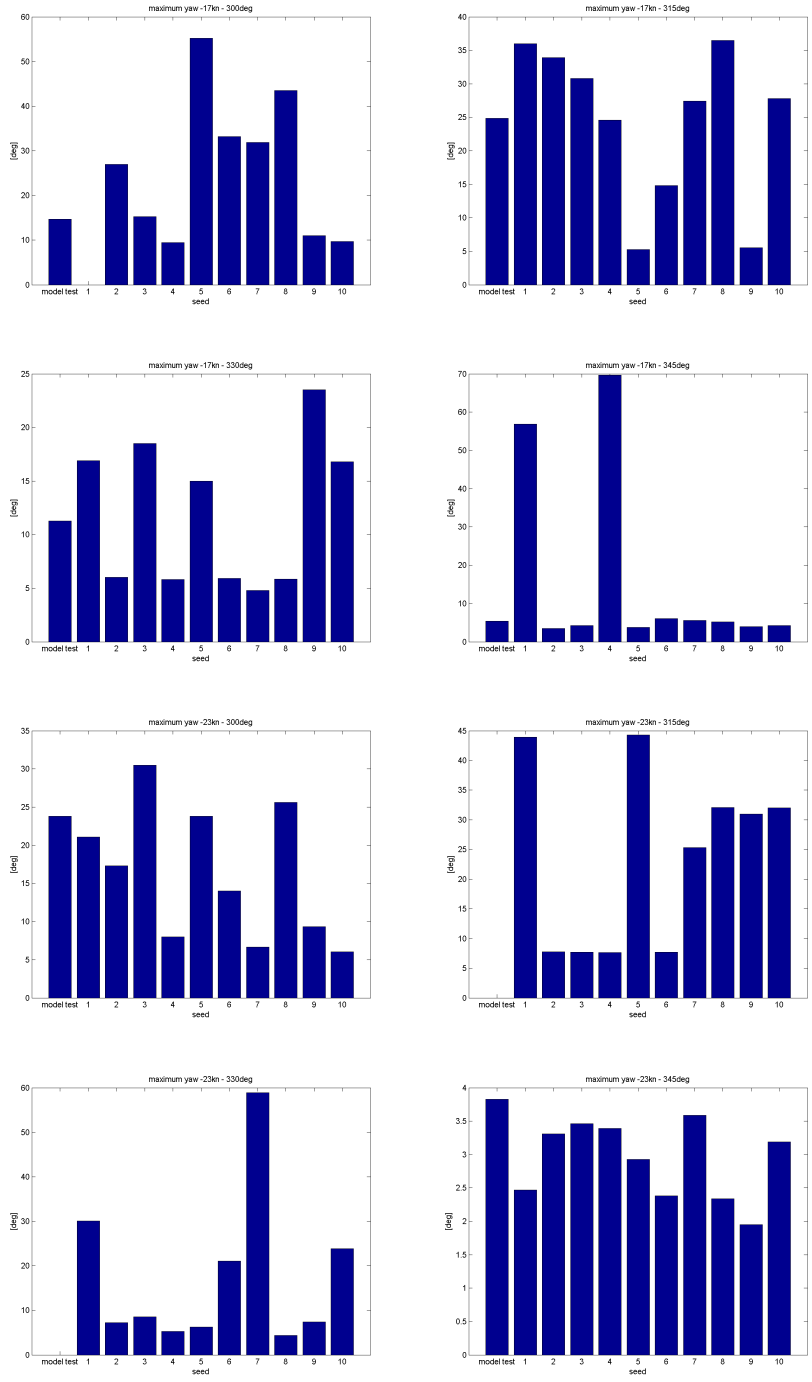

Figure 62: Maximum encountered yaw angle during tests

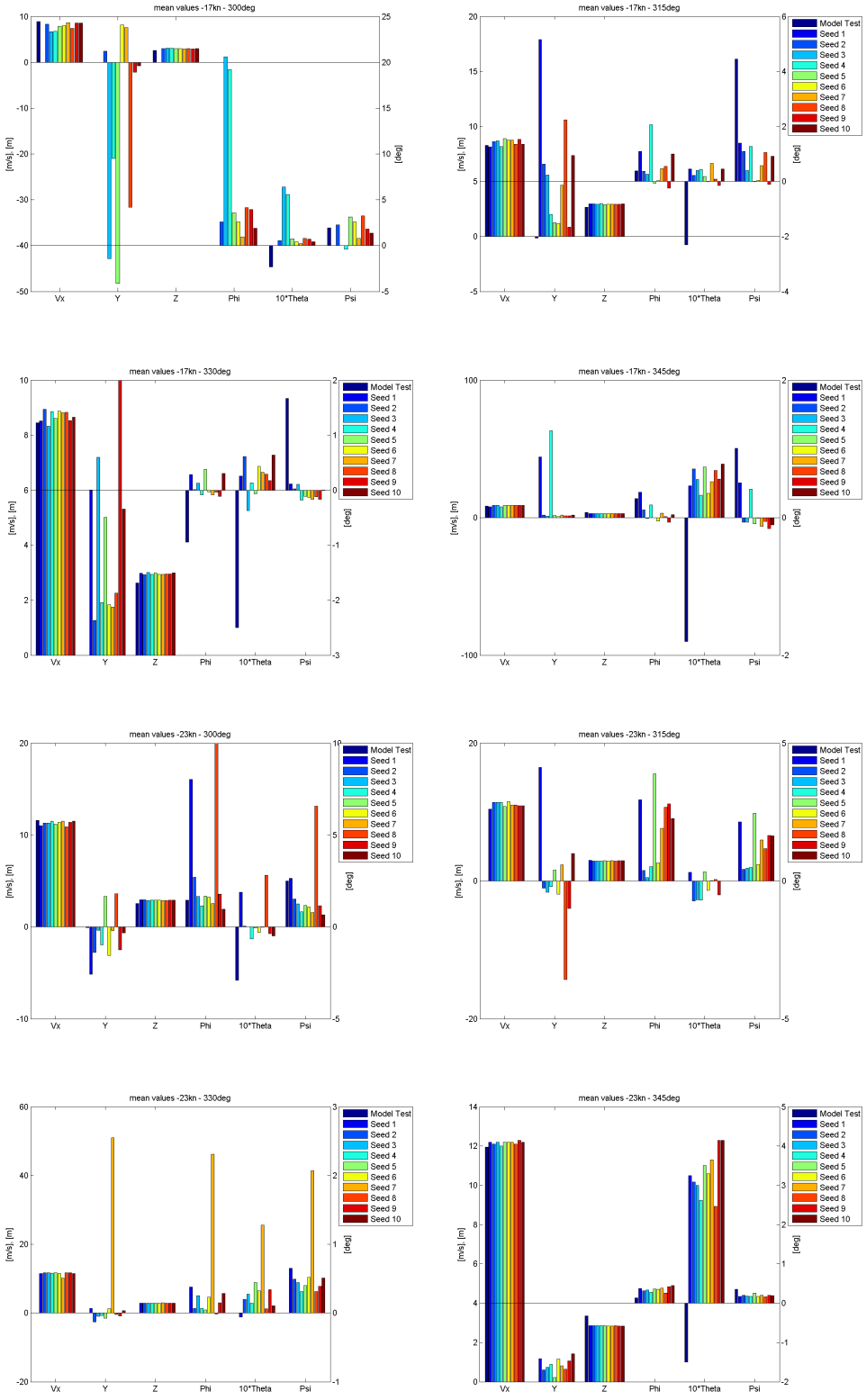

Figure 63: Mean values of ship motions in stern quartering waves

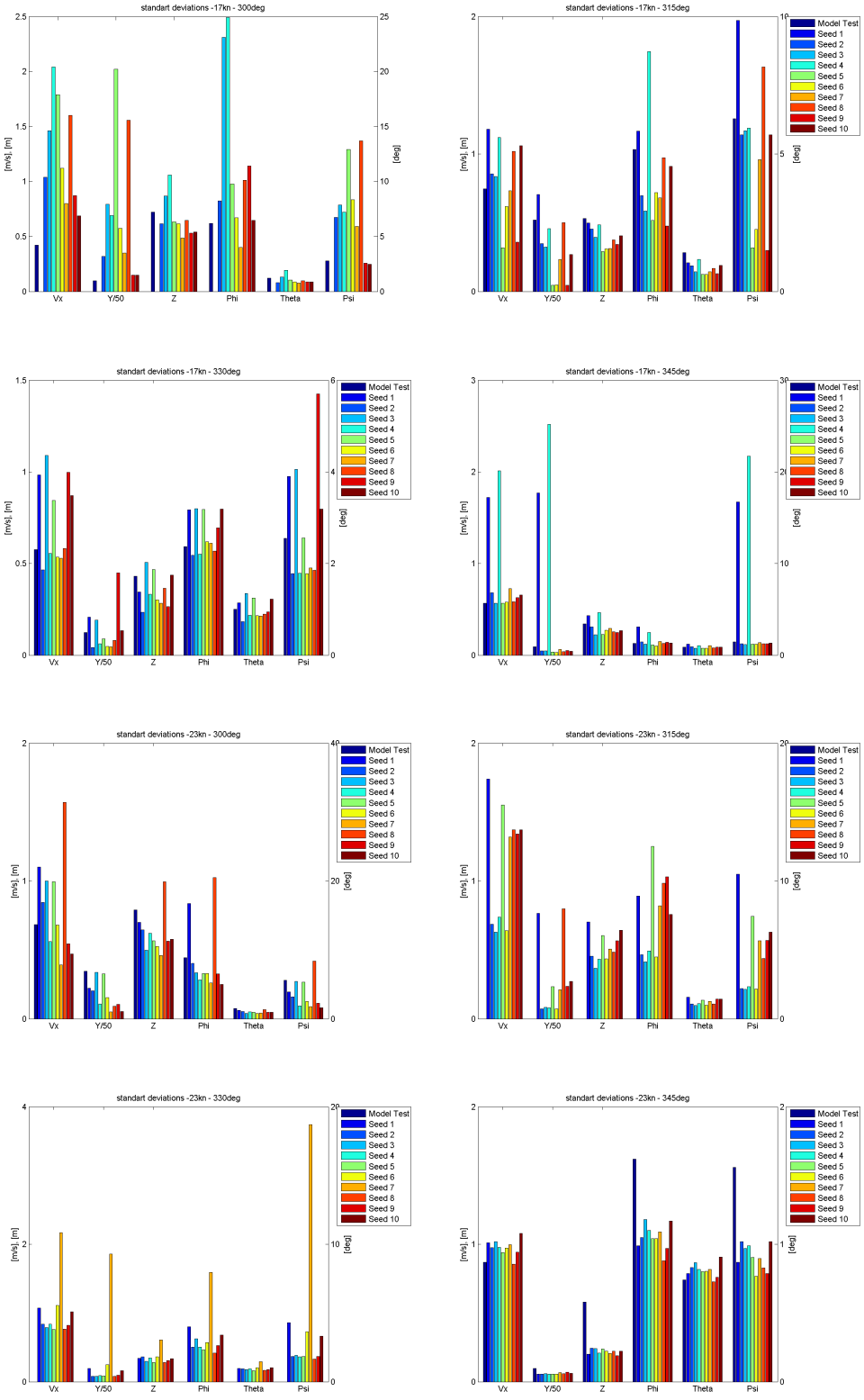

Figure 64: Standard deviations of ship motions in stern quartering waves

E.2 IFSWAV 2

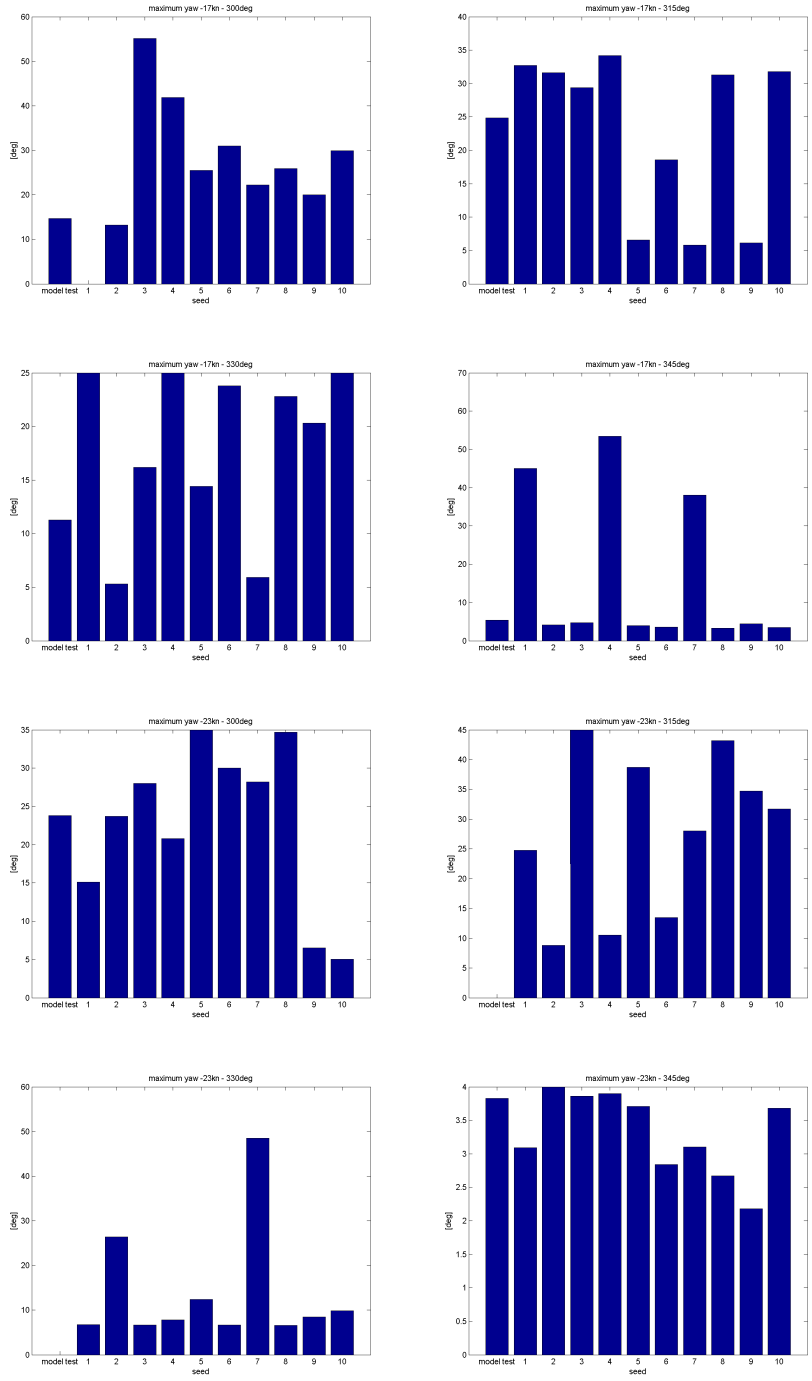

Figure 65: Maximum encountered yaw angle during tests

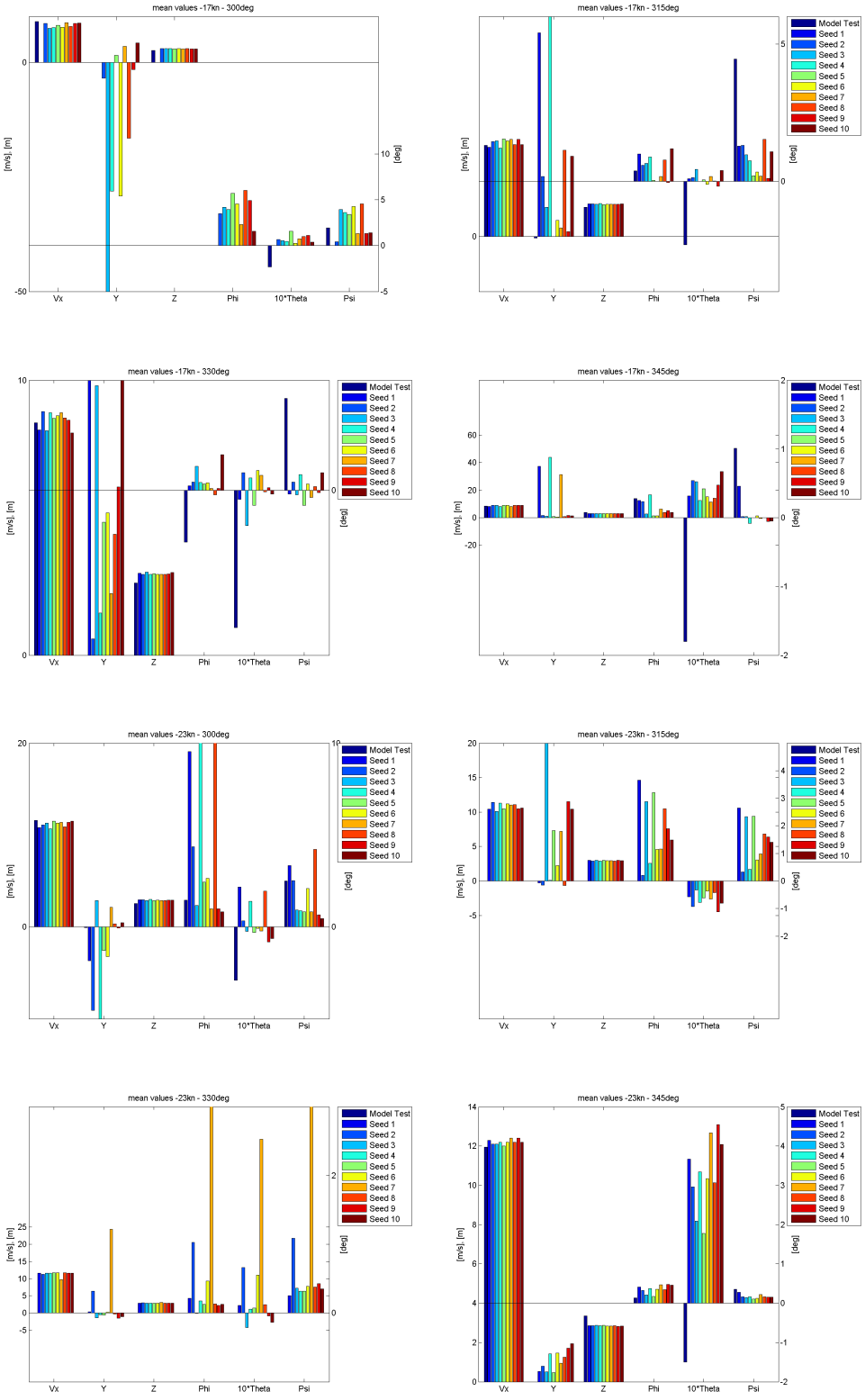

Figure 66: Mean values of ship motions in stern quartering waves

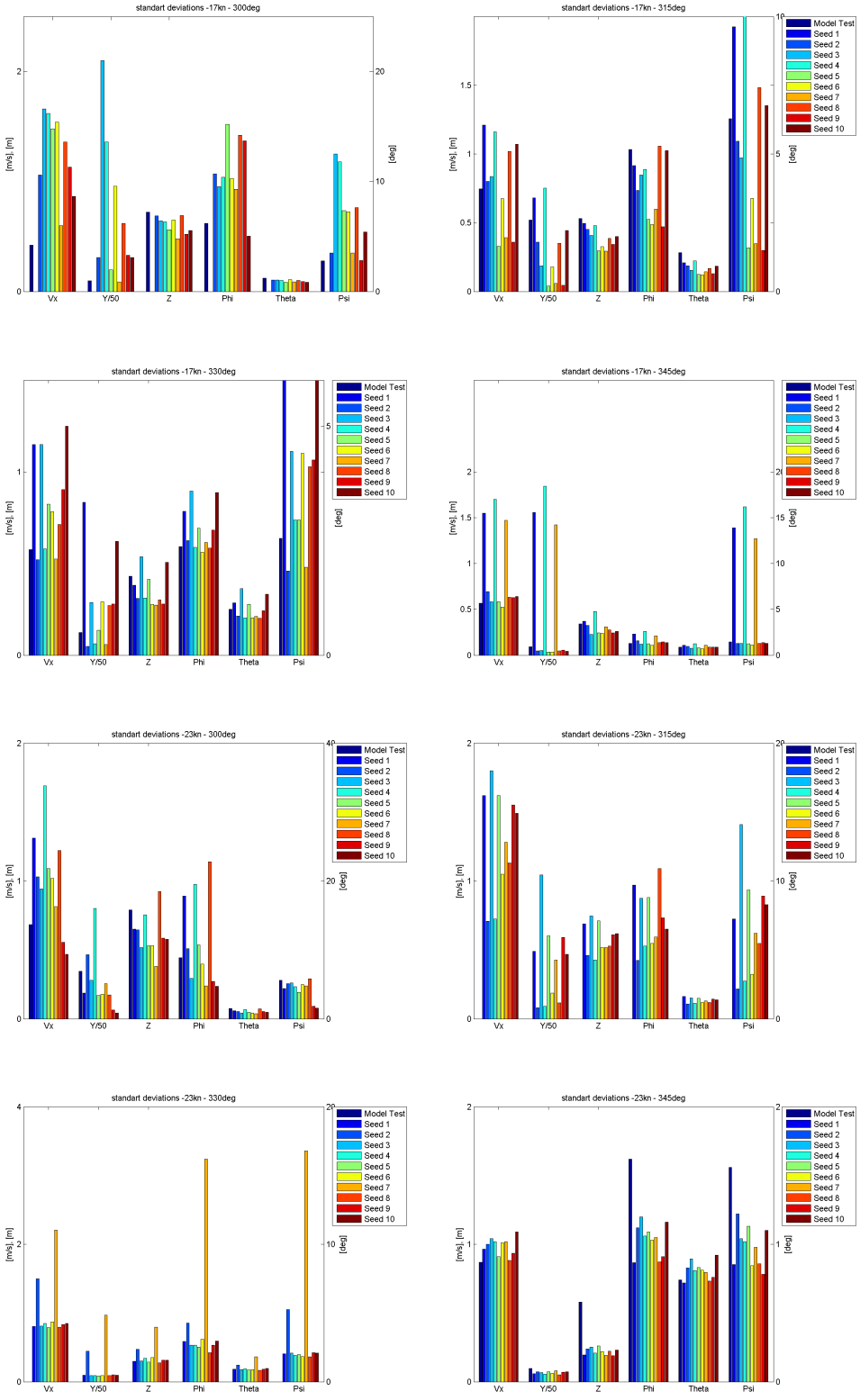

Figure 67: Standard deviations of ship motions in stern quartering waves

F Random seeds for wave train realizations

train realization	seed
1	847235
2	123456
3	654321
4	321654
5	456123
6	456789
7	987654
8	654987
9	789456
10	123789

Table 10: Initial random seeds, used for wave train realizations

G Probability of Exceedance Functions

G.1 Roll Motions

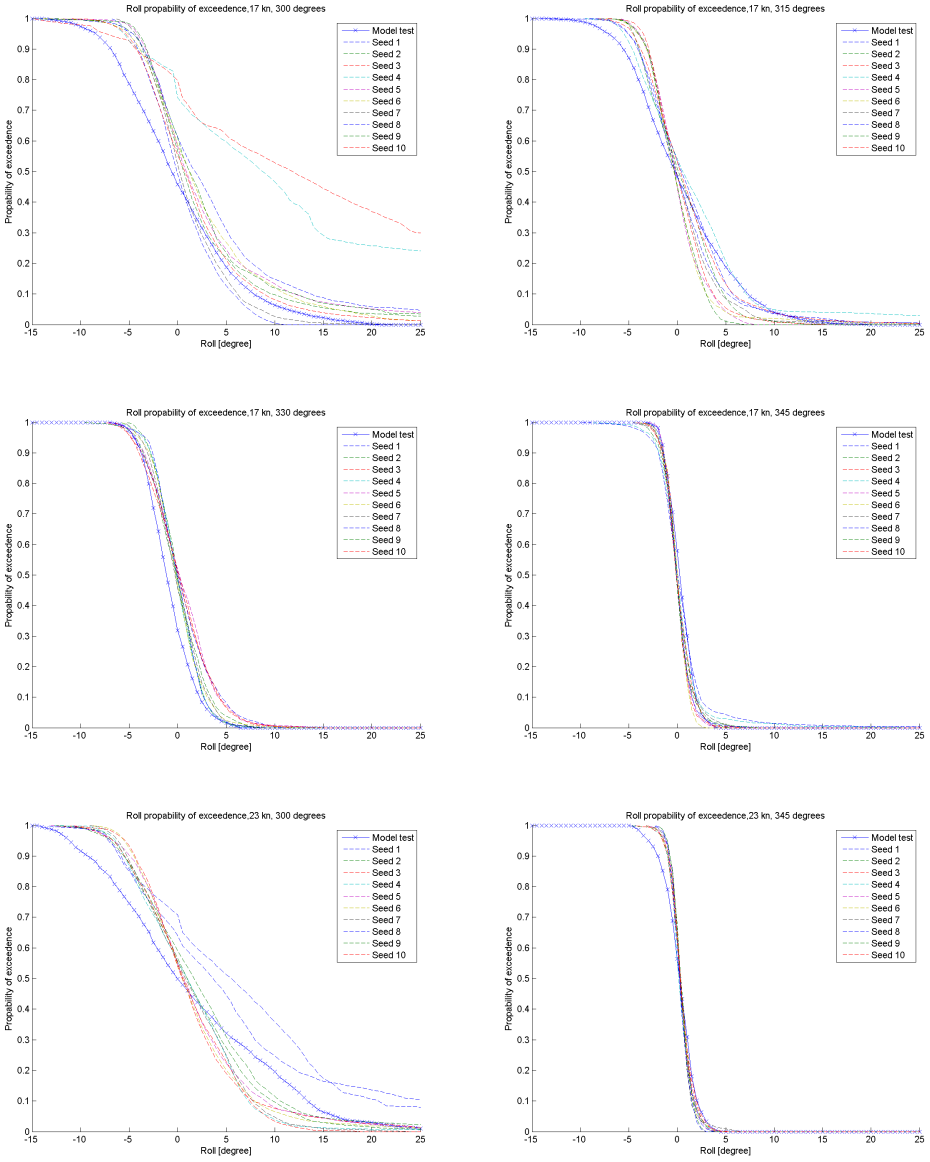

Figure 68: Probability of exceedance functions for roll motions in 6 conditions.

G.2 Yaw Motions

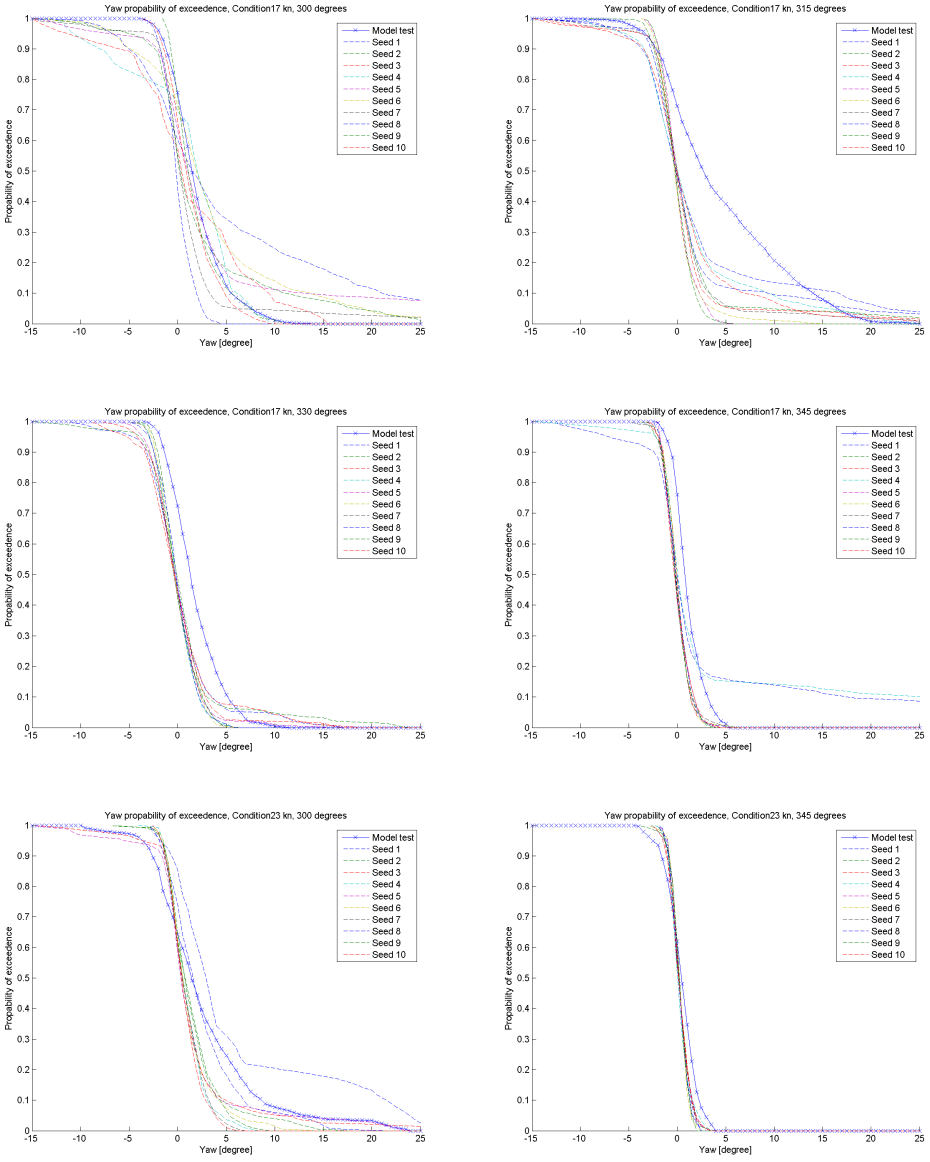

Figure 69: Probability of exceedance functions for yaw motions in 6 conditions.

H Results of Deterministic Validation

H.1 Wave Trains

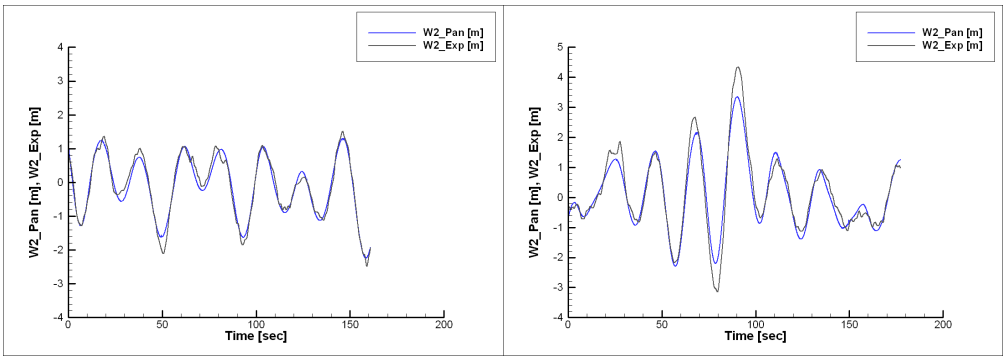

(a) Run 704002

(b) Run 704003

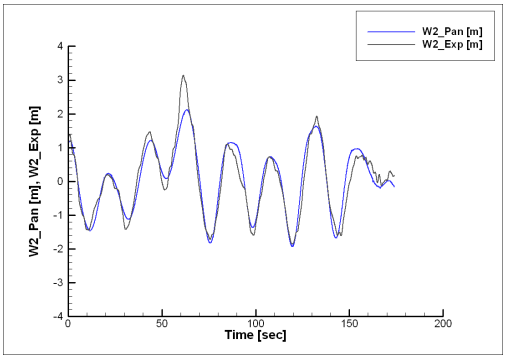

(c) Run 704006

Figure 70: Wave train reproductions of all runs at 17 knots in waves from 345 degrees.

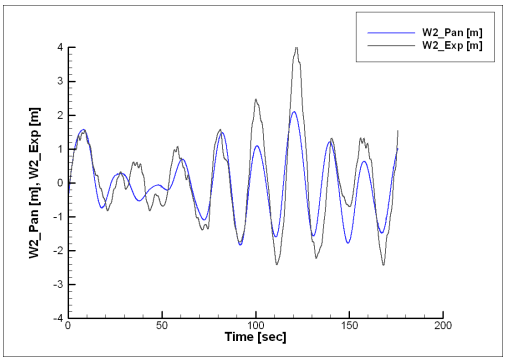

(a) Run 706003

Figure 71: Wave train reproductions of all runs at 17 knots in waves from 330 degrees.

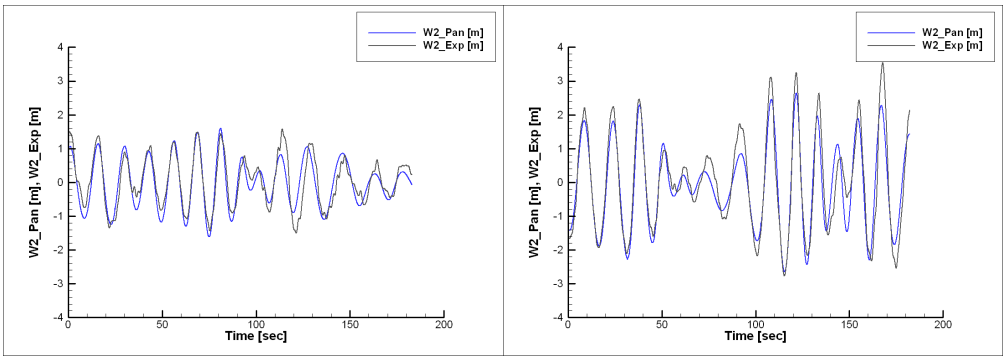

(a) Run 707001 (b) Run 707005

Figure 72: Wave train reproductions of all runs at 17 knots in waves from 315 degrees.

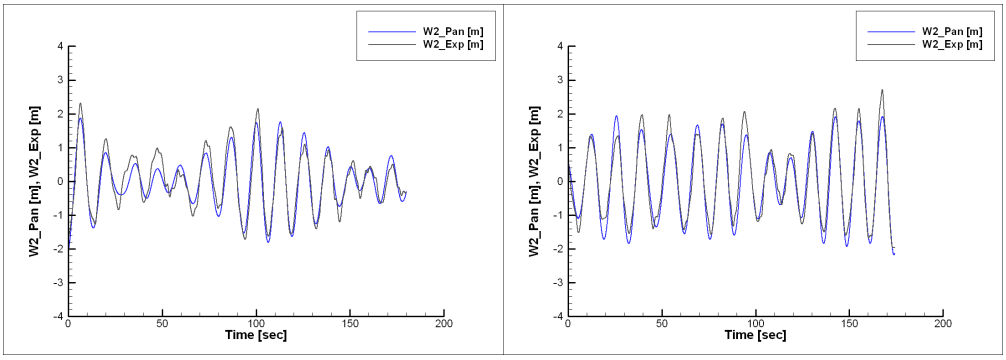

(a) Run 708004 (b) Run 708005

Figure 73: Wave train reproductions of all runs at 17 knots in waves from 300 degrees.

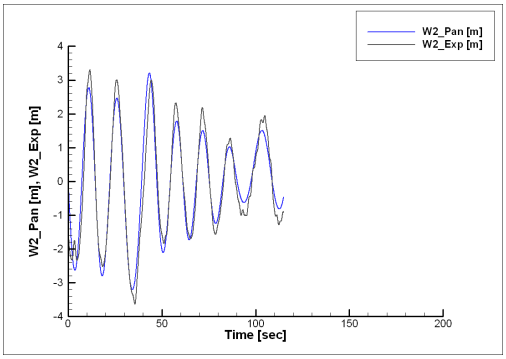

(a) Run 709003

Figure 74: Wave train reproductions of all runs at 23 knots in waves from 300 degrees.

H.2 Motions

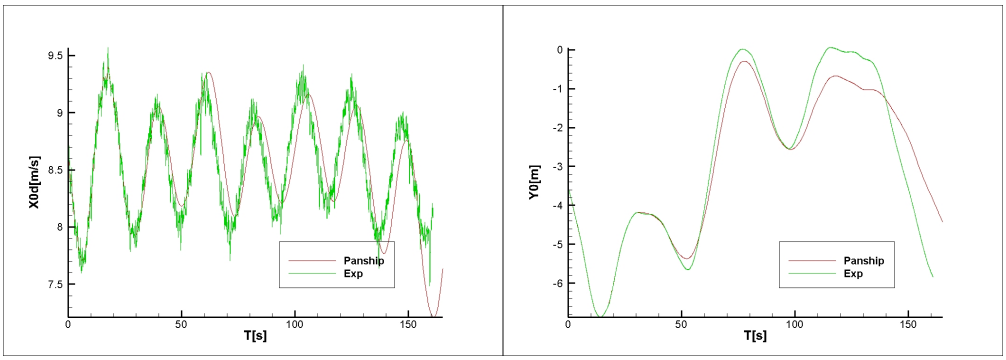

(a) Speed

(b) Sway

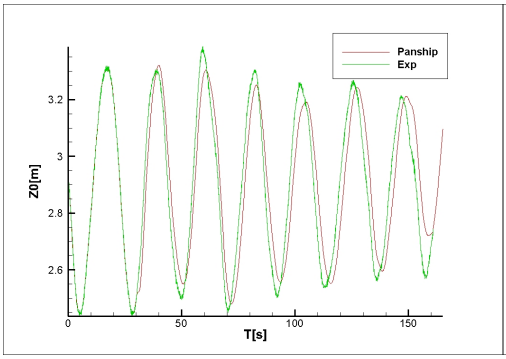

(c) Heave

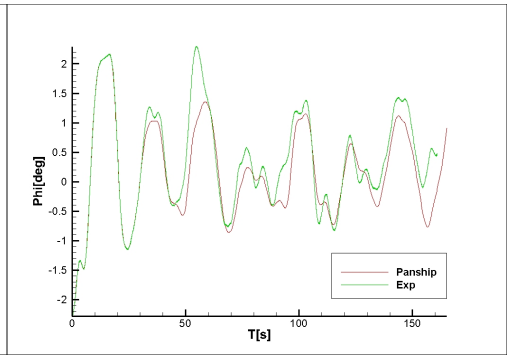

(d) Roll

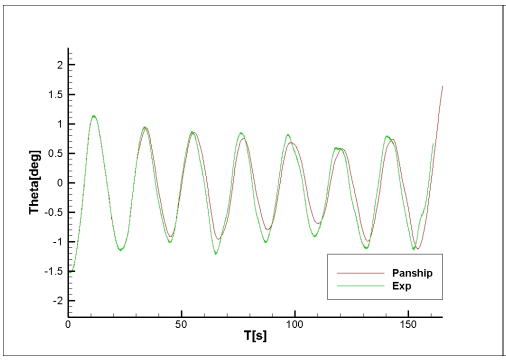

(e) Pitch

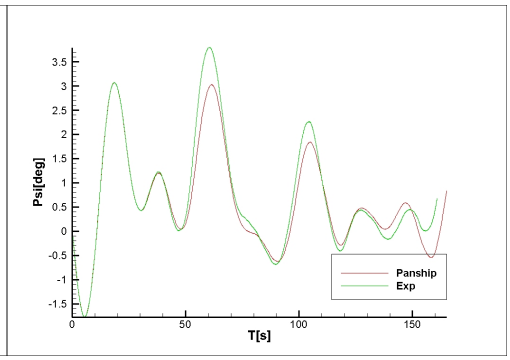

(f) Yaw

Figure 75: Time traces of model test and Panship for run 704002.

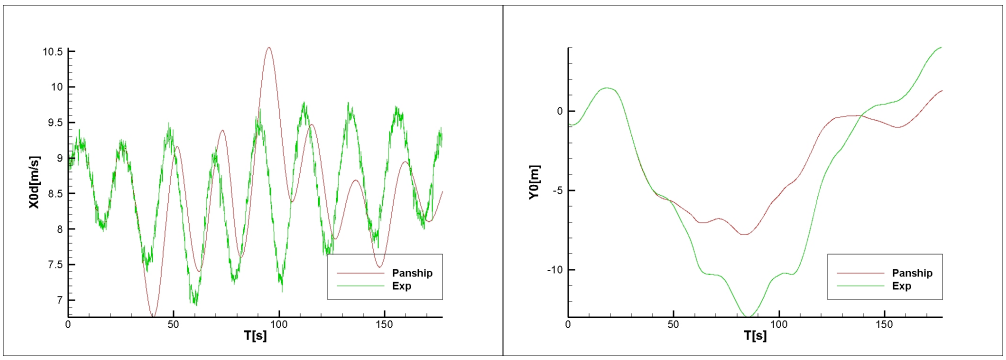

(a) Speed

(b) Sway

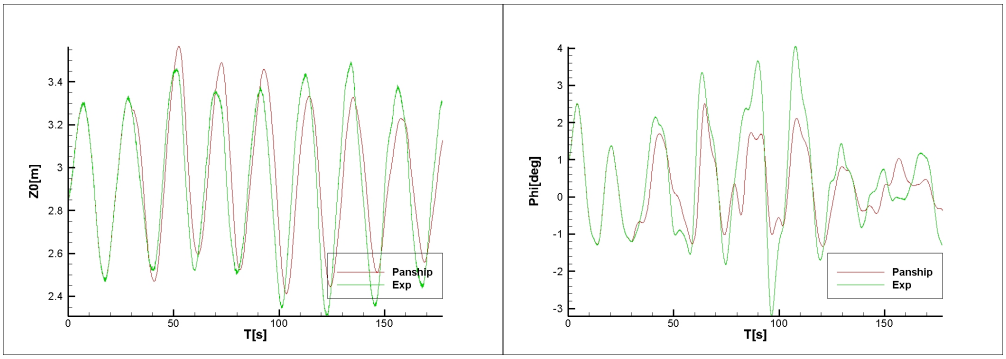

(c) Heave

(d) Roll

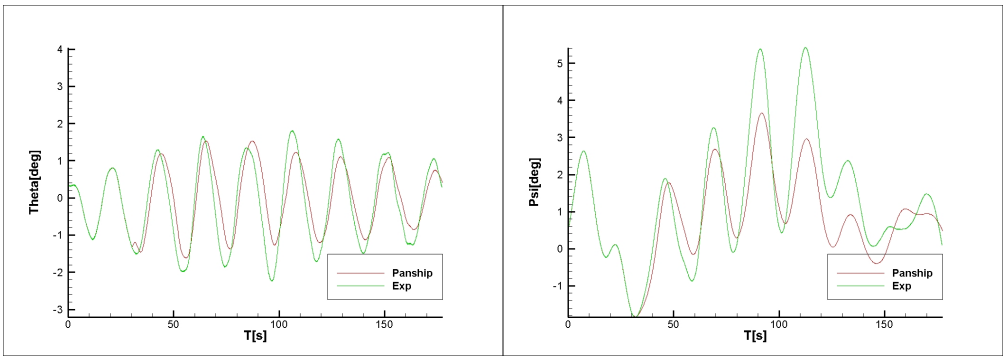

(e) Pitch

(f) Yaw

Figure 76: Time traces of model test and Panship for run 704003.

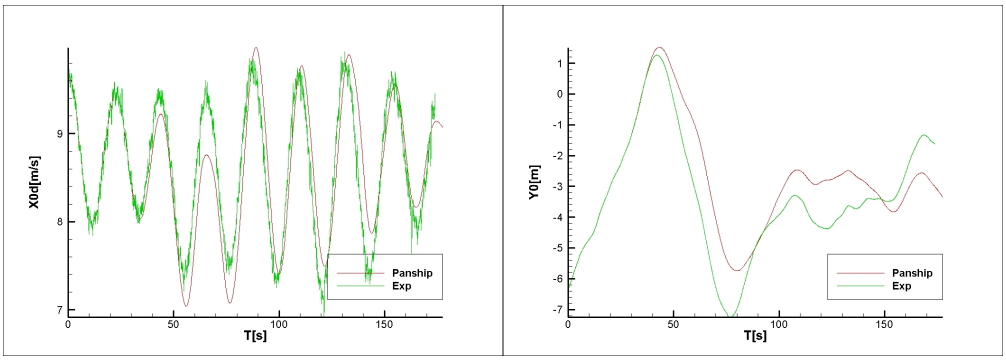

(a) Speed

(b) Sway

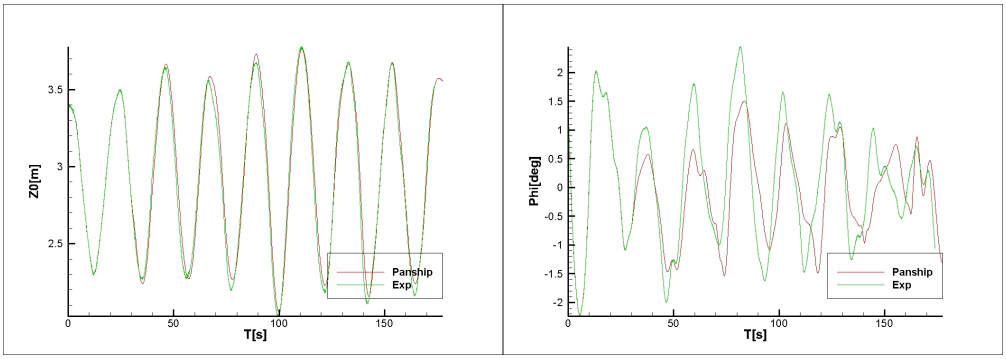

(c) Heave

(d) Roll

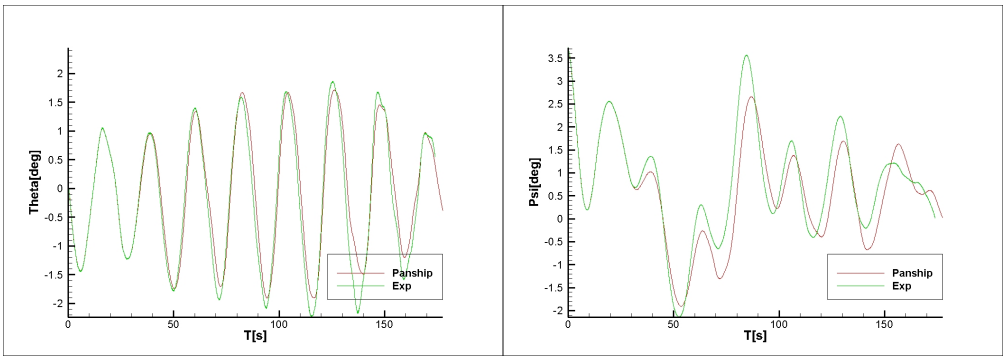

(e) Pitch

(f) Yaw

Figure 77: Time traces of model test and Panship for run 704006.

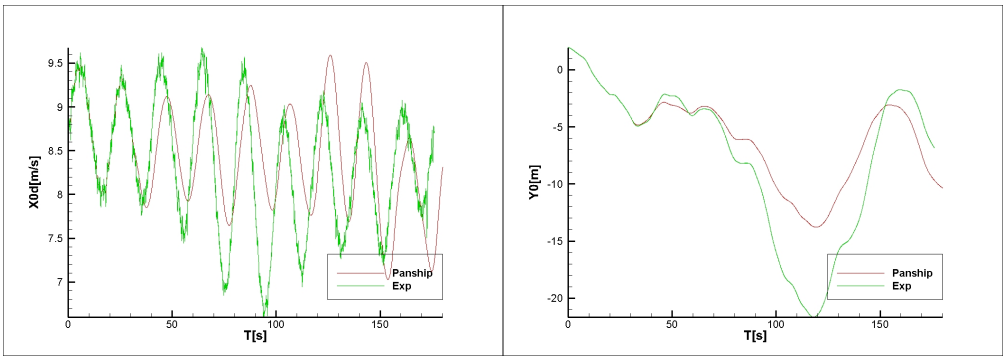

(a) Speed

(b) Sway

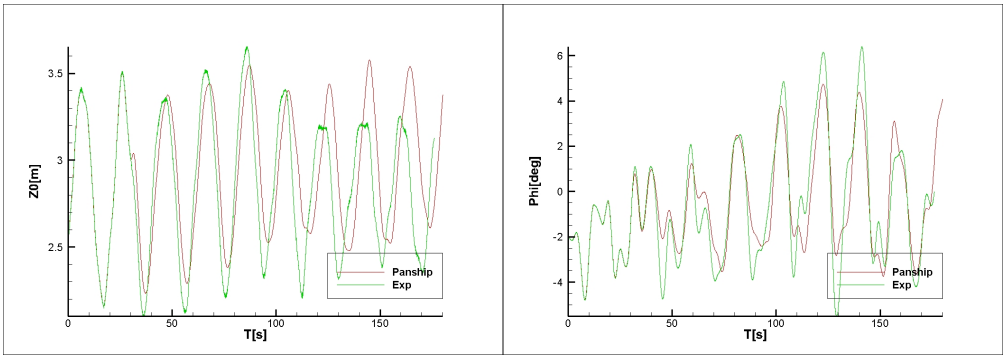

(c) Heave

(d) Roll

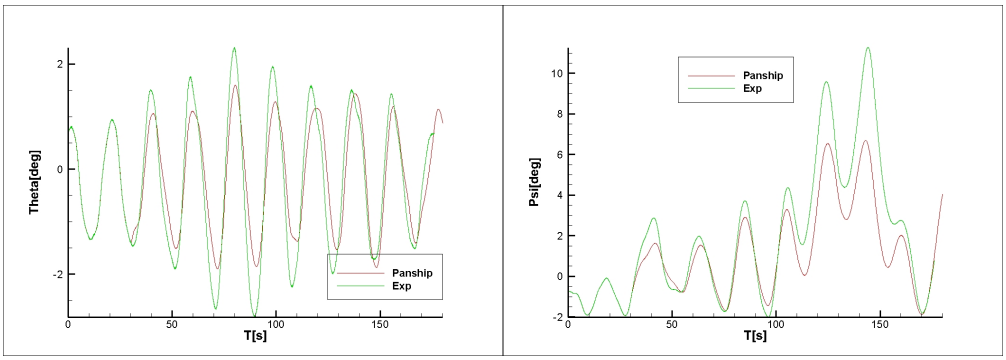

(e) Pitch

(f) Yaw

Figure 78: Time traces of model test and Panship for run 706003.

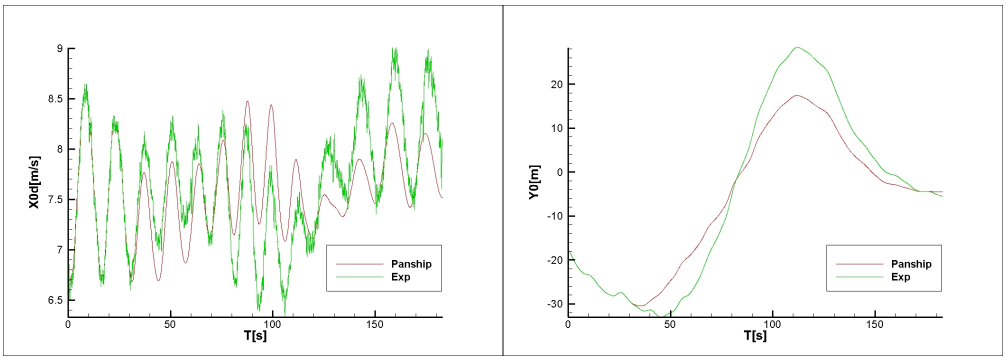

(a) Speed

(b) Sway

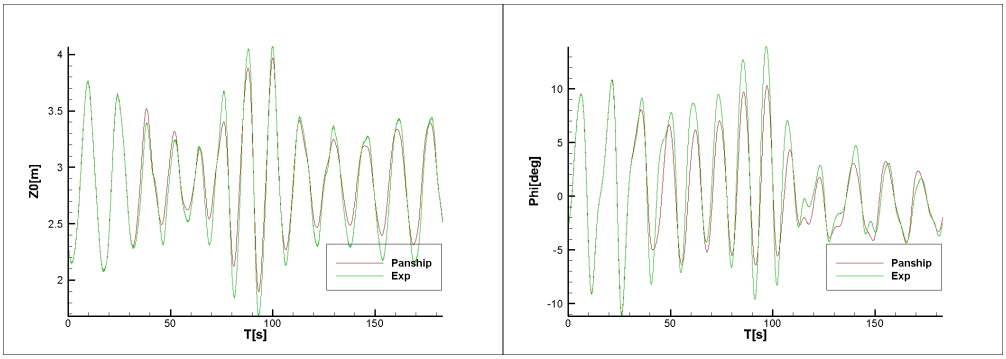

(c) Heave

(d) Roll

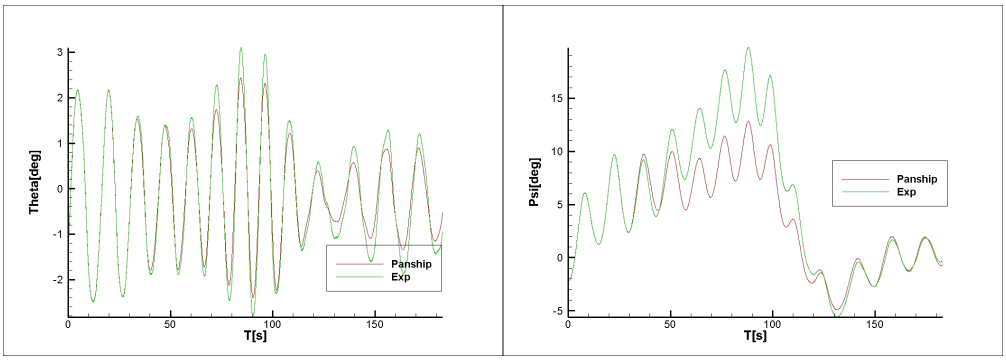

(e) Pitch

(f) Yaw

Figure 79: Time traces of model test and Panship for run 707001.

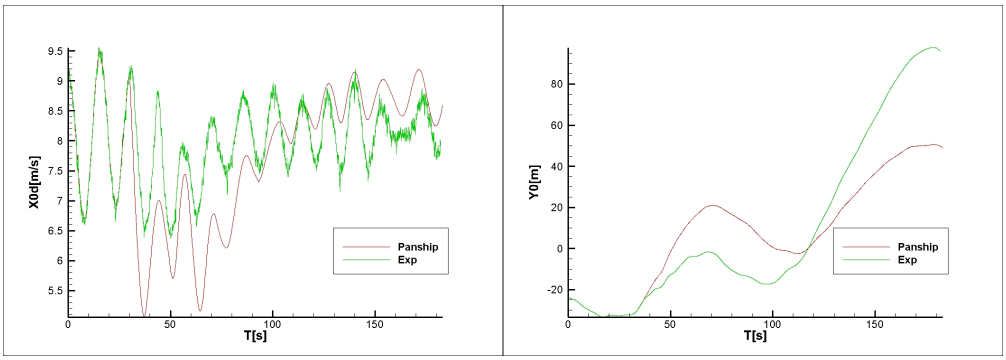

(a) Speed

(b) Sway

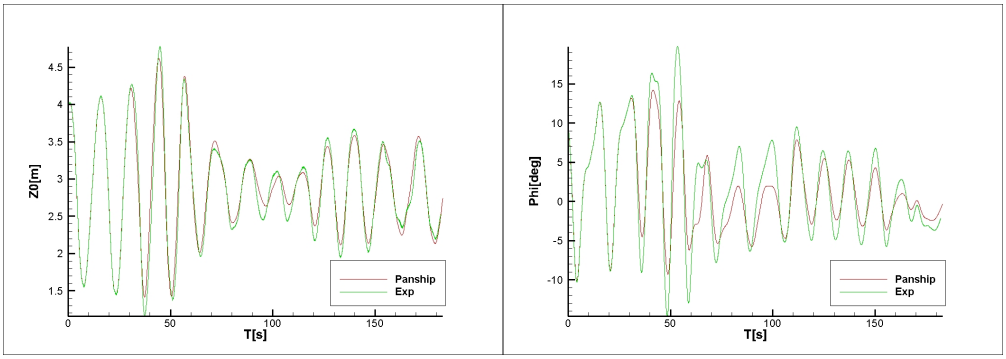

(c) Heave

(d) Roll

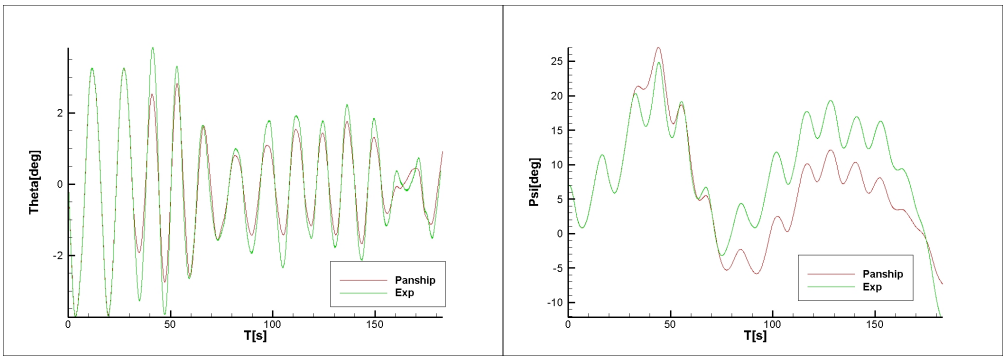

(e) Pitch

(f) Yaw

Figure 80: Time traces of model test and Panship for run 707005.

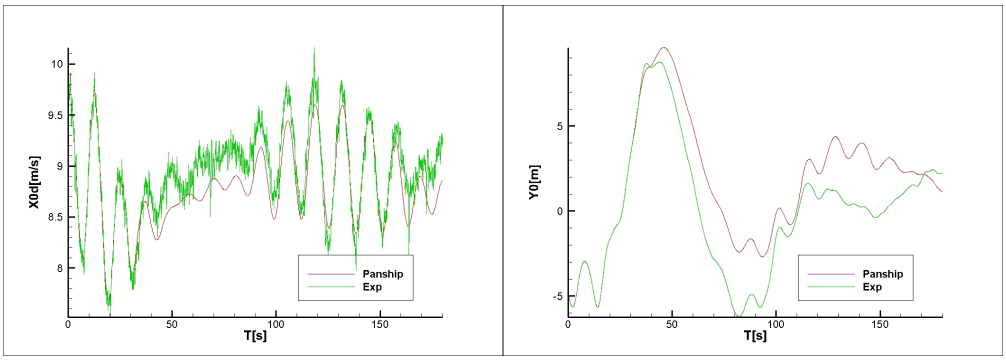

(a) Speed

(b) Sway

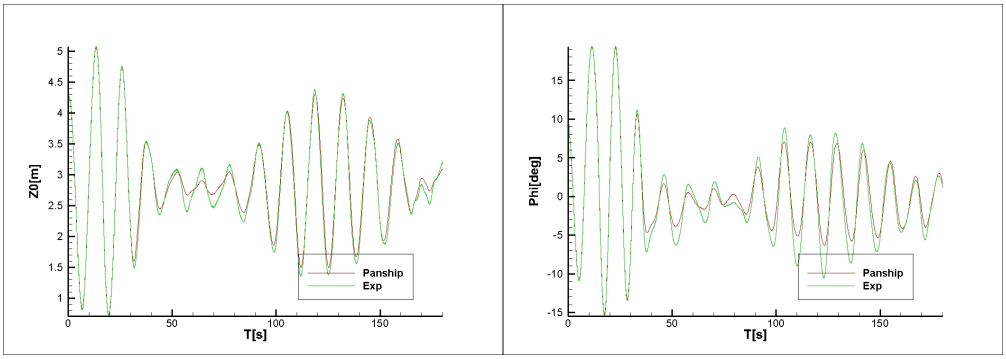

(c) Heave

(d) Roll

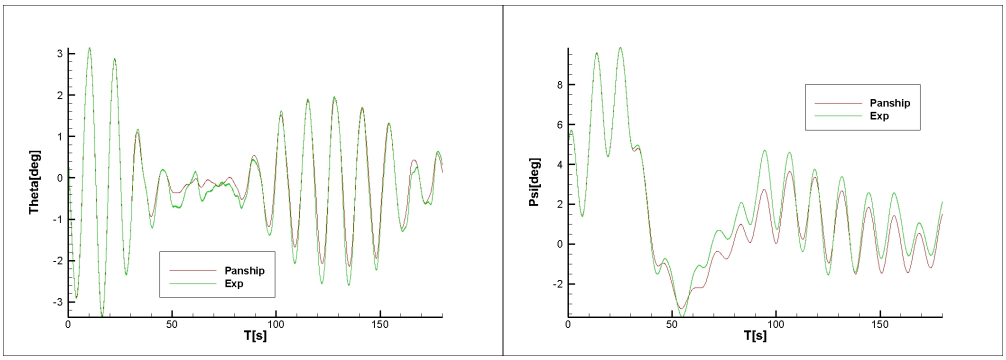

(e) Pitch

(f) Yaw

Figure 81: Time traces of model test and Panship for run 708004.

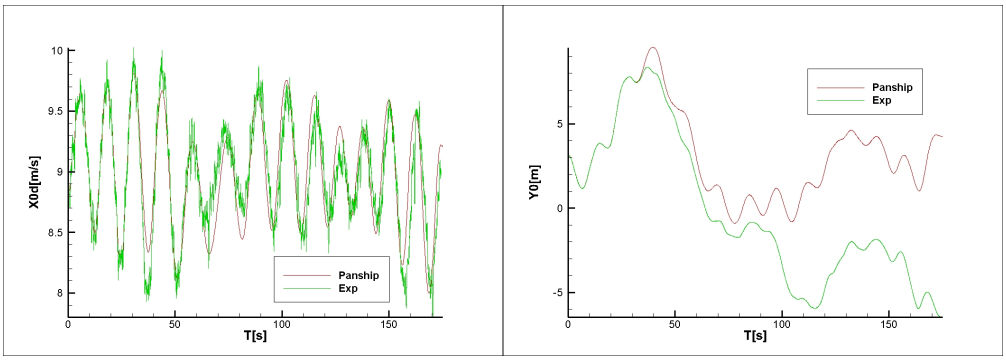

(a) Speed

(b) Sway

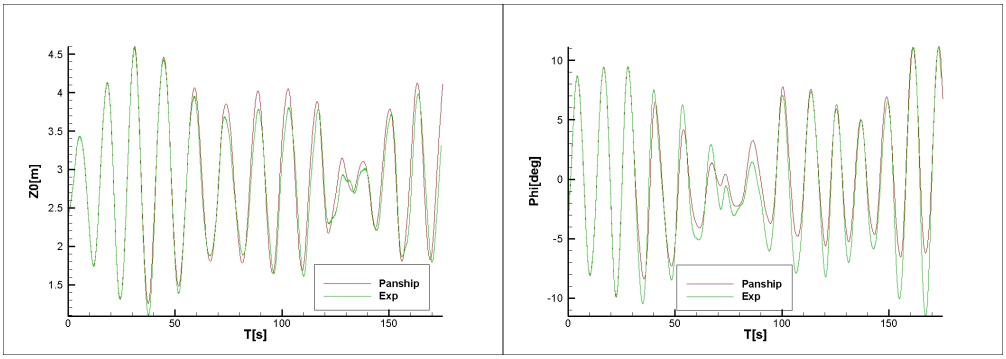

(c) Heave

(d) Roll

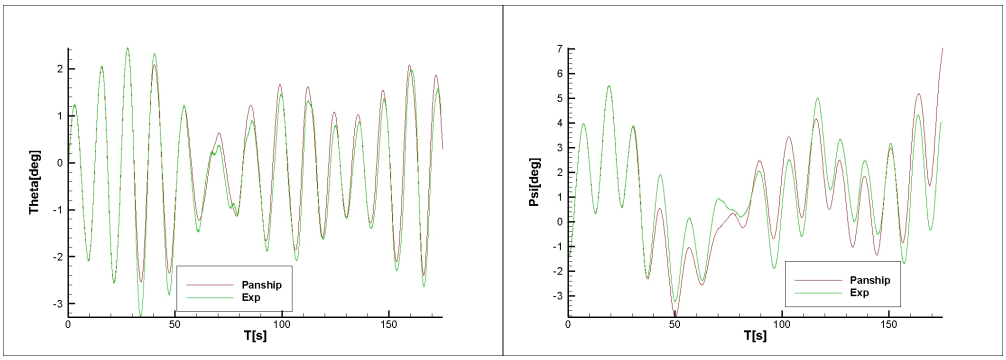

(e) Pitch

(f) Yaw

Figure 82: Time traces of model test and Panship for run 708005.

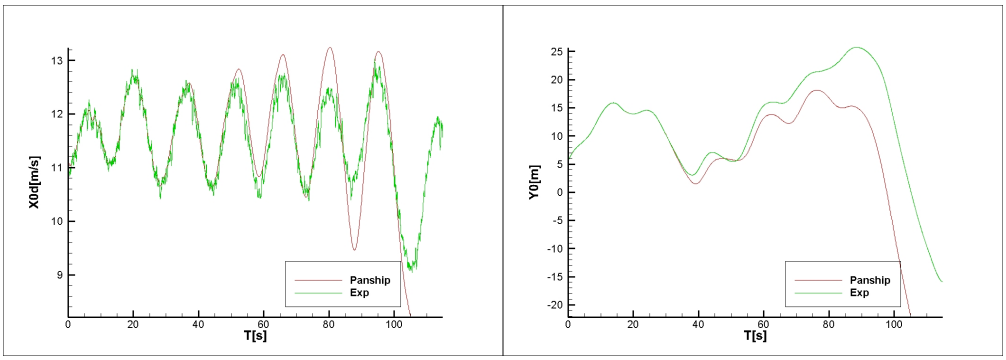

(a) Speed

(b) Sway

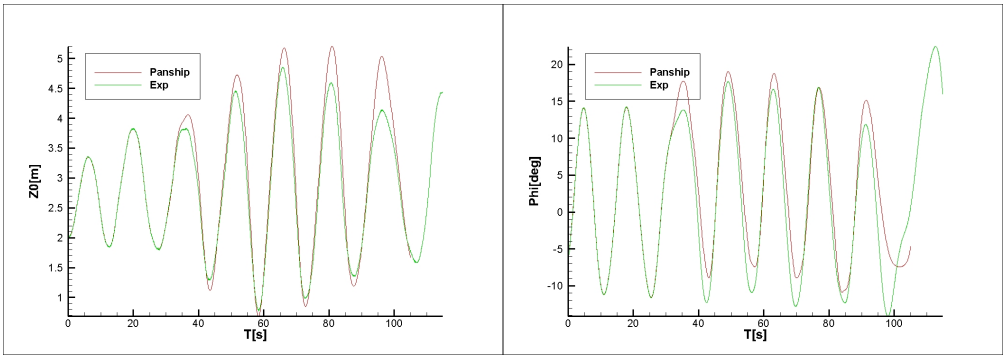

(c) Heave

(d) Roll

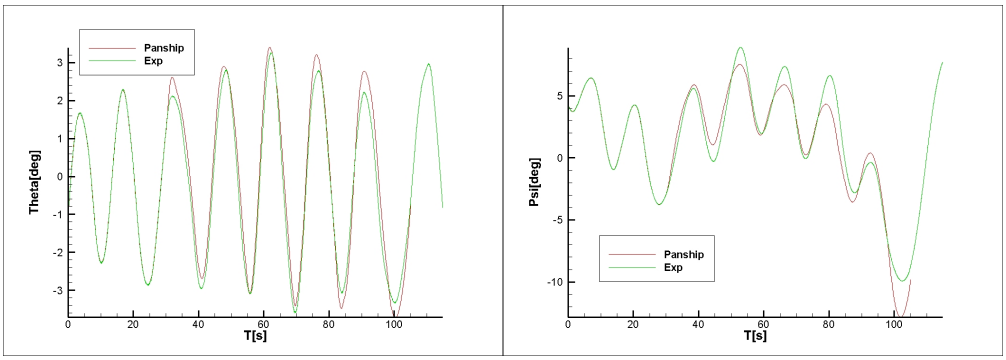

(e) Pitch

(f) Yaw

Figure 83: Time traces of model test and Panship for run 709003.

I Results of different Viscous drag calculations

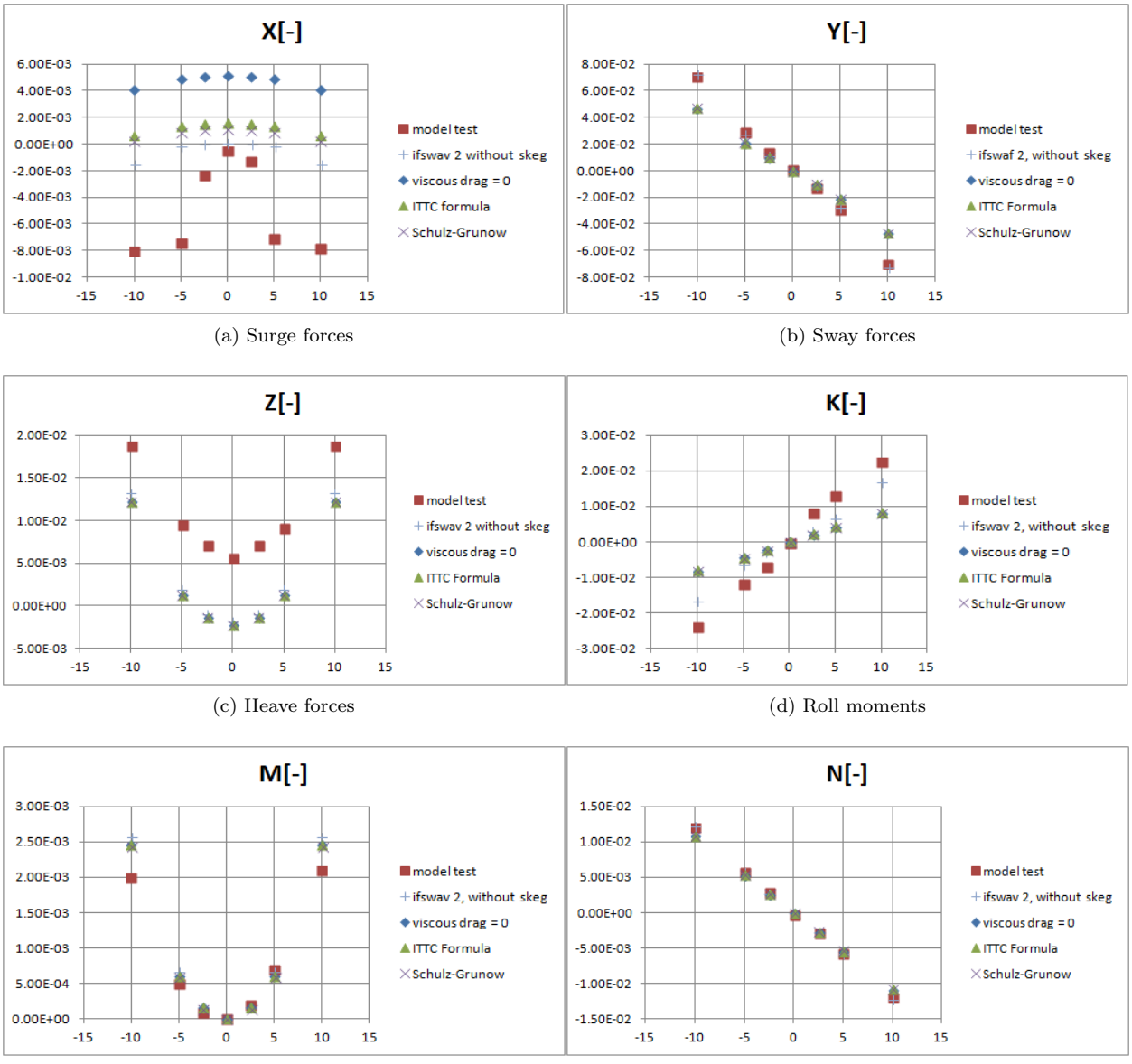

(a) Surge forces

(b) Sway forces

(c) Heave forces

(d) Roll moments

(e) Pitch moments

(f) Yaw moments

Figure 84: Forces and moments measured in model tests and calculated with simulations including different viscous drag calculations